DISCLAIMER NOTICE

THIS DOCUMENT IS BEST QUALITY AVAILABLE. THE COPY FURNISHED TO DTIC CONTAINED A SIGNIFICANT NUMBER OF PAGES WHICH DO NOT REPRODUCE LEGIBLY.

ASD-TDR-63-820

STRUCTURAL DESIGN
for
ACOUSTIC FATIGUE

TECHNICAL DOCUMENTARY REPORT NO. ASD-TDR-63-820

October 1963

AF Flight Dynamics Laboratory
Research and Technology Division
Air Force Systems Command
Wright-Patterson Air Force Base, Ohio

Project 1370, Task 137001

NOTICES

When Government drawings, specifications, or other data are used for any
purpose other than in connection with a definitely related Government
procurement operation, the United States Government thereby incurs no
responsibility nor any obligation whatsoever; and the fact that the
Government may have formulated, furnished, or in any way supplied the said
drawings, specifications, or other data, is not to be regarded by implica-
tion or otherwise as in any manner licensing the holder or any other person
or corporation, or conveying any rights or permission to manufacture, use,
or sell any patented invention that may in any way be related thereto.

FOREWORD

The research work reported herein was conducted by the Aircraft Division, Douglas Aircraft Company, Inc., Long Beach, California. The work was administered by the Aero-Acoustic Branch, Vehicle Dynamics Division, AF Flight Dynamics Laboratory, Research and Technology Division, Wright-Patterson Air Force Base, Ohio, under Contract No. AF33(657)-8217. This research is part of a continuing effort to obtain tolerance levels and design criteria for flight vehicles which is part of the Air Force Systems Command's Applied Research Program 750A, "Mechanics of Flight". The work was conducted under Project 1370, "Dynamic Problems in Flight Vehicles", Task 137001, "Resonant Fatigue of Structure." Mr. M. J. Cote of the Aero-Acoustics Branch was the Project Engineer.

The Douglas program was conducted under the direction of Mr. G. E. Anderson, Chief of the Structures Section, Engineering and Product Development, Aircraft Division. Mr. P. R. McGowan served as principal investigator aided by Mr. R. L. Frasca. Additional personnel of both the Structures Section and the Structural Mechanics Section aided in this project.

Testing in the High Intensity Sound System of the Douglas Santa Monica Acoustics Laboratory was under the control of Mr. J. E. Apple assisted by Mr. M. R. Ballard.

The testing and the analysis of the aluminum structure was performed by Mr. J. D. Van Dyke and Mr. A. L. Eshleman and credit must be extended to them for these results.

The time period covered by this contract was June 11, 1962 to September 30, 1963.

The corresponding Douglas number for this report is LB-31354.

ASD-TDR-63-820

ABSTRACT

The results of acoustic testing on several types of aircraft structure
are compiled and are used to produce acoustic fatigue design charts.
The theory on which the charts are based is explained. A method of
converting constant amplitude S-N data to random data is presented,
as is a method of converting discrete frequency test results to
equivalent random data. Test results from various other companies
test facilities are compared.

PUBLICATION REVIEW

This report has been reviewed and is approved.

FOR THE DIRECTOR

WALTER J MYKYTOW
ASSISTANT FOR RESEARCH AND TECHNOLOGY
VEHICLE DYNAMICS DIVISION

ASD-TDR-63-820

TABLE OF CONTENTS

LIST OF ILLUSTRATIONS

LIST OF ILLUSTRATIONS (cont)

LIST OF TABLES

ASD-TDR-63-820

LIST OF SYMBOLS

A   Cross Sectional Area, square inches; also amplification factor

AR   Aspect ratio; a/S

B   Factor, $f\ (^t2/^t1)$

C   Aspect ratio correction factor

D   Damage, in the cumulative damage concept

E   Young's modulus, psi

E_c Modulus of elasticity in compression, psi

F_{bru} Ultimate bearing stress, psi

F_{bry} Bearing yield stress, psi

F_c Allowable column buckling stress, psi

F_{cy} Compressive yield stress, psi

F_{su} Ultimate shearing stress, psi

F_{tu} Ultimate tensile stress, psi

F_{ty} Tensile yield stress, psi

G   Shear modulus, psi

I   Moment of inertia, inches^4

I_{cg} Moment of inertia about the center of gravity, inches^4

I_x Moment of inertia about the x axis, inches^4

K   Proportionality constant; also $\propto$

K_b Bending - Buckling coefficient

K_{ss} Buckling coefficient for plates with simply supported edges

L   Bead length, inches; also corrugation length, inches; also length of cutout

L'   Effective column length, inches

M   Bending moment, inch-pounds

N	Constant amplitude fatigue life, cycles
N_R	Total number of random cycles to failure; also N_r
N_x	Number of cycles to failure at $\sigma = x \sqrt{\sigma^2}$
P	Sound Pressure, psi; also load, pounds
P_H	RMS sound pressure for discrete frequency loading, psi
P_R	RMS sound pressure in one cps band width
$P(x)$	Rayleigh probability density function for one variable $= xe^{-\frac{x^2}{2}}$
R	Radius of cutout, inches
S	Support spacing, inches; also short side of panel, inches
S_{PD}	Stress at which maximum fatigue damage occurs under random loading, psi
W	Weight per inch of section, pounds per inch; also bead width, inches
X	Ratio of peak stress in one cycle of response to random loading to RMS stress due to random loading
Y	Relative damage
Z	Section modulus, inches^3
a	Long side of panel, inches
b	Bead height, inches
b_c	Cap width, inches
b_w	Web width, inches
c	Distance from the neutral axis to the outer most fibers, inches
d	Distance from the x axis to the outer most fibers, inches; also Rivet diameter, inches
db	Sound pressure level, decibels
db_R	Random sound pressure level, decibels
dA	Incremental area under the Rayleigh probability curve
e	Depth of flange or eccentricity, inches
f	Applied stress, average, psi; also frequency, cps
f_s	Applied stress in the skin, psi

h	Rib-beam height, inches
i	Subscript used for the "i" th mode
l_1	Corrugation peak to peak length along the cover plate, inches
l_2	Developed peak to peak length along the cover plate, inches
n	Distance between faces, inches
n_x	Number of stress cycles at stress defined for N_x
t	Skin thickness, inches
t_B	Bead inner skin thickness, inches
t_d	Doubler thickness, inches
t_E	Edge thickness, inches
t_{min}	Minimum face thickness, inches
t_p	Pan thickness, inches
t_r	Rib thickness, inches
t_w	Web and cap thickness, inches
t_1	Outer skin thickness, inches
t_2	Inner skin or corrugation thickness, inches
w	Density, pounds per cubic inch
w_e	Effective width, inches
y	Distance from x axis to centroid location, inches
α	Coefficient of thermal expansion (mean), inches per inch per Degree Fahrenheit
α_d	Stress load ratio at design
α_t	Stress load ratio at test
ϵ	Elongation, percent
γ	Poisson's ratio
δ	Deflection of beam, inches
ζ	Damping ratio

θ	Angle between cover plate and corrugation, degrees
λ	Nonlinearity factor
ρ	Radius of gyration, inches
$\sqrt{\sigma^2}$	RMS stress due to random loading, psi
σ_{HD}	Harmonic stress equal to random discrete stress, psi
σ_M	Peak stress in one cycle of response to random loading, psi
σ_{al}	Allowable pressure buckling stress, psi
σ_{ap}	Applied stress for bending of corrugation, psi
σ_E	Stress in panel edge, psi
σ_o	Stress load ratio at resonance; for a sinusoidal load, divided by the amplification factor, $1/2\zeta$ (in the linear range of response)
σ_p	Pressure stress, psi
γ	Shear stress, psi
γ_{cr}	Critical shear buckling distribution
ω	Natural frequency, cps
ω_f	Resonant frequency, cps
$\propto$	Proportional symbol

SECTION 1   INTRODUCTION

Acoustic fatigue is a subject that is no longer new. However, due to the
many factors which must be considered for design, and allowed to vary for
a comprehensive test program, the amount of data available for general
design purposes is almost nil. To partially eliminate that condition this
study extends results of either discretely or randomly excited structural
acoustic tests through an analytical approach and presents the extended
results as design nomographs.

The source of acoustic excitation was considered to be the propulsion system
and the structure of main interest was the lighter structural configuration
common to wing trailing edges, empennage, or fuselage afterbody. These
structural components are most commonly exposed to acoustic environments and
are such that other design criteria is not critical.

The design results as presented are a function of the allowable random
fatigue life of the material. Use of elevated temperature data for this
fatigue life would account for the direct effect on the material of elevated
temperature. No attempt was made to account for the overall effect of
elevated temperature. This depends so greatly on the response of the
adjoining structure that it is beyond the scope of this study. Additionally,
for a majority of the structural components under study the damage occurs at
takeoff when temperatures are nominal and combined effects are insignificant.

ASD-TDR-63-820   1

SECTION 2 SUMMARY

This investigation has been directed towards developing design data for acoustic fatigue. The factors that enter into the design of structures for acoustic fatigue and the manner in which each of these factors affect the life of various typical aircraft structure is considered. The acoustic environments considered are those resulting from typical jet propulsion systems as distinct from aerodynamic noise.

The final results of this study are design charts to aid the designer in the selection of structural elements to meet the requirements for acoustic fatigue. These charts are based on an analytical approach to determine the relationship of the various parameters which affect the design and are presented in Section 6.

The analytical expressions developed are for (1) structural mechanical relationships, (2) equivalent random and discrete acoustic loading or response and (3) equivalent random and constant amplitude material fatigue allowable data. These expressions are used in conjunction with the test results to develop the design charts mentioned above. The analytical expressions and relationships are developed in Section 5.

The results reported herein cover two phases of the study

    1) Study of conventional - subsonic structure

    2) Study of advanced structure

The structure considered in the first phase consists of six types fabricated of 2024S-T3, 2024S-T4 or 7075S-T6 aluminum alloy

    1) Skin and rib construction

    2) Skin and rib with a doubler at the rib

    3) Edge attachments

    4) Ribs with lightening holes

    5) Beaded inner skin panels

    6) Honeycomb panels

The second phase of this study is conducted on two types of structure suitable for a portion of a supersonic or aerospace vehicle. The material for construction is titanium 6Al-4V sheet annealed. The test configurations are:

1) Corrugated inner skin with a single face
2) Skin with welded stringers

A detailed description of the test specimens is presented in Section 3.

The tests were conducted in the Douglas Santa Monica Acoustics Laboratory facilities. Either the siren or the random noise generator was used in these tests. The siren, producing a discrete frequency output, was used for the conventional -subsonic structure. The random generator, which was not available in the early part of the program, was used for testing the advanced structure specimens. This test equipment and the test procedures employed with each are described fully in Section 4.

Test data were obtained from other sources and, where possible, were compared with data from this study. Due to data limitations and variation in test methods, there was little correlation of results. This information also is presented in Section 4.

SECTION 3   TEST SPECIMENS

The test specimens for this program are separated into two general types based on the structure which they represent. These two types of structure can be defined roughly as 1) Conventional-Subsonic Structure and 2) Advanced Structure. While variations in basic structure between these types exist, it will be found that the variation in material and in methods of assembly are as much a criteria defining the types as is the basic structural concept. Thus, while the specimens for the first type are all fabricated from aluminum alloy (2024S-T3, 2024S-T4 or 7075S-T6), the advanced specimens are fabricated of titanium 6Al-4V sheet annealed, with however, one of these specimens being, in form at least, a conventional skin and stringer.

Both types of specimens are confined to structure that is most susceptible to damage from acoustic fatigue. This normally imposes the two restrictions, that the parts be in a relatively high level area of the sound field and that other design criteria does not dictate such a high strength capability that acoustic fatigue is insignificant as a design factor. Structures which usually meet both restrictions are the "minimum gage" structure of the wing trailing edge, wing control surfaces, fuselage afterbody and empennage.

CONVENTIONAL-SUBSONIC STRUCTURE

Simple specimens were evaluated, initially, using the siren to determine the best configurations for the various structures. These specimens included skin and rib box panels with closely spaced ribs which simulate control surface construction, honeycomb panels, and bonded-beaded panels. The materials used were 2024S-T3, 2024S-T4 and 7075S-T6 clad sheet. Based on these tests, various improvements were made and appropriate rib spacing, rib gages, skin gages and rib lightening holes were determined for a useful range of sound levels. Skin capability was improved through the use of bonded skin-doublers at the ribs. These doublers provided a reinforcement at locations of high stresses near rivet holes. The doublers were scalloped to reduce stress concentration at their edges. Improvements were made on

bead ends to balance the end and center strength. The honeycomb panel edge
designs and attachments were selected. Material gages and other pertinent
dimensions were varied from specimen to specimen within each configuration.
The limits of these dimensions are indicated in the following paragraphs and
the combinations tested are presented in detail in Table 4.

The aluminum alloy conventional structures tested were:
1) Skin and rib construction
2) Skin and rib with a doubler at the rib
3) Ribs with lightening holes
4) Beaded inner skin panels
5) Honeycomb panels

The specimen overall dimensions were approximately 3 x 4 feet.

Skin and Rib

The skin and rib specimens were representative of a control surface section
with ribs joining an upper and a lower skin and shear webs representative
of spars completing the box section. Various combinations of rib and skin
gage and rib spacing were tested within the following limits:

Skin gage	.025	-	.063
Rib gage	.032	-	.063
Rib spacing	4.0	-	9.5 inches

Skin and Rib with Doubler

These specimens were fabricated as indicated in the previous paragraph with
a finger or scalloped doubler bonded to the skin at the rib locations.
Specimens were fabricated with doublers of various thicknesses but generally
within one gage of the skin itself. These specimens ranged within the
following limits:

Skin gage	.020 -	.050
Rib thickness	.040 -	.063
Doubler thickness	.012 -	.032
Rib spacing	4 and 8 inches	

Rib with Lightening Hole

The affect of lightening holes on ribs was evaluated in the box specimens in conjunction with the other panels. The ribs had standard "C" flange stiffened edges on the cutouts. The ends of the cutouts were circular in shape with two alternate radii, 1-1/8 inch or three inches. The rib thicknesses varied from .050 to .032. The lengths of the lightening holes tested were either three or 13-1/2 inches.

Beaded Inner Skin Panels

Panels with various forms of beaded inner skins were tested and most failed through the bead end. Redesign developed a bead end which was equally fatigue resistant with the other parts of the panel. Only the test results for this improved bead, described below, are presented herein. The beads tested were one inch deep and the material was .020 in thickness. The width and length were 5-1/8 and 29-1/2 inches, respectively.

Honeycomb Panels

The honeycomb panels were sandwich construction with the aluminum face sheets bonded to the aluminum core. A formed doubler was added around the edges and the edge core was stiffened by the addition of a foam filler. The panels tested were square, 21 inches on a side, and the overall thickness was 7/16 inches.

ADVANCED STRUCTURE

The advanced panels tested in this program are of two basic types. These represent control surface and trailing edge structure, areas susceptible to acoustic fatigue. The material for all items, with the exception of the lower surface in the stringer configuration, is titanium 6Al-4V sheet annealed. Mechanical properties for this material are shown in Table 1. This lower surface is aluminum of a thickness to simulate the stiffness of the "built-up" test surface but offers simplicity for fabrication.

TABLE 1

MECHANICAL PROPERTIES

Titanium 6Al-4V Annealed Sheet (.020 - .187)

Mil-Hdbk-5, "A" Value

F_{tu} = 130.0 ksi (Long)
130.0 ksi (Trans)

F_{ty} = 120.0 ksi (Long)
120.0 ksi (Trans)

F_{cy} = 126.0 ksi (Long)
126.0 ksi (Trans)

F_{su} = 76.0 ksi

F_{bru} = 244.0 ksi (e/D = 2.0)

F_{bry} = 198.0 ksi (e/D = 2.0)

E = 15.4×10^6 psi (Long)
16.4×10^6 psi (Trans)

E_c = 16.0×10^6 psi (Long)
16.9×10^6 psi (Trans)

$\in$ = 10.0% (Long)
10.0% (Trans)

α = 4.6×10^{-6} in/in/$^{\circ}$F (70 - 200°F)

$\sqrt{}$ = .33 (Long)
.32 (Trans)

w = .160 - .161 lb/in^3

Corrugated Inner Skin with a Single Face

The configuration proposed for a control surface is a corrugation stiffened panel with formed angles, representative of spar caps, at each end and running normal to the direction of the corrugations. Welded tees, representative of rib caps, parallel to the corrugations, located at the ends and two positions in the central portion of the panel, are clipped to the spar cap angles and form three bays. Formed angles in each bay are positioned against the lower crest of and transverse to the direction of the corrugation to tie each end to the spar cap. These two attachments are by spotwelds as is the corrugation to skin, the skin to spar cap and the rib clips to spar. The ribs are fastened through the skin and corrugation by A286 rivets, 5/32 inches in diameter. The corrugations extend in the chordwise direction. This orientation permits the rib cap to tie directly to the outer skin and the inner skin to efficiently work with the outer skin to supply a torsionally stiff path for actuation loads. Under conditions of spanwise bending, the inner skin will offer very little restraint which will result in a comparatively flexible structure. This condition will alleviate the induced loads which result from deflection of the supporting surface. This construction also eliminates the need for rib cutouts which increase the fatigue susceptibility. These panels overall are 24 by 36 inches. The combination of skin and corrugation thicknesses tested is indicated below:

Outer Skin Thickness	Corrugation Thickness
.025	.016
.025	.020
.020	.016
.020	.020

Photographs of these panels are presented in Figures 1 and 2. The manner of selecting the skin and corrugation test combinations is presented in Appendix I.
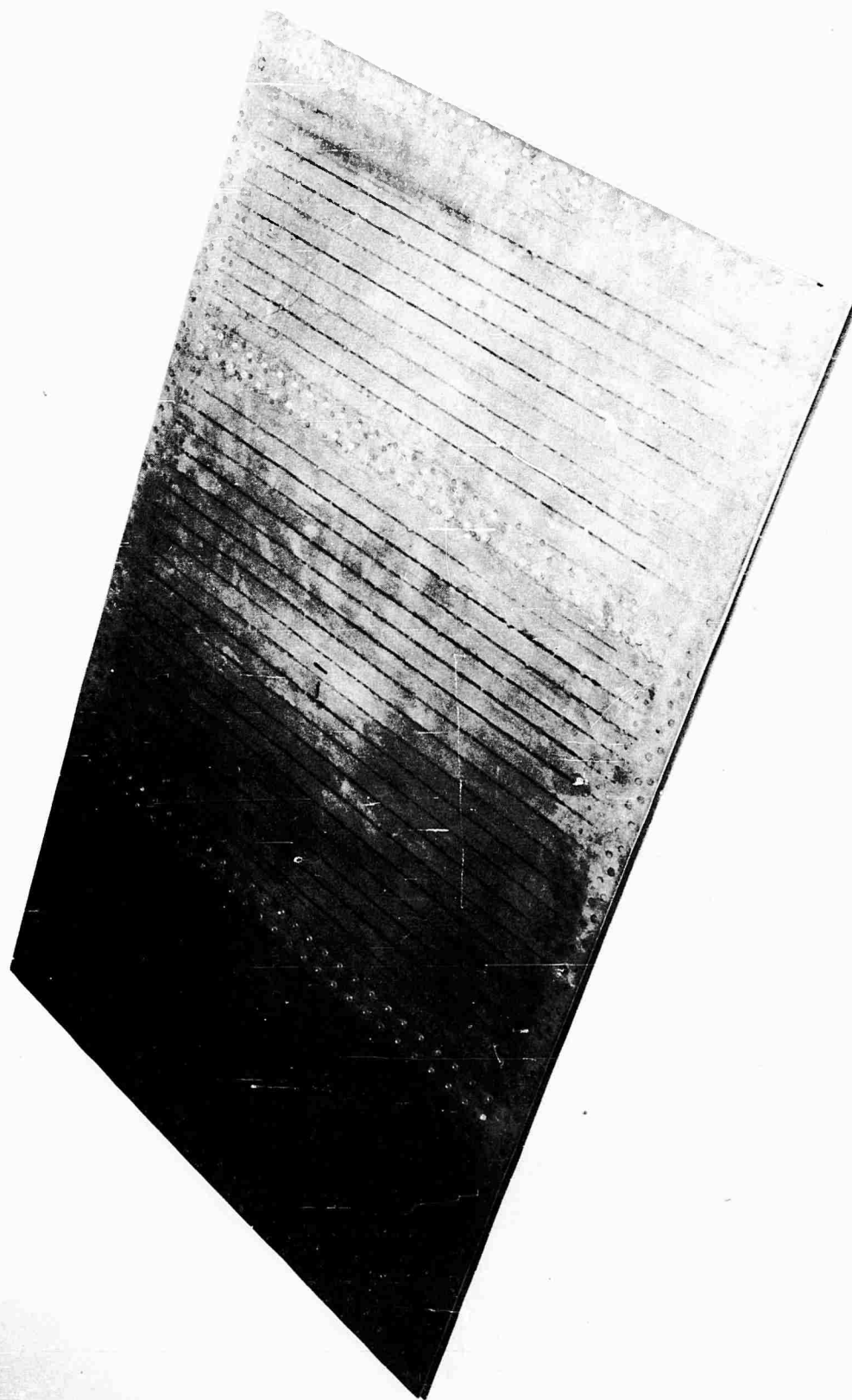
FIGURE 1   CORRUGATED PANEL - SKIN

9
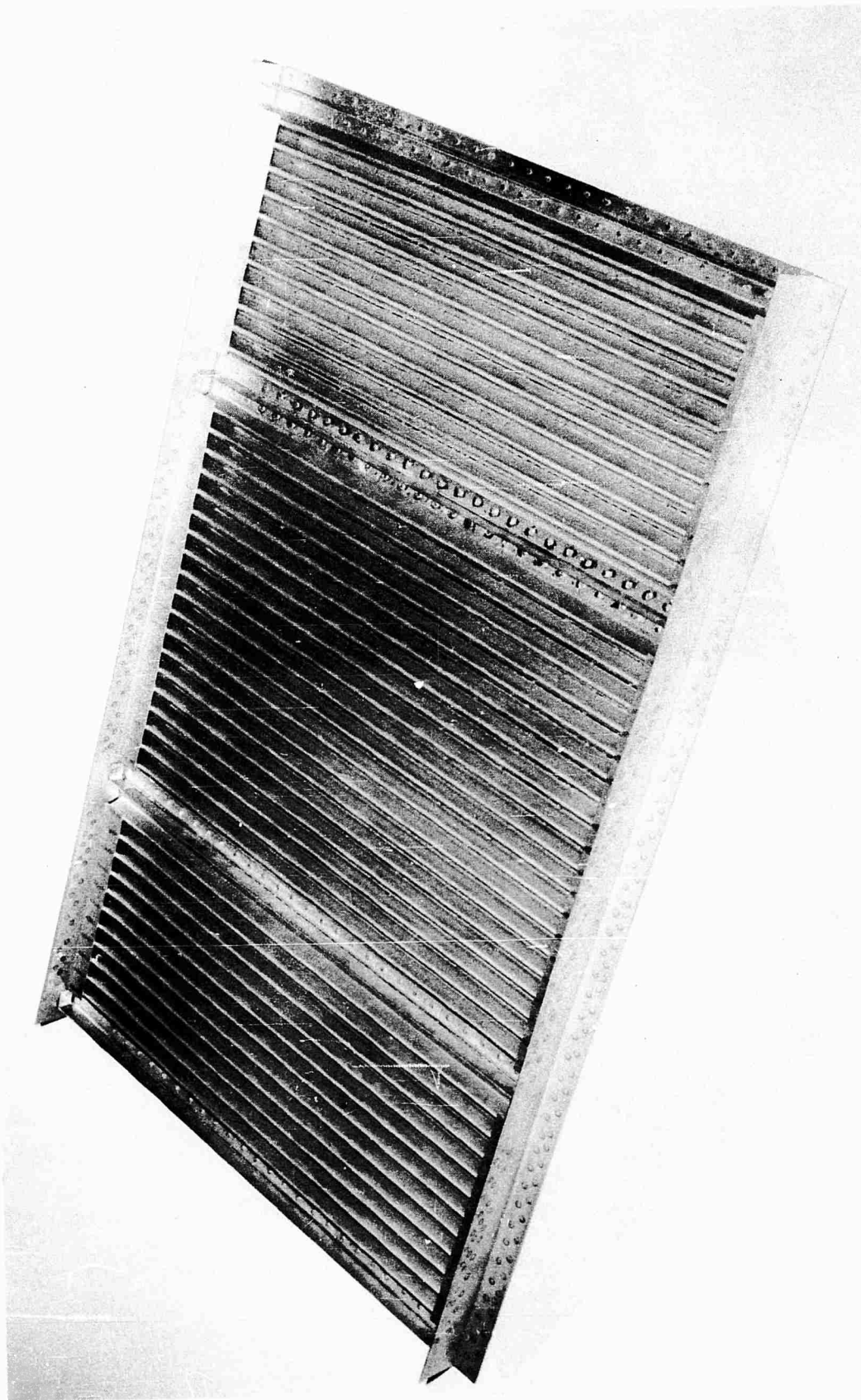
FIGURE 2 CORRUGATED PANEL - CORRUGATION

10

Skin with Welded Stringers

The trailing edge structure, in form, is a conventional skin-stringer-rib configuration. The panels are supported by a representative sub-structure consisting of four ribs, a front and rear spar and a lower closing panel. The structure is unusual in that it is of all welded construction and the stringer-skin attachment is achieved by means of a melt-thru weld process.

The stringer does not have a flat against the skin but the web is welded directly to the skin eliminating duplicate area at this point. The attachments of the ribs, skin and spars is all by resistance spotwelds. At the stringer-rib intersection, the two elements are clipped together to prevent stringer rolling. This attachment is by resistance spotweld to the rib but the attachment to the stringers is by fusion spotwelds. These panels have overall dimensions of 24 by 36 inches with the stringers running in the longer direction, approximately four inches on center. The stringers are .032 inches thick material and are formed by using a melt-thru weld to form a tee which is then welded to the skin. Two skin thicknesses were tested: .025 and .020. Photographs of the panels are presented in Figures 3 thru 5.
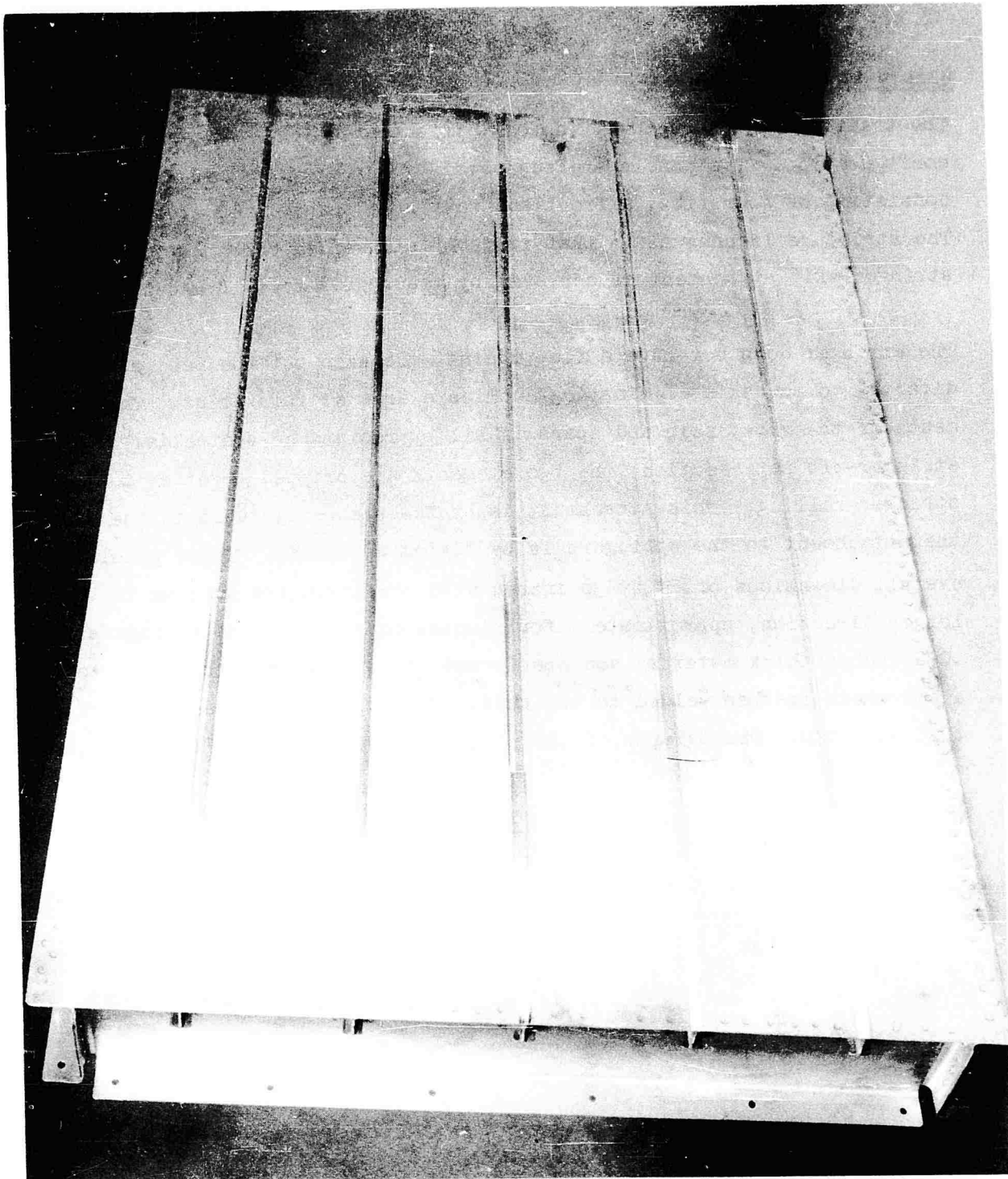
FIGURE 3 SKIN AND STRINGER - UPPER EXTERIOR
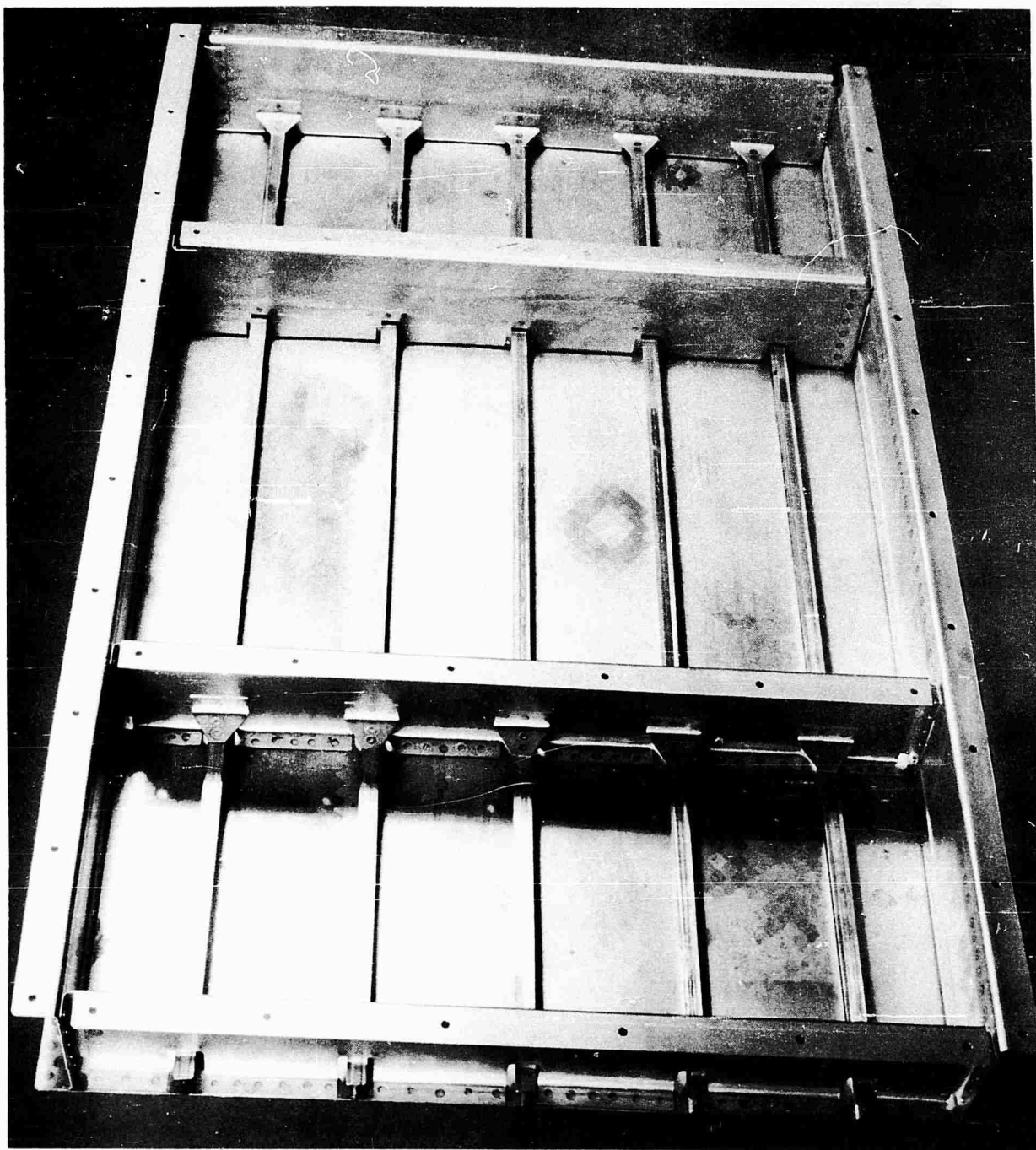
FIGURE 4   SKIN AND STRINGER - LOWER COVER REMOVED

13
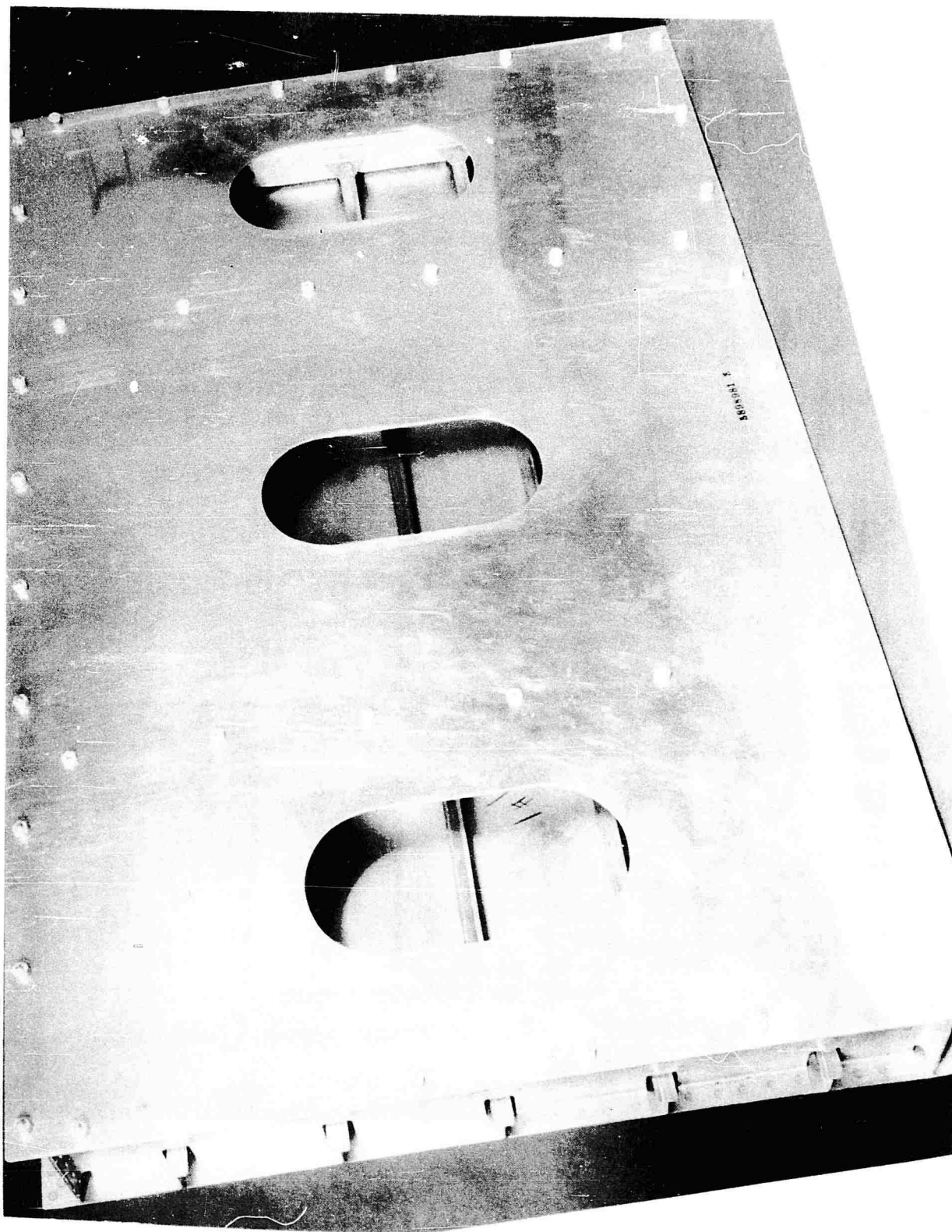
FIGURE 5   SKIN AND STRINGER - LOWER COVER INSTALLED

14

SECTION 4 TESTING - FACILITIES, PROCEDURES, RESULTS

The testing in this investigation was conducted for the most part in one of
two test facilities at the Douglas Company Acoustics and Vibration laboratory
in the Santa Monica Division. In addition, some of the tests on the conven-
tional structure were conducted in the noise field of an actual jet engine.
The following paragraphs describe the test facilities, the test procedures
and present the test results.

TEST FACILITIES

The two test facilities located at the Santa Monica Division consist of a
siren of Douglas design and a High Intensity Sound System (HISS) designed by
the Ling-Altec Company.

Siren

The siren produces discrete frequency noise up to a sound pressure level of
160 db. The available frequency range is from 50 to 1000 cps. Air for this
facility is furnished by a squirrel cage blower driven by a 100 horsepower
motor. The air passes through the siren which is driven by a variable speed
motor and produces noise of the required frequency. This noise passes
through an expansion horn to the test section where it impinges on the test
specimen with a grazing incidence. Test panels can be accommodated up to
3 feet by 4 feet in size.

High Intensity Sound System (HISS)

The HISS is an electrically controlled system which has a capability of
reproducing random, sinusoidal or a taped signal as desired. The limitations
are an overall output of 170 db random and a frequency range of 50 to 10,000
cps. The random output is adjustable in octave band widths. The air for
this equipment is supplied from a plant compressor and is used up to 50 psi.
The air flow is modulated by an electrical signal to the ten transducers in
the system to produce the desired noise. This noise then passes through
exponential horns to the test section when it impinges on the specimen with

a grazing incidence. The test section has a width of six inches and is capable of accommodating test specimens up to 5 feet by 10 feet in size. A general view is shown in Figure 6.

The instrumentation is by Brüel and Kjaer and provides a capability of using up to 50 strain gages with an automatic selector type 1542 which monitors the gages in sequence. Strain gage response was viewed on a 502 dual beam oscilloscope. Peak and RMS strains were read off a voltmeter. A level recorder type 2305 in conjunction with a beat frequency oscillator type 1014 was used to determine strain response as a function of frequency. A multiple octave band equalizer was used to obtain the desired shape spectrum. This spectrum was checked with an octave band noise analyzer type 1350-A. Strain gage output was recorded on an Ampex 600 magnetic tape recorder. This tape is reduced through use of a Techno analyzer. During the test, an audio frequency spectrometer type 2112 which filters to 1/3 octave band was used. A 527B power supply and a 30 db amplifier model 442C were also used.

TEST PROCEDURE

The test procedure varied slightly with the two facilities to accommodate the differences in equipment. For each of the facilities, however, the specimens were first excited with a stress-coat applied to the surface to determine the most appropriate location for strain gages. Photographs showing typical stress-coat results and strain gage positions are shown in Figures 7 through 16.
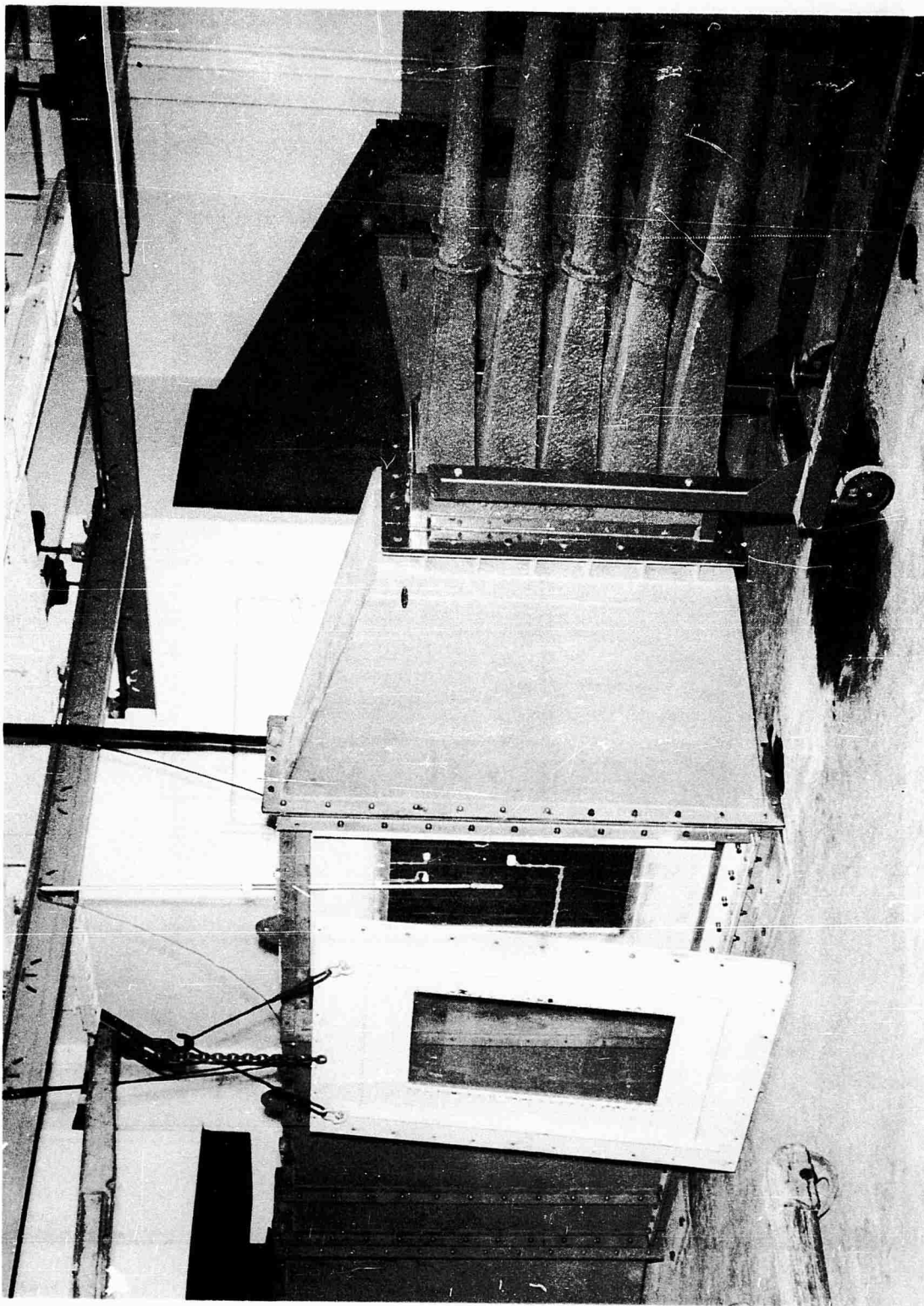
FIGURE 6   GENERAL VIEW HIGH INTENSITY SOUND SYSTEM
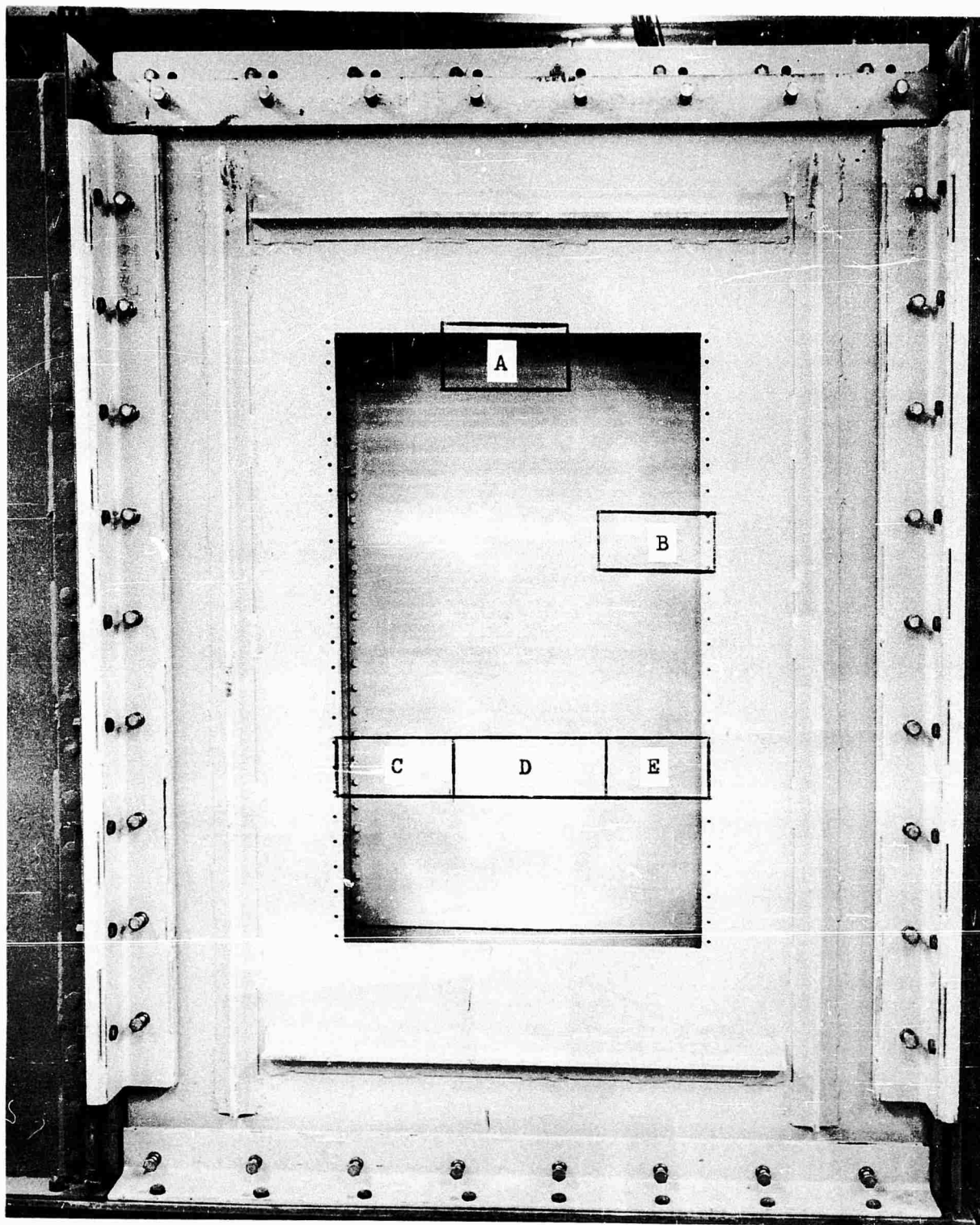
FIGURE 7   CORRUGATED PANEL INSTALLED FOR TEST (VIEW THROUGH WAVE TUBE)
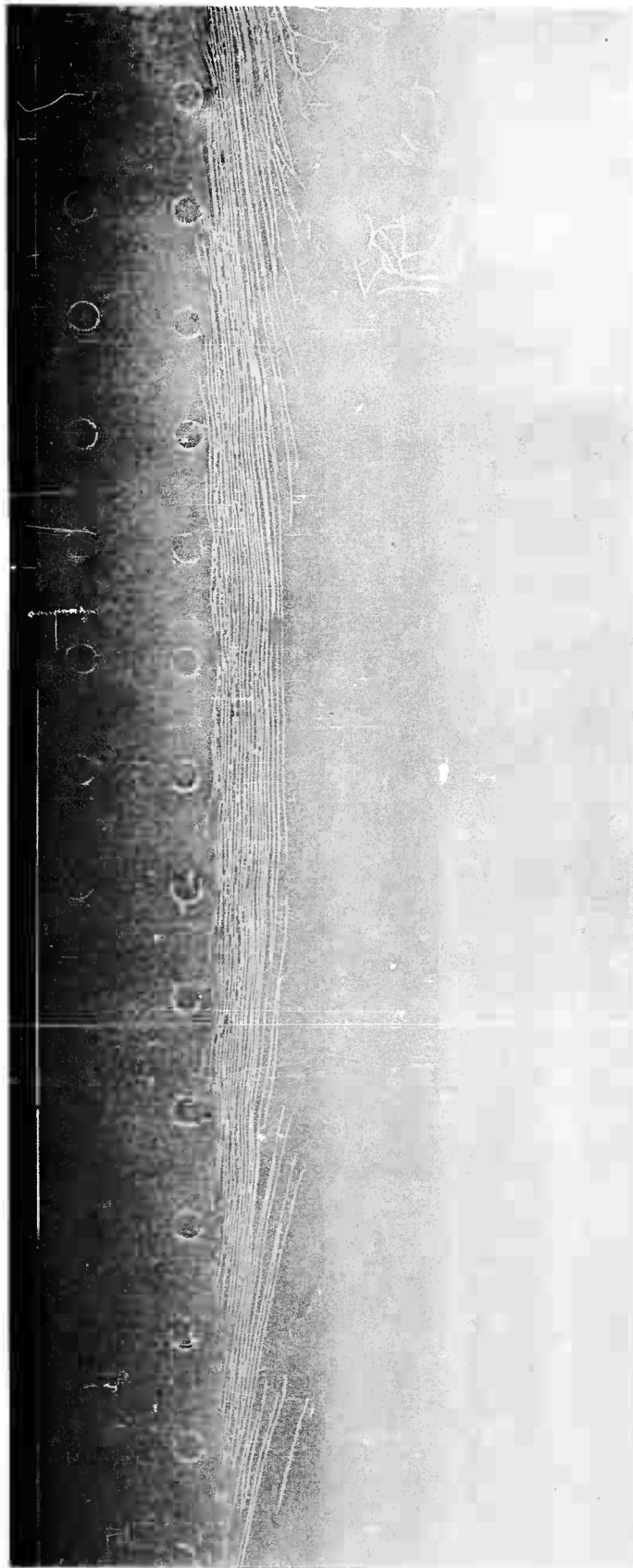
FIGURE 8 STRESS COAT (AREA A, FIG 7)

FIGURE 9 STRESS COAT (AREA B, FIG 7)

FIGURE 10 STRESS COAT (AREA C, FIG 7)
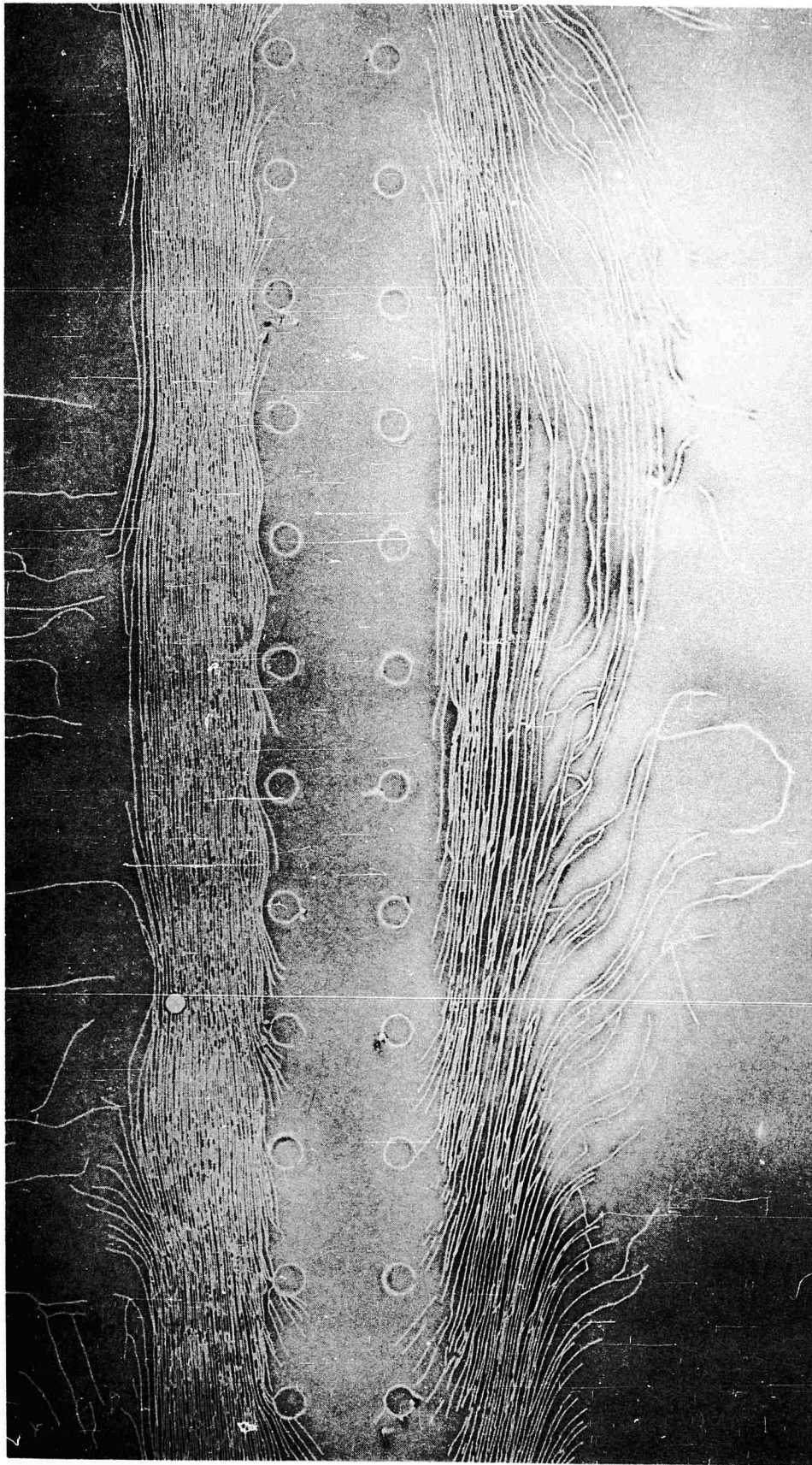
FIGURE 11 STRESS COAT (AREA D, FIG 7)
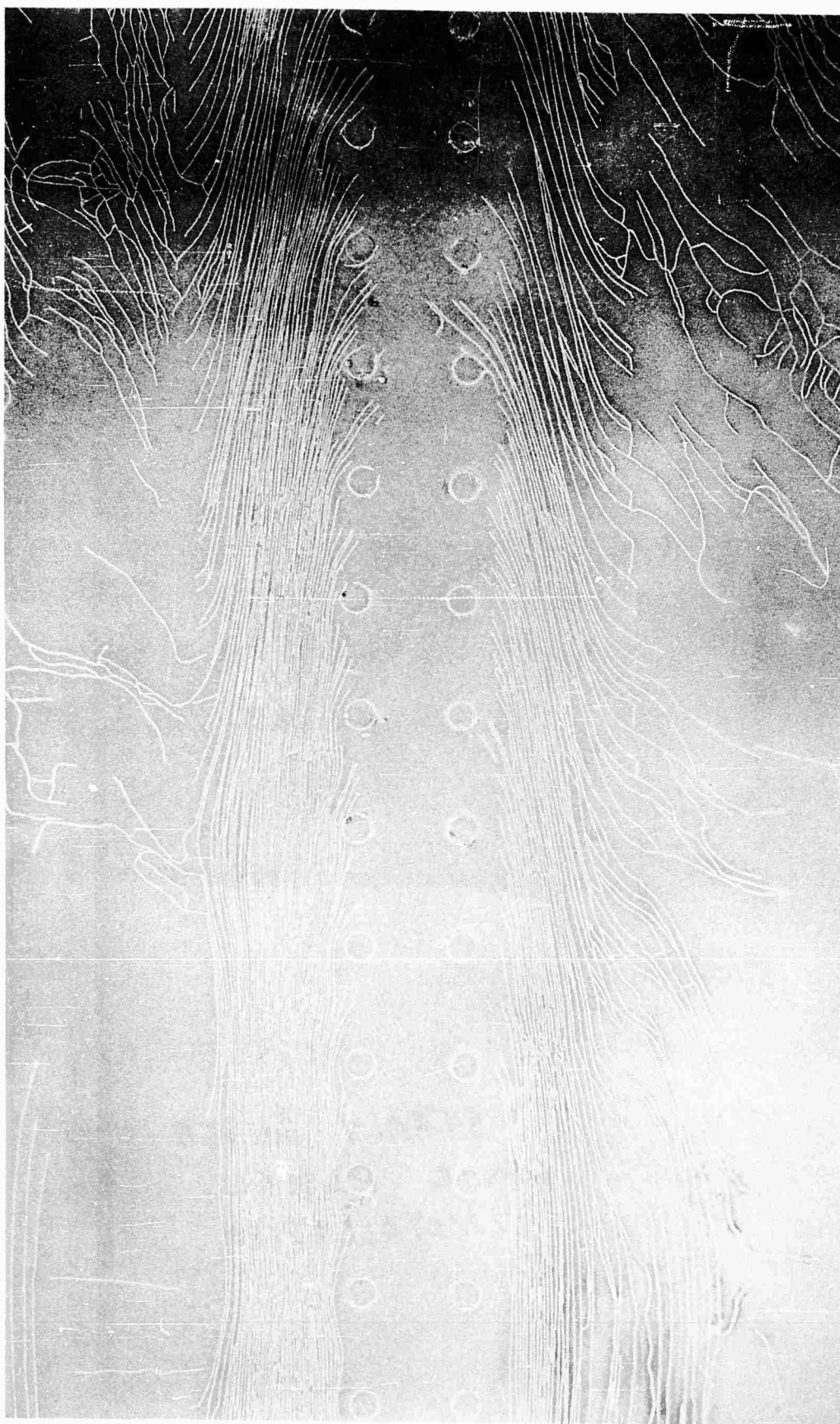
FIGURE 12 STRESS COAT (AREA E, FIG 7)
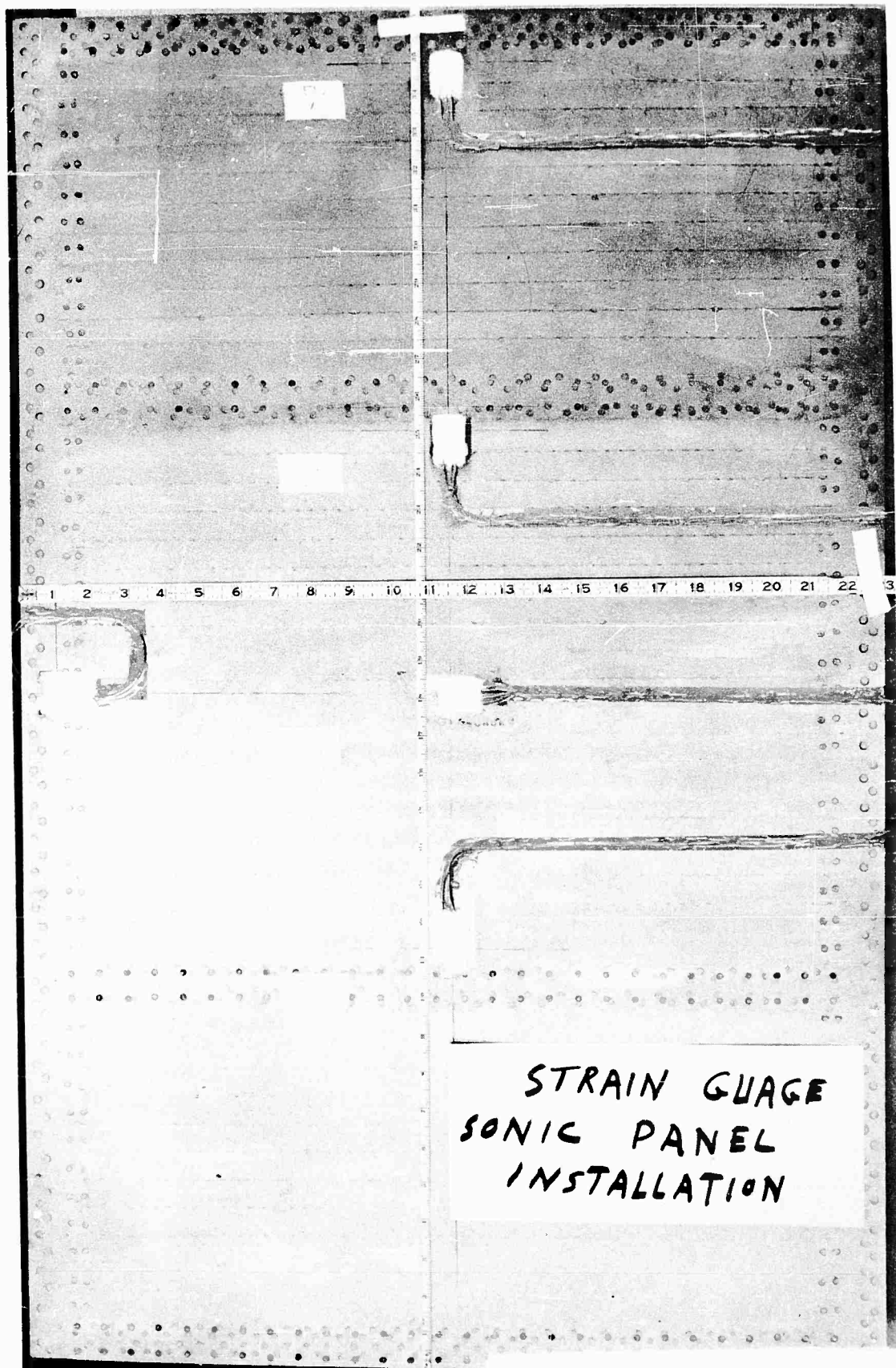
FIGURE 13   TYPICAL STRAIN GAGE INSTALLATION CORRUGATED PANEL

STRAIN GUAGE
SONIC PANEL
INSTALLATION
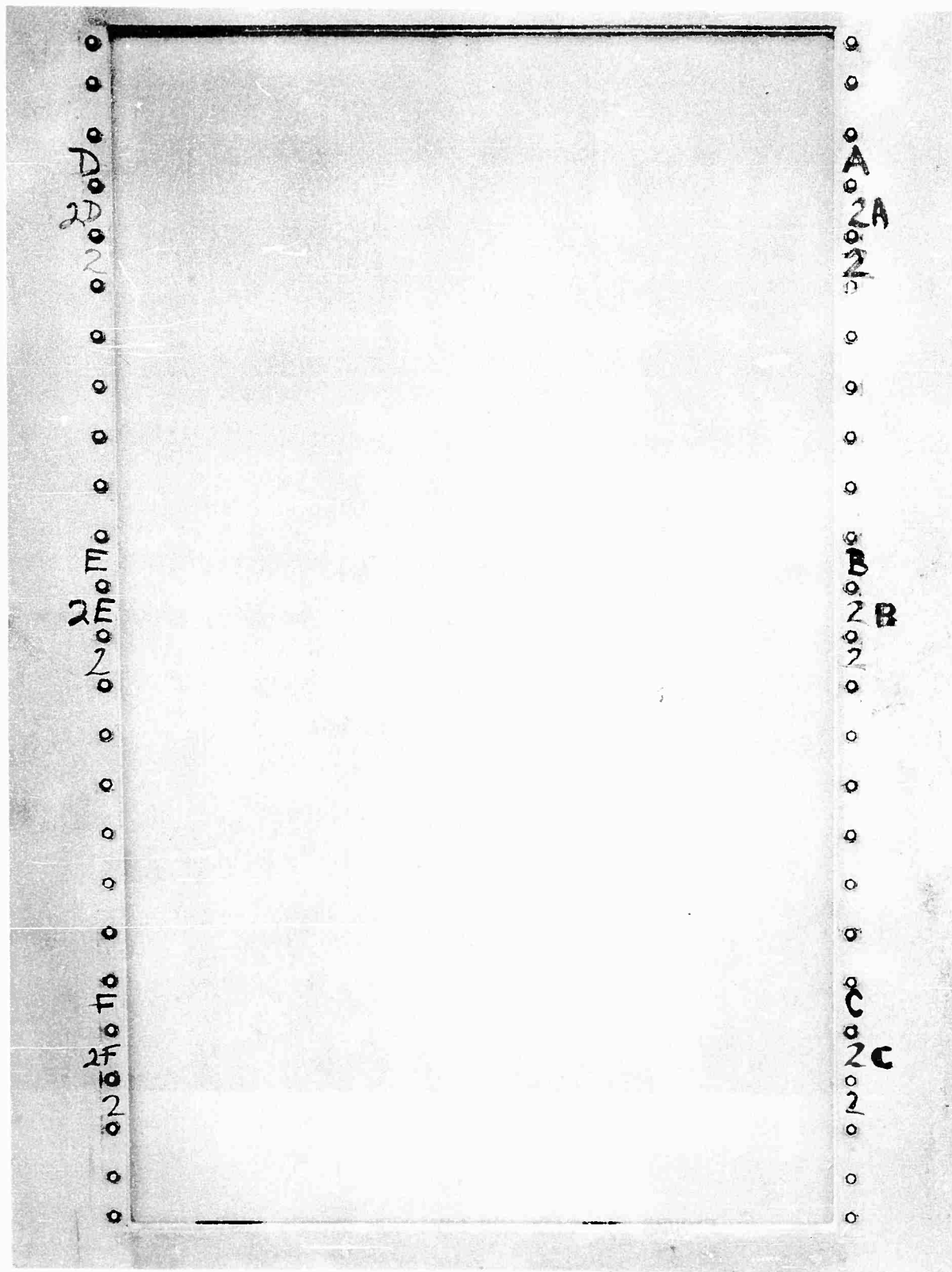
FIGURE 14 SKIN AND STRINGER STRESS COAT OVERALL VIEW
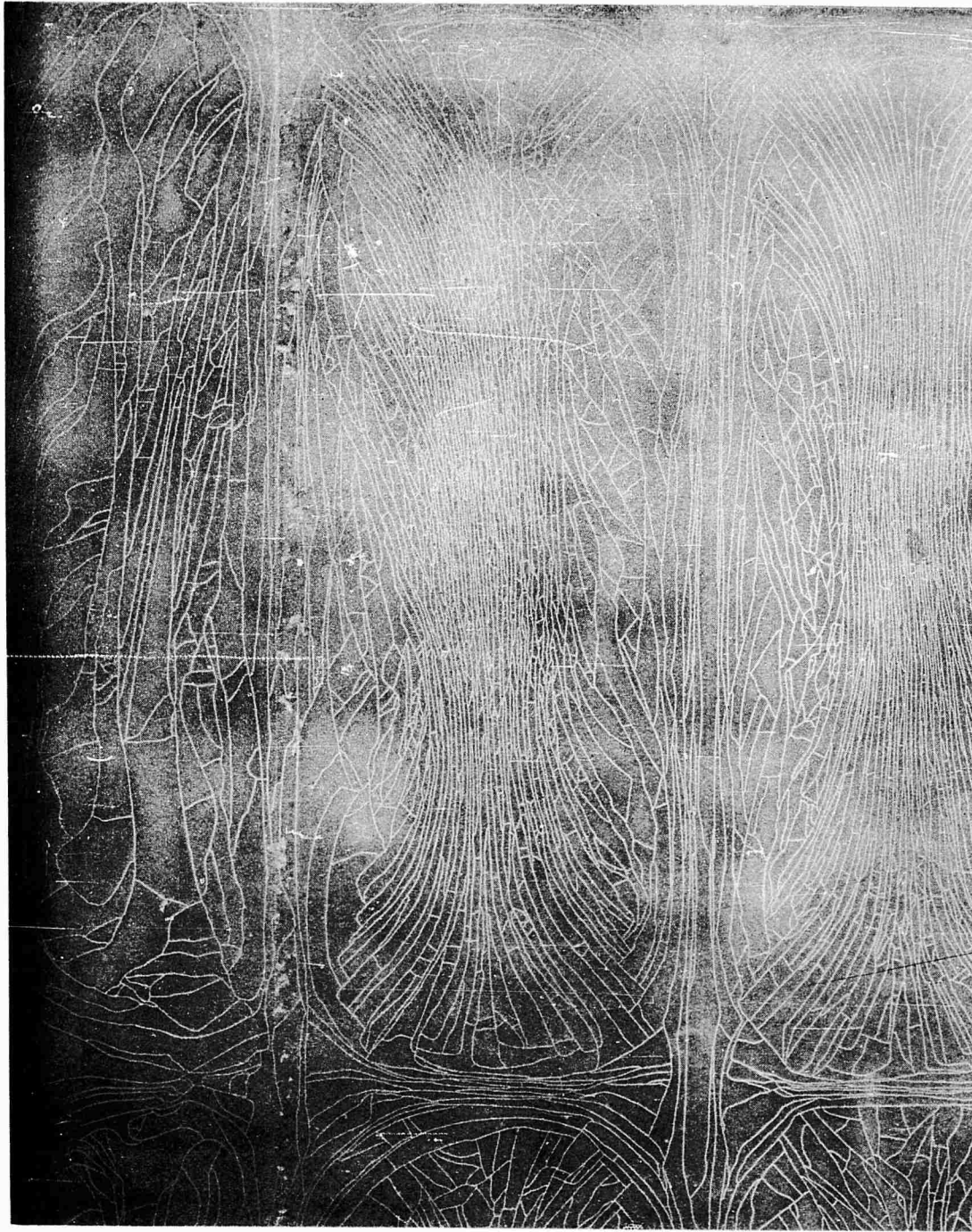
FIGURE 15   SKIN AND STRINGER STRESS COAT CENTER

FIGURE 16   SKIN AND STRINGER STRESS COAT CORNER

Siren Test Procedure

In conducting the siren tests on the specimens with strain gages installed, the resonant frequencies were determined by exciting the panel at a low sound pressure level in increasing frequencies and noting those of most response. A more detailed survey was then made of the points of interest and the critical frequency was determined with the variation in response of near frequencies to permit determination of the damping factor. Mode shapes were determined through the use of a stroboscopic light. Response readings were taken at each of the critical frequencies while varying the sound pressure level. This data results in a linearity factor as explained in Section 5. After these data were obtained the specimens were tested to failure. To accomplish this the panels were exposed to a chosen lower intensity sound level at each of the more critical frequencies for a period of 20 minutes. If failure did not occur, the sound pressure level was increased 3 db and the specimens again excited at each frequency for 20 minutes. This was repeated until failure occurred.

HISS Test Procedure

In using the HISS equipment, the test procedure was similar to that described above. The strain gaged specimen was first excited by a low level random noise to determine which of the gages were indicating the most critical stress to establish limits of pre-fatigue test noise levels. Using a sinusoidal excitation, critical frequencies and mode shapes were determined. Linearity data were then determined as indicated for the siren. The fatigue portion of the test was then conducted, using a white noise excitation. Testing was all at a single sound pressure level for each panel. The manner in which an appropriate test level was arrived at is indicated below. Testing was conducted for various periods of time varying from three minute intervals at the start of a run to 15 minute intervals after completion of an hour of excitation.

The preliminary analysis showed that the corrugated panels with the equal thickness corrugations had almost equal critical stress levels for the same noise input. Thus, these four panels were tested in two sets of two each. The skin and stringer panels were tested individually.

Test Sound Pressure Levels

The test sound pressure levels were chosen at a level which was computed to cause failure in approximately one hour of testing. For the corrugated panels this was 134 db_R per cps and 128 db_R per cps for the skin and stringer panels. Within the ability of the test equipment to produce white noise at these levels, the overall equivalents from test were $163-1/2$ and $158-1/2$ db_R, respectively. The method employed to arrive at an appropriate test level is detailed in the following paragraphs.

The two general types of configurations being tested, (skin-stringer, and corrugation) were analysed through the use of a Douglas developed computer program. This program considers an element of the panel as a two-dimensional beam with multiple supports of varied translational and rotational stiffnesses. The critical stress and frequency for the beam are obtained as part of the program output.

To determine the test sound pressure level to cause failure in a given time, for example: one hour, the following procedure was followed. Using the computer program, the critical stress is determined for a trial sound pressure level (131 db or .01 psi was used). The program also indicates the critical frequency which permits an analytical determination of the number of load cycles which are applied in one hour. Having the number of cycles and making use of the appropriate random fatigue curve, the random stress corresponding to this life is determined. A simple proportion, based on the computed pressure and stress, determines the pressure which should be applied to cause test failure in the desired time. This method was employed for all the titanium specimens. The skin and stringer panels were checked both normal and parallel to the stringer direction while the corrugated panels were checked only in the direction of the corrugations. A sample calculation is presented below.

The skin and stringer is checked in the direction of the stringer. The assumed beam is a stringer with its adjacent skin supported at the four rib points.

The computer program indicated that the maximum stress occurred in the middle of the short bay with the following analytical results:

$$P_R \quad = \quad .01 \text{ psi } (131 \text{ db})$$

$$\sqrt{\sigma^2} \quad = \quad 7950 \text{ psi (max)}$$

$$f \quad = \quad 970 \text{ cps}$$

$$N_{1 \text{ hour}} = \quad 3.5 \times 10^6$$

From the titanium random S-N curve, stress for failure in one hour $(3.5 \times 10^6$ cycles) is:

$$\sigma_{1 \text{ hour}} = \quad 22,800 \text{ psi}$$

and the pressure to cause this stress

$$P_{R \ 1 \text{ hour}} = \frac{P_R \sqrt{\sigma^2}_{1 \text{ hour}}}{\sqrt{\sigma^2}} \quad = .029 \text{ psi } (140 \text{ db}) \qquad (1)$$

Computations are presented in Table 2 for the pressure to cause failure at various numbers of cycles for each of the titanium test specimens and the results are plotted in Figures 17 and 18.

The computer results for each of the cases are presented in Table 3, along with the selected test conditions.

Table 2

CALCULATED VARIATION OF SOUND PRESSURE LEVEL WITH TEST PANEL LIFE

N_R	$\sqrt{\sigma^2}$	P_1	P_2	P_3	P_4
10^5	44,000	.00993	.01363	.0190	.0216
3×10^5	36,000	.00813	.01114	.01555	.01764
10^6	29,500	.00666	.00913	.0127	.0144
3×10^6	26,000	.00587	.00806	.01123	.01275
10^7	23,000	.00518	.00713	.00995	.01127
3×10^7	22,000	.00496	.00682	.00953	.01077
10^8	21,000	.00473	.00650	.00907	.0103
3×10^8	20,000	.00451	.00620	.00865	.0098

$$P_1 = (.01) \frac{\sqrt{\sigma^2}}{44,300} \quad - \text{ Skin-Stringer } (t_s = .020")$$

$$P_2 = (.01) \frac{\sqrt{\sigma^2}}{32,270} \quad - \text{ Skin-Stringer } (t_s = .025")$$

$$P_3 = (.01) \frac{\sqrt{\sigma^2}}{23,140} \quad - \text{ Corrugation } (t_s = .020")$$
$$(t_c = .016")$$

$$P_4 = (.01) \frac{\sqrt{\sigma^2}}{20,400} \quad - \text{ Corrugation } (t_s = .025")$$
$$(t_c = .020")$$

Table 3

TEST SOUND PRESSURE LEVELS

| | SKIN - STRINGER Z5898981 | | | | CORRUGATIONS Z5898980 | | | |
| | 1 SKIN -501 | | 2 STRINGER | | -1 | -501 | -503 | -505 |
	$t = .020''$	$t = .025''$	-501 $t = .020''$	-1 $t = .025$	$t = .025''$ $t_2 = .020''$	$t = .025''$ $t_2 = .016''$	$t = .020''$ $t_2 = .020''$	$t = .020''$ $t_2 = .016''$
3 $\sqrt{\sigma^2}_{max}$	22,148	16,133	7,950	7,600	10,201	11,317	10,458	11,670
3 f	226	278	970	908	145	147	145	147
4 db	128.0	128.0	140.0	140.0	134.0	134.0	134.0	134.0
Time Hours	0.7	7.0	1.0	1.0	1.7	0.9	1.7	0.9

1   Location of highest stress was at midpoint of 16 inch bay. A concentration factor of two was applied.

2   Location of highest stress was at the attachment point of rib and skin. A concentration factor of two was applied.

3   The RMS stress $(\sqrt{\sigma^2})$ and resonant frequency (f) were obtained from the computer program results with the loading of 131 db white noise.

4   The random test db which must be applied in order to fail the panel at the indicated time.

CORRUGATED SPECIMENS

TI 6AL - 4V

LIMITS FOR SELECTION OF TEST LEVEL
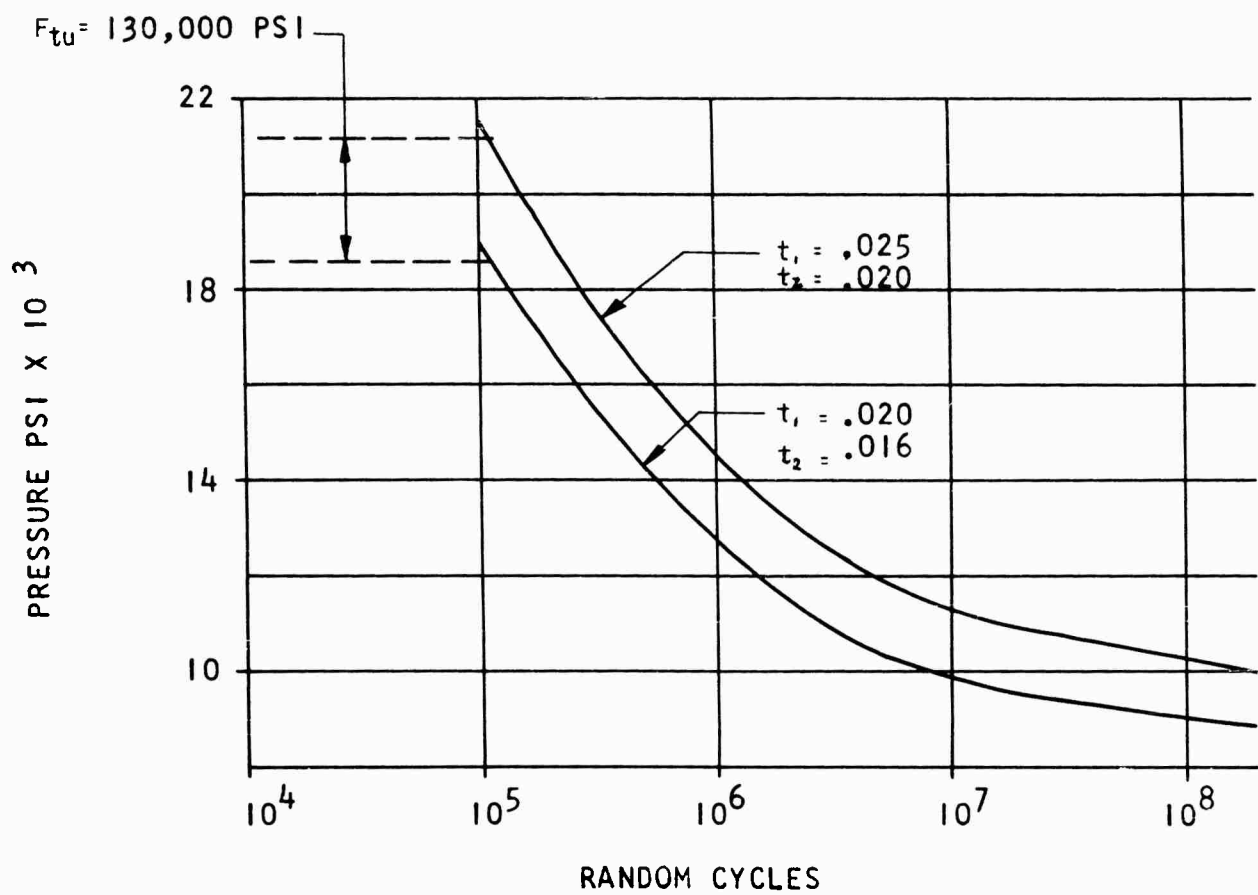
FIGURE 17 RANDOM LIFE VS PRESSURE CORRUGATED PANEL

SKIN AND STRINGER SPECIMEN

TI 6AL-4V

LIMITS FOR SELECTION OF TEST LEVEL
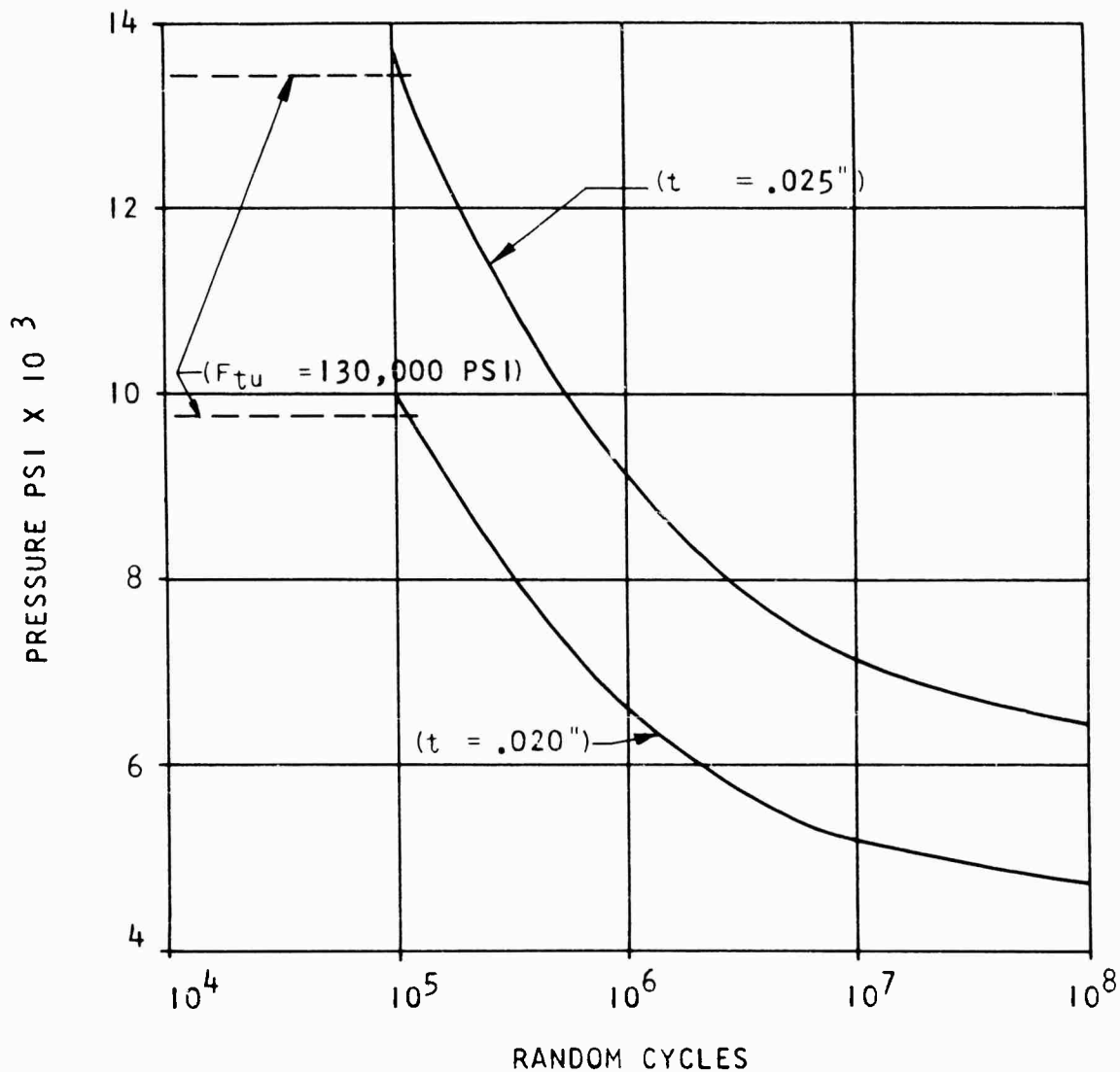
FIGURE 18 TEST RANDOM LIFE VS PRESSURE SKIN STRINGER PANEL

34

TEST RESULTS

The following paragraphs discuss the test results available from this program. These results are presented in a tabular form.

Conventional -Subsonic Structure

The data for the conventional structure was obtained from tests which were conducted from 1956 through 1958. The required data from these tests are presented in Table 4 but much of the related detail is not available.

Advanced Structure

The corrugated skin and the skin and stringer specimen results which were tested with a random sound pressure are discussed below.

The .016 corrugated skin panels were tested first. The first failure occurred in the panel with the .020 outside skin after 10 minutes of excitation. These failures were of two types. Cracks occurred in the corrugation crests at the ends and extended down the side of the corrugation. Two of these cracks had occurred at the 10 minute period. The other failure type was in the attachment of the corrugation to the formed angle which connected the corrugation to the spar cap. In these failures the spotweld pulled out of the corrugation.

These failures continued at different locations on the panel for the duration of the test run. A third type of failure occurred along the skin to spar cap row of welds after 19 minutes. These failures occurred first at the 1/3 points of the center panel. At this point, the panel was considered to have failed completely. It was allowed to remain in the test position, however, until completion of testing on the companion panel. The test failures are shown in the photographs in Figures 19 and 20.

The companion panel with the same .016 thick corrugation but with .025 skin experienced the same failure types but these did not occur until 13 minutes of run time had elapsed. The extension of the failures in this panel was also delayed. The first failure in the skin to spar cap attach did not occur until after 79 minutes of excitation.

Table 4

SUMMARY OF TEST RESULTS

SKIN AND RIB CONSTRUCTION

S	t	t_r	f (cps)	db*	T (min)
8	.040	.040	202	157	50
8	.050	.050	223	160	40
8	.063	.063	315	160	60
6	.032	.032	366	154	20
4	.025	.040	480	153	1
4	.025	.032	357	156	10
4	.025	.040	168	150	10
4	.025	.032	376	153	65
9.5	.050	.063	171	153	20
9.5	.050	.063	163	150	60

SKIN AND RIB WITH A DOUBLER AT THE RIB

S	t	t_r	t_d	f (cps)	db*	T (min)
4	.032	.050	.020	333	163	10
4	.025	.040	.016	380	166	22
8	:050	.063	.032	397	160	40
4	.020	.040	.012	400	163	20
4	.032	.050	.020	333	163	26

RIB WITH A LIGHTENING HOLE

S	R	L	t_r	e	h	f (cps)	db*	T (min)
4	3	13.5	.040	1/2	3	393	149	21
4	3	13.5	.050	1/2	3	368	153	29
4	1-1/8	3	.032	3/8	1-3/4	333	163	10
4	1-1/8	3	.050	3/8	1-3/4	318	151	40
4	1-1/8	3	.032	3/8	1-3/4	362	160	20
6	1-1/8	3	.032	3/8	1-3/4	366	154	20
4	1-1/8	3	.032	3/8	1-3/4	376	147	10

* Discrete Frequency

ASD-TDR-63-820

Table 4 (cont)

HONEYCOMB PANELS

t_1 or t_2	n	S	a	t_E	f (cps)	db*	T (min)	Type Failure
.01	7/16	21	26-1/4	.050	210	153	45	Edge
.01	7/16	21	26-1/4	.050	167	150	24	Edge
.016	7/16	21	26-1/4	.061	198	156	30	Edge
.016	7/16	21	26-1/4	.061	189	156	75	Edge
.016	7/16	21	26-1/4	.061	259	156	37	Unbonding
.010	7/16	21	26-1/4	.050	206	156	60	Skin
.016	7/16	21	26-1/4	.061	239	159	38	Edge
.016	7/16	21	26-1/4	.061	240	159	10	Unbonding
.010	7/16	21	26-1/4	.050	245	159	2	Skin
.016	7/16	21	26-1/4	.061	140	159	5	Skin

BEADED INNER SKIN PANEL

t_B	t_E	W	L	b	f (cps)	db*	T (min)	Type Failure
.020	.060	5-1/8	29.5	1	131	147	21	Skin

* Discrete frequency

Table 4 (cont)

WELDED SKIN AND STRINGER PANELS

S	t	f (cps)	db_R **	T (min)	Type Failure
4	.025	286	128	90	Skin
4	.025	286	128	10	Attachment
4	.020	215	128	10	Skin
4	.020	215	128	10	Attachment

CORRUGATED PANELS

S	t_1	t_2	l_1	f	db_R **	T (min)	Type Failure
23	.025	.020	.75	150	134	16	Corrugation
23	.025	.020	.75	150	134	40	Attachment
23	.025	.020	.75	150	134	60	Edge
23	.025	.016	.75	215	134	13	Corrugation
23	.025	.016	.75	215	134	13	Attachment
23	.025	.016	.75	215	134	79	Edge
23	.020	.020	.75	148	134	14	Corrugation
23	.020	.020	.75	148	134	25	Attachment
23	.020	.020	.75	148	134	60	Edge
23	.020	.016	.75	123	134	10	Corrugation
23	.020	.016	.75	123	134	10	Attachment
23	.020	.016	.75	123	134	19	Edge

** White noise
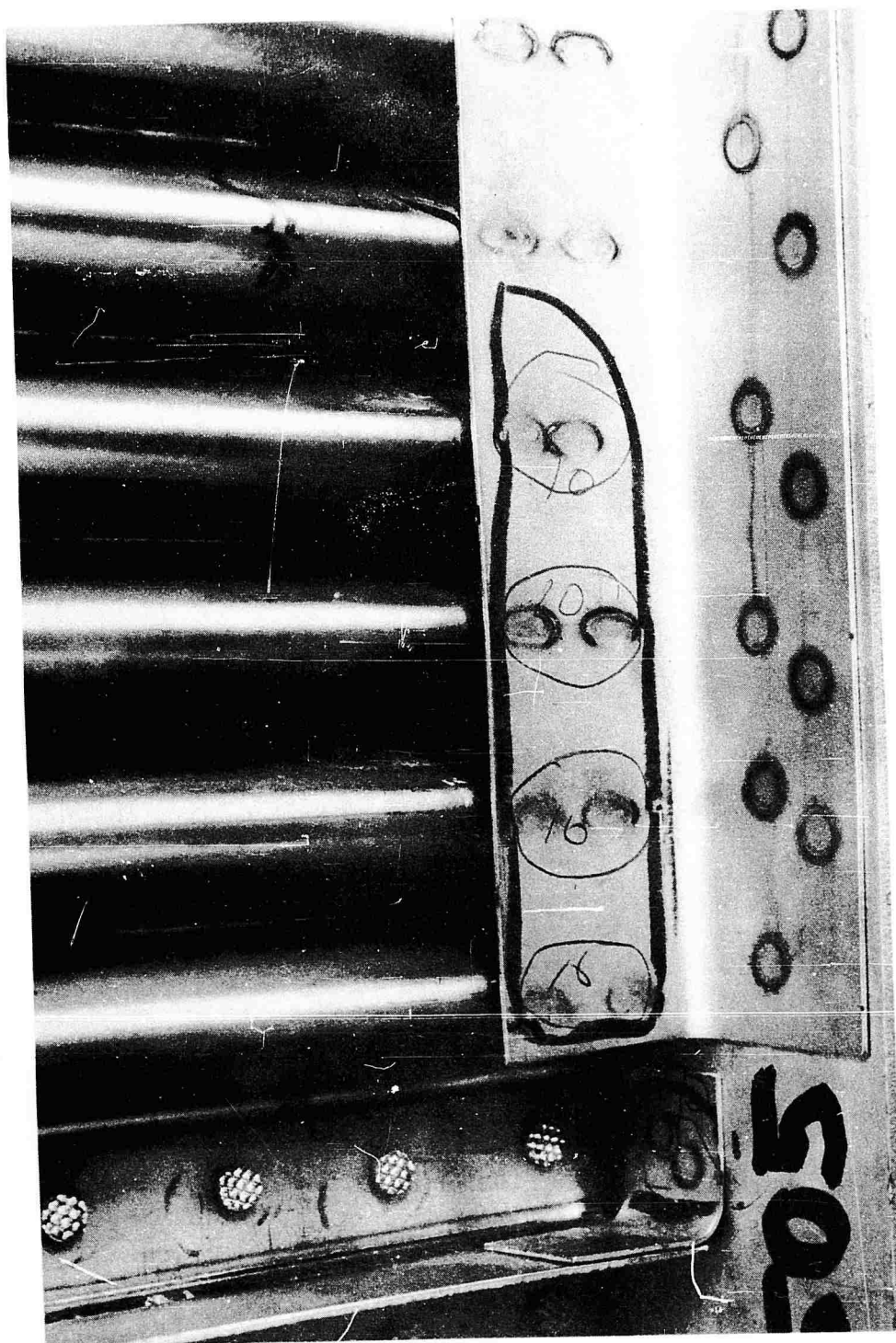
FIGURE 19   CORRUGATED PANEL FAILURES EDGE

FIGURE 20   CORRUGATED PANEL FAILURES CORRUGATION

The other set of corrugated panels failed in a manner similar to that described above for the first set. In these panels, however, due to the thicker .020 corrugation, the spotwelds did not pull out and failure at this point occurred within the attaching angle. The cracks in the corrugation occurred as before. The first failure in the corrugation occurred at 14 minutes for the .020 outer skin panel and at 16 minutes for the .025 outer skin panel. The angle failure which did propagate though the spotwelds occurred at 40 minutes and 25 minutes for the .020 and .025 skin panels respectively. In these panels, the skin to spar cap failures occurred at 60 minutes for each.

The skin and stringer panels were tested as an element of a complete box structure. The first failures occurred in the substructure attachments. In the .025 skin panel cracks were observed across several of the fusion spotwelds which attached the stringer to rib clips on to the stringer after 10 minutes of testing. These cracks did not propagate into the clip proper until approximately 50 minutes after which complete failure of a few of the clips occurred rather rapidly. In approximately the same time period some of the fusion welds failed leaving the clips unattached to the stringer. An additional substructure failure which occurred was in the rib at the clip attach. Cracks were initiated at the clip to rib spotweld and propagated approximately 1/4-inch to the stringer cutout on the rib. These failures were first observed at 24 minutes. No failure of the rib proper or of a stringer occurred. The critical failure within this panel occurred in the .025 skin along the short edge of one of the small panels defined by the stringer and rib grid. The failure was along the line of spotweld skin to rib flange attach and occurred after 90 minutes of excitation. This failure is shown in Figure 21.

The skin and stringer panel with the thinner .020 skin experienced very little substructure damage before critical damage occurred in the skin at 10 minutes. This failure occurred in two locations on the panel and was along the stringer and had extended the full length of the bay between ribs in each case. Photographs of these failures are shown in Figures 22 and 23.

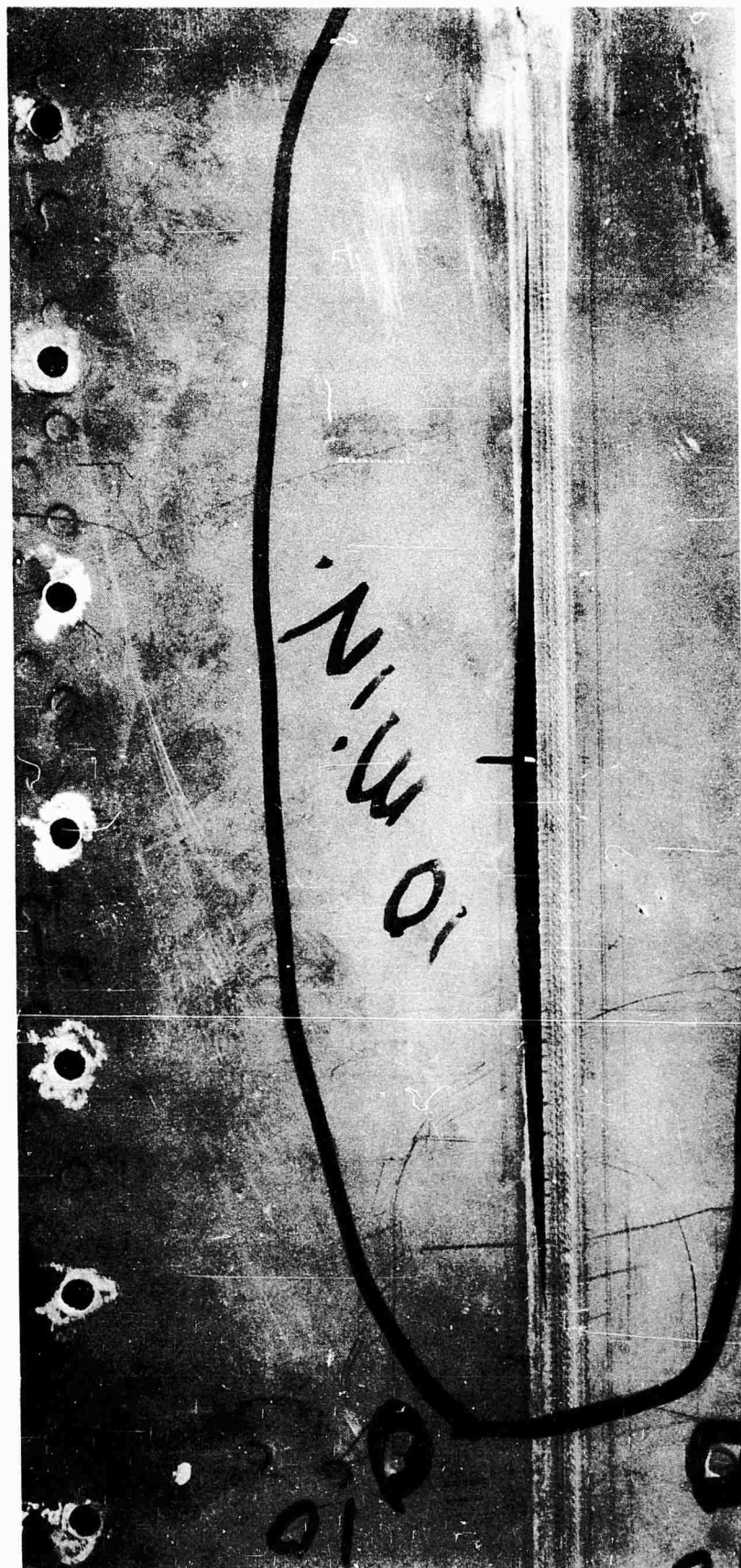FIGURE 21   SKIN AND STRINGER FAILURE SKIN AT RIB

FIGURE 22 SKIN AND STRINGER FAILURE SKIN AT WELD (1)

FIGURE 23 SKIN AND STRINGER FAILURE SKIN AT WELD (2)

COMPARISON WITH OTHER TEST DATA

Results of acoustic tests from various companies is presented along with pertinent test data in Table 5. A method of comparing test results to the predicted results from the Douglas design charts is given, and comparisons made using the method are presented in tabular form grouped according to company.

The testing as performed by these companies was for a normal incidence with no baffling of the sound pressure while the Douglas tests were conducted using grazing incidence with an infinite baffle. Either grazing or normal incidence could be more representative of actual conditions depending on the location and type of structure being considered. Another variation in test technique was in the test frequency. The other companies in general tested at only the lowest resonant frequency. The Douglas procedure consisted of exciting the specimen at each of the resonant frequencies at each sound pressure level which more nearly simulates the broad band excitation of actual engine exposure. The stresses from the several modes were then combined to compute a "multi-mode factor" which was applied to reduce the apparent single mode allowable stress at the critical frequency.

The Douglas results indicated a lower allowable SPL than the other tests and the differences probably are attributable to two factors. The above indicated discrepancy in test procedures probably contributes appreciably to the variation in predicted and test results. In addition, the panels for both the Martin and the Boeing tests were curved. Limited Douglas data indicates that curvature can increase the allowable SPL from 7 to 14 db. The Douglas method is the most conservative and where it differs, it is on the safe side, which is appropriate for design.

The coorperation of the companies supplying these data is appreciated.

Boeing

These panels were tested at normal incidence in front of a siren fitted with an exponential horn. A typical control panel was tested at 143 db, at its resonant frequency of 125 cps and lasted 7.0 hours. To use the Douglas design

45

charts, the conversion of discrete pressure (P_H) to random pressure (P_R) through the use of the following equation was made:

$$\frac{\sqrt{\overline{\sigma}^2}}{\sigma_H} = \frac{P_R}{P_H} \quad (\pi \delta f)^{1/2} \tag{2}$$

$$P_R = (P_H) \left(\frac{\sqrt{\overline{\sigma}^2}}{\sigma_H}\right) \Big/ (\pi \delta f)^{1/2} \quad (\delta = .01 \text{ assumed}) \tag{3}$$

$$N = (125 \text{ cps}) (60 \text{ sec/min}) (60 \text{ min/hr}) (7.0 \text{ hr})$$

$$N = 3.15 \times 10^6 \text{ cycles to failure}$$

Using random and normal S-N curves for 2024-T4, the panel material, the random stress ($\sqrt{\overline{\sigma}^2}$), and harmonic stress (σ_H), corresponding to the number of cycles to failure (N), were found to be 8500 and 18,300 psi respectively. The peak harmonic stress is converted to an RMS stress (σ_H) by multiplying by .707. Assuming a 3 db correction to the indicated test level for band width effect and converting from decibels to psi, P_H, is .029 psi. P_R was computed to be .00962 psi or 130.5 db_R A 3 db correction was found to be appropriate in the Douglas siren facility for modifying unfiltered data.

The panel parameters necessary for use with the design charts to determine the random db level for which failure will occur are: life, skin thickness (t), and rib spacing (S). For these panels, t = .040 inches and S = 8 inches. Under these conditions, for the same life and 3.15×10^6 cycles, the Douglas chart indicates this panel should have failed with a random loading of 120.0 db_R

General Dynamics

The specimens were subjected to sonic vibration at resonant frequencies. A typical panel subjected to 158 db overall SPL had a resonant frequency of 401 cps for 59 minutes at which time the resonant frequency changed to 410 cps and failure occurred 31 minutes later. This panel had a t = .060 inches and S = 7 inches. Under these conditions, following the previous method of analysis, for the same life, the actual and the critical P_R were found to be 140.0 and 131.0 db respectively. The panel material used was 7075-T6. The values for support spacing were scaled.

Martin-Denver

Each specimen was edge supported by knife edges to permit flexure while static compressive loads were applied to simulate expected forces during lift off. The panels were subjected to sonic vibration at resonant frequencies by an exponential horn coupled to a discrete frequency siren noise generator.

For these data, the actual and theoretical P_R's were found to be 137.0 and 123.0 db_R respectively. These panels were not directly comparable to the Douglas design charts because they were curved and subjected to static compressive loads.

Data Presentation

A short explanation of the other companies' test results presented in Table 5 follows. These data were gathered from test reports made available by the cooperating companies. The first four columns in the table identify the test and define the specimen. The next two columns present the applied test siren harmonic spectrum pressure level in db's and the test frequency. The seventh and eighth columns indicate the test time for each phase of the test. Where test conditions were varied as the test continued, the time for each condition is indicated. The test time at the test conditions at which failure occurred is indicated separately. The ninth column indicates a random sound pressure level which is equivalent to the test condition. Column ten compares this to the random sound pressure level the design charts would indicate for the test panel.

Table 5

PANEL AND TEST DATA DESCRIPTION OF VARIOUS TESTS FROM OTHER COMPANIES

Case	Material	t (in)	s (in)	Applied Panel SPL Discrete (db)	Resonant Frequency (cps)	Exposure Time to failure (min)	Total (min)	P_R Equivalent (db)	P_R Theoretical for equal life (db)
				GENERAL DYNAMICS					
1	7075 T-6	.060	7	158 158	401 410	31	59	141	130.0
2	7075 T-6	.060	7	158 158	233 244	71	5	143	132.0
3	7075 T-6	.060	7	158 158	415 412	58	32	140.5	131.0
4	7075 T-6	.06	8	164 164 164	316 297 315	18.75	10 10	148.0	131.0
5*	7075 T-6	.06	8	158 158 164 164 170	548 549 551 557 581	36.75	60 62 8 20	145	126.0
6**	7075 T-6	.06	8	158 164 170 170	256 268 280 286	2.3	120.0 3.0 51.5	151.7	129.0

* Average values of 164 db and 581 cps were used to calculate P_R

** Average values of 168 db and 280 cps were used to calculate P_R

Table 5 (cont)

PANEL AND TEST DATA DESCRIPTION OF VARIOUS TESTS FROM OTHER COMPANIES

Case	Material	t (in)	s (in)	Applied Panel SPL Discrete (db)	Resonant Frequency (cps)	Exposure Time to failure (min)	Total (min)	P_R Equivalent (db)	P_R Theoretical for equal life (db)
				GENERAL DYNAMICS (cont)					
7*	7075 T-6	.06	8	158	308		11.5	147.5	129.0
					307		2.5		
					305		4.0		
					308		13.0		
					311		3.0		
					312		6.0		
					315		4.0		
				158	316		41.5		
				164	312		32.0		
				170	323		27.5		
					333		2.0		
					331		2.5		
					353		1.0		
					354		1.5		
				170	355	4.5			

* Average values of 164 db and 316 cps were used to calculate P_R

Table 5 (cont)

PANEL AND TEST DATA DESCRIPTION OF VARIOUS TESTS FROM OTHER COMPANIES

Case	Material	t (in)	s (in)	Applied Panel SPL Discrete (db)	Resonant Frequency (cps)	Exposure Time to failure (min)	Total (min)	P_R Equivalent (db)	P_R Theoretical for equal life (db)
	MARTIN-DENVER*								
8	2014 T-6	.040	14	152	130	10		143.0	123.0
9	7075 T-6	.040	14	151	118	17		140.0	121.0
	BOEING								
10	2024 T-4	.040	8	160	133	180		148.0	121.5
11	2024 T-4	.040	8	160	217**	54		147.0	124.5
12	2024 T-4	.040	8	143	125	420		130.5	120.5
13	2024 T-4	.040	8	150	120	57		139.3	124.5

* These panels were curved and subjected to applied static compressive loads of 37,300 pounds.

** Panel excited above first resonant frequency

SECTION 5   DEVELOPMENT OF DESIGN CHARTS

The information required to produce a design chart for a specific type of structure is an analytical expression for the stress which is caused by a distributed air load; the allowable fatigue stress and life relationship; and the test life or stress and air load causing failure in an actual test. The analytical expression combines certain constants representing such effects as dynamic response, boundary conditions or stress concentration factors which are unknown. Substitution of the test conditions and results into the proper analytical expression permits the evaluation of these unknown constants as a factor which can be used to extend the expression to similar structure with different dimensions.

APPLIED STRESS-ANALYTICAL EXPRESSION

In the following paragraphs expressions will be developed for the stress existing in structure as a function of the structural parameters and the sound pressure loading. This stress, as a function of the sound pressure level, can be expressed in terms of peak values or root mean square values. For discrete frequency excitation peak values are useful. However, noise, in general, is a random phenomena and most easily described for analytical purposes by a distribution of peaks and an RMS value of intensity. The stresses in a structure which is being excited by this random noise phenomena will be random in distribution. This stress distribution is not directly correlated to that of the exciting force due to the effect of the structural system. The net result over a sufficient period of time will, however, permit direct comparisons on the basis of mean values. For these reasons, the stresses defined in this work are expressed as RMS stresses.

The important frequencies for structural consideration have wave lengths such that it is possible to consider the panel to experience loads, from the air pressure fluctuation, that are independent of location on the panel. These loads are functions of time only. Thus, the stress expressions are developed as if the panel is responding to a distributed air load that is equal to the RMS values of the sound pressure.

In the following paragraphs, the analytical expressions will be developed for specific configurations.

Skin and Rib Construction

For the conventional skin and rib or skin and stringer construction subjected to an air load applied normal to the skin, the derivation of an expression for the stress in the skin is presented below with the pertinent limitations and approximations.

The skin is considered to be acting as a series of unit width strips oriented in the direction of the smaller panel dimension. If these strips are assumed to act as separate beams supported with an unknown restraint at the rib or stringer, the expressions for moment and stress can be written as

$$M \propto PS^2 \qquad (4)$$

and

$$\sigma \propto \frac{M}{t^2} \qquad (5)$$

for a rectangular cross section beam of unit width.

Substituting

$$\sigma = \frac{K \; PS^2}{t^2} \qquad \text{or} \qquad \sigma \propto \frac{PS^2}{t^2} \qquad (6)$$

The constant (K) is introduced into the formula to represent the various numerical constants which are suppressed and the various factors previously mentioned, the effect of which will be evaluated through the introduction of the test data.

Skin and Rib with a Doubler at the Rib

This configuration is the same as that just described with a finger doubler added between the rib and skin such that the doubler further reduces the shorter panel dimension and the fingers act to produce a discontinuous or soft edge.

52

The parameters which enter the stress expression for this configuration are identical to those for the previously considered configuration and the variation between the two only enters into the design data through the test results.

Rib

The ribs proved, in test, to be most critical in the bend radius of the flange. The expressions for the rib stress are a function of the load the skin strip transfers to the rib and are therefore similar to the skin stress expressions. One factor entering the rib moment expression is the rib-flange width. This dimension varies only with rib thickness for good design practice and therefore is evaluated through the test results.

Then, the stress in the rib is expressed as:

$$\sigma \propto \frac{PS}{t_r^2} \tag{7}$$

Edge Attachments

The proper edge attachment can be a critical design consideration for panels of the types presented in the preceding paragraphs. If the attachment spacing is too close, panel strength is reduced by the excess material removed or if the spacing is too great, the attachments do not obtain the best load distribution to the skin and portions of the skin are permitted to work below their capability.

The required attachment is developed on the basis of utilizing the full potential of the skin panels. The development here is slightly different from that used elsewhere in this report. This is because the attachment limitation is not based directly on the design sound pressure level but is instead related to the SPL only through the panel which controls the attachment limits. These relationships are established below:

Allowable rivet load is proportional to d^2

Applied load per inch is proportional to PS

ASD-TDR-63-820

and

$$A \propto \frac{d^2}{PS} \tag{8}$$

To express the attachment spacing in terms of the optimum structural parameters, consider the maximum of the relationship previously developed for the skin-rib structures

$$\sigma_{max} \propto \frac{P_{max}S^2}{t^2} \tag{9}$$

Where σ_{max} is constant with a given material and a fixed desired life, the maximum permissible pressure for a panel is

$$P_{max} \propto \frac{t^2}{S^2} \tag{10}$$

Substituting this for "P" in the attachment spacing as above results in the following expression:

$$A \propto \frac{d^2S}{t^2} \tag{11}$$

Ribs with Lightening Holes

The cutout lightening holes used for ribs have many designs and modifications each of which requires a somewhat different approach to obtain the neccessary design data. Only one type of cutout was investigated in this study and the design data presented is only strictly applicable to this design. The general method, however, is demonstrated and can be used with available test data for the required configurations as a means of extending that design data.

In arriving at the stress expression for the rib with a cutout that portion of the rib between the cutout proper and the skin is considered to act like a beam loaded by the air loading on the skin and transferring its load fore and aft to the full depth rib.

In testing, the failures in the ribs were at the ends of the cutout area in the bend radius of the stiffening element. This failure was caused by an out of plane reaction to the "rib-beam" moment which resulted in bending moments

normal to the rib web and failure at the concentration point. The moment
acting on the "rib-beam" may be expressed as:

$$M \propto PSL^2 \tag{12}$$

Which derives directly from the standard expression for a beam with a distributed loading. The stress in the "rib-beam" is

$$\sigma \propto \frac{M}{Z} \qquad \propto \frac{PSL^2}{Z} \tag{13}$$

where Z, the section modulus is primarily a function of "h" and "t" .

The force (F) in the flange of the "rib-beam" is proportional to the product
of the flange area and the flange force or

$$F \propto te \frac{PSL^2}{Z} \tag{14}$$

Where the flange area is considered to be proportional to the flange width
or eccentricity and the rib web thickness.

The moment acting on the rib web is proportional to the flange force and the
distance of its application from the rib web, the eccentricity. This moment
is reacted by a portion of the rib along the cutout-end, the length of which
is a function of the cutout radius. Thus, the expression for the stress in
the web can be considered as

$$\sigma \propto \frac{F\,e}{t^2 R} \tag{15}$$

or substituting the previous expression for F

$$\sigma \propto \frac{PSL^2 e^2}{R}\ f(h,t,) \tag{16}$$

The best fit to the test results is obtained with negative exponents of approximately 2.5 and 1.5 for "h" and "t" respectively.

Beaded Inner Skin Panels

Various designs of beaded-bonded panels were tested and the results presented
here are for the one found to be most effective. Beads with smooth ends were
tested early in the program. These contained a built-in stress concentration

at the point of greatly reduced moment of inertia, such that the failures always occurred at this point. The double-ended bead was developed to alleviate this condition. Panels of this type will usually fail in the outer skin, the bead crown at midspan or the unsupported overhang at the panel edge.

The bead acts like a beam and the parametric relationships for the midspan failure are similar to those developed for the plain panel. The bead and its associated width of skin is treated as a beam loaded by the sound pressure and supported at the panel edge adjacent to the bead end. The moment expressions for this configuration which has a running load equal to PW pounds per inch is

$$M \propto PWL^2 \tag{17}$$

The section modulus for the bead can be shown to be

$$Z_b \propto \frac{Wb^2 t}{b} \sim Wbt \tag{18}$$

and the bead stress is

$$\sigma \propto \frac{PL^2}{bt} \tag{19}$$

The failing stress at the panel edge is not clearly definable analytically. It is, of course, proportional to the load transferred from the bead to the support, ie., bead width and length, and the distribution of the load at the bead end. However, this distribution at the end is also dependent on the bead dimension and requires that the final relationships be developed in compliance with the test results. The edge stress expression is used in the form

$$\sigma_E \propto f \frac{(W,L,)P}{t_E^2} \tag{20}$$

56

Honeycomb Panels

The stress expression for honeycomb panels is much the same as that for the simple panel and is developed using an assumed one inch wide strip. The honeycomb panel however usually has proportions which require that the effect of the interaction of the end and side supports must be considered. This factor (C) for aspect ratio correction is applied directly to the derived stress expression. For these panels the moment on the strips is assumed reacted as concentrated loads in the faces with the core carrying shear loads only. This results in the minimum thickness face having the critical stress. The critical panel dimesnion for bending is the shorter length. For a one inch wide strip, the stress expression is as follows:

$$\sigma \propto \frac{PS^2C}{nt_{min}} \tag{21}$$

As was previously mentioned for the beaded panel, the edge condition stress is not clearly definable. The panel geometry, aspect ratio factor and air load enter into the expression and it is used as

$$q_E \propto \frac{f(S)PC}{t_e^2} \tag{22}$$

Corrugation Stiffened Panels

The corrugation stiffened panels experience failure at two locations: The corrugation crown and the skin to spar cap attach line. The analytical expressions for these two locations are developed in the following paragraphs.

For a corrugation peak to peak length (l_1) and an unsupported span (S) in the direction of the corrugations, the bending moment acting on a single corrugation and related skin under a distributed pressure (P) is:

$$M \propto Pl_1S^2 \tag{23}$$

For the optimum condition l_2 equals $2(l_1)$, the section modulus Z is

$$Z \propto l_1^2t_1B \tag{24}$$

Where B is a factor to account for the thickness ratio t_2/t_1

This expression is developed in Appendix I as are the optimum design conditions. Combining these two produces the stress expression

$$\sigma \propto \frac{PS^2}{1t_1 R} \tag{25}$$

The attachment of the skin to the spar cap load for a minimum unsupported length consistent with good design practice is a function only of the span (S), the pressure (P) and the skin thickness (t). This analysis is similar to the edge analysis for the beaded inner skin or for the honeycomb panels considering a unit width of skin and minimum unsupported skin

$$\sigma \propto \frac{PC}{t_1} \tag{26}$$

Skin and Stringers

The skin and stringer panels are from the general analytical view of the same form as the skin and rib. The material and the fabrication techniques are different but this does not affect the analytical expression as it is developed for this study. The one factor which does change and which is added, due to the skin and stringer geometry, is the aspect ratio correction as indicated for the honeycomb panels. With this addition, the stress expression for the skin and stringers is

$$\sigma \propto C \frac{PS^2}{t^2} \tag{27}$$

ALLOWABLE STRESSES

The above stresses, which are computed as a function of, or are attributable to, an external exciting force, are in normal design designated as "applied" stresses. For design purposes these stresses must be compared to an "allowable" stress. This allowable stress can be either an ultimate stress which should not be exceeded or, for fatigue, it can be a stress which is dependent on the number of load applications and will vary with the desired life. For usual long life, lower-stress design, the latter consideration is the only one of importance. However, for short life design or for accelerated test procedures, the possibility of exceeding the ultimate stress with one of the peak applied

stresses must be considered.

The allowable fatigue stresses, as described above, are to be compared to applied stresses which result from noise and are random in nature and thus these allowable stresses must also be random. A method to obtain allowable life data or number of load applications for a random distribution of stresses is presented later in this section. These data then express the allowable random stress as a function of the life.

APPLICATION OF TEST DATA

If now the applied stresses and the allowable stresses are equated, a relationship is obtained for the life of the structure under consideration in terms of the structural parameters and the sound pressure level. Were it possible to exactly define the applied stress in an analytical manner, the relationship between sound pressure, structural parameters and life would be complete, analytically. Due to practical limitations this relationship is completed through the use of test data. These test data supply the missing factors in the stress expressions and permit generalization of the analytical relationships.

The test specimens, procedure, equipment and results for the structural types presented in this study are presented in detail in Section 3 and Section 4.

Discrete Frequency Conversion

Portions of the testing were accomplished using a random noise generator. The test results obtained thus were directly applicable as coordinating data. Other tests were conducted using a discrete frequency siren as a means of exciting the structure. The results of these tests could not be used directly but required a conversion to equivalent random data to be applicable. The expression used for this purpose is developed in the following paragraphs.

59

DEVELOPMENT OF RANDOM STRESS - LIFE DATA

In measuring the allowable life of structure which is subject to a random loading such as that produced by acoustic excitation, it is necessary to have random stress-life data. This information could be obtained directly by the same method as is employed in obtaining standard data but substituting a random loading. This is a costly and time consuming process however, and if possible, should be avoided. A method of obtaining random data with sufficient accuracy from constant amplitude reverse bending data is indicated in the following paragraphs.

The two assumptions with which the data are derived are: 1) that the probability of obtaining a certain peak value of stress for each cycle follows a Rayleigh distribution, where the most probable stress is the root mean square stress; and 2) that the linear cumulative damage theory of fatigue is valid.

A typical response for a single degree of freedom system subjected to random loading is indicated in the sketch, Figure 24. It has a constant frequency with varying amplitude and a Rayleigh distribution of peaks is assumed.
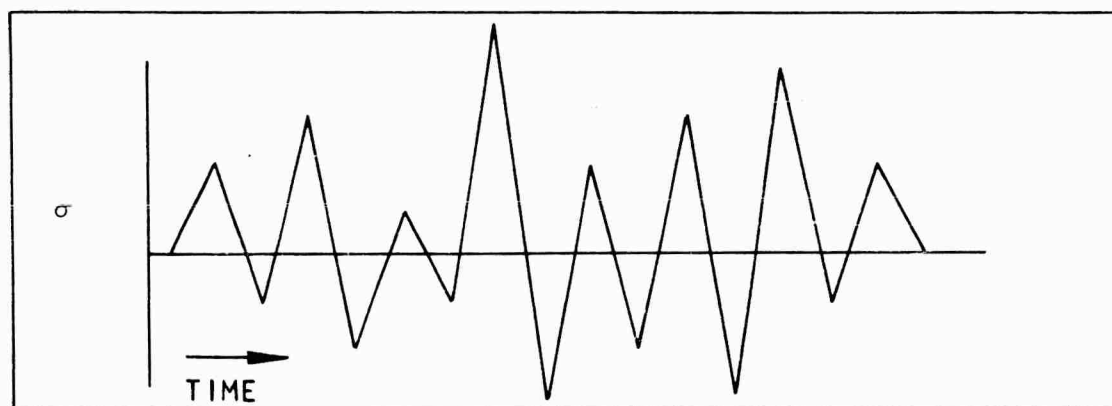

FIGURE 24   SKETCH RANDOM RESPONSE

An example of a Rayleigh probability curve is shown in Figure 25. This figure also presents terms which will aid in the following development.

$$P_{(x)} = x\,e^{-\left(\frac{x^2}{2}\right)}$$

$$dA = P(x)\,dx = \frac{n_x}{N_R} \tag{28}$$

$$n_x = N_R\,P(x)\,dx \tag{29}$$

REF (1)

$P_{(x)}$

dA

dx

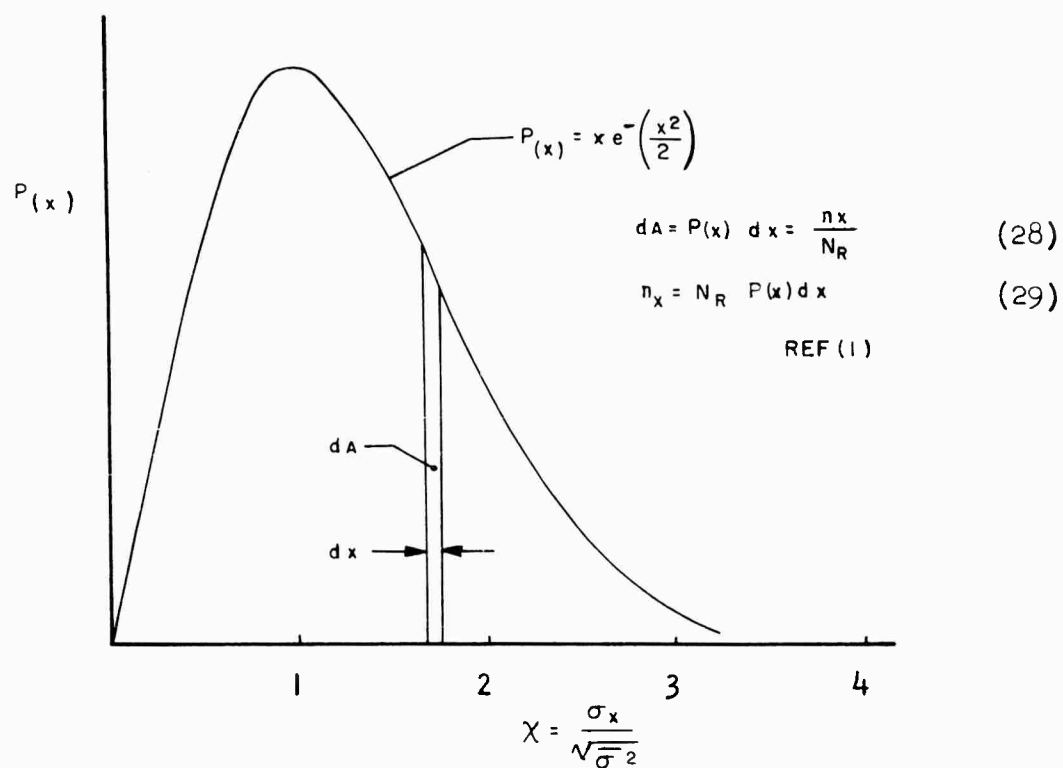$$\chi = \frac{\sigma_x}{\sqrt{\overline{\sigma^2}}}$$

FIGURE 25 RAYLEIGH STRESS DISTRIBUTION

As the area under the probability curve is equal to unity and also represents the total number of cycles to failure, an element of area under the curve, dA, may be thought of as representing a proportionate number of the total cycles to failure.

$$dA = \frac{n_x}{N_R} \tag{30}$$

n_x = the number of cycles at a stress σ_x

N_R = the total number of cycles to failure with random loading.

From the probability curve, Figure 25, it is obvious that

$$dA = P(x)\, dx \tag{31}$$

Substituting and rearranging

$$n_x = N_R\, P(x)\, dx \tag{32}$$

From the linear accumulative damage concept the damage at failure is represented as

$$D = 1 = \sum_{1}^{\infty} \frac{n_x}{N_x} \tag{33}$$

Where N_x is the number of cycles to failure at the stress σ_x.

Substituting from the previous expression and bringing the constant N_R out from under the integral sign results in the following:

$$1 = N_R \int_0^{\infty} \frac{P(x)\, dx}{N_x} \quad \text{or} \quad N_R = \left[\int_0^{\infty} \frac{P(x)dx}{N_x} \right]^{-1} \tag{34}$$

Evaluation of this integral results in the random life for only one value of the mean stress and must be repeated several times to arrive at a random Stress-Life curve.

Integration of this expression by analytical methods is usually impossible, therefore, numerical methods of solution are employed. This may be accomplished by hand by plotting the values $P(x)/N_x$ and solving graphically. An example of such a procedure is presented in Table 6 and Figure 26 to clarify the technique.

Table 6

SAMPLE COMPUTATION-RELATIVE DAMAGE

$$\sqrt{\sigma^2} = 20,000 \text{ psi}$$

x	σ_m	N_x	$P(x)$	$\dfrac{P(x)}{N_x}$
2.95	59,000	2.2×10^6	3.80×10^{-2}	1.72×10^{-8}
2.9	58,000	5.5×10^6	4.33×10^{-2}	$.787 \times 10^{-8}$
2.8	56,000	3.3×10^7	5.55×10^{-2}	1.68×10^{-9}
3.0	60,000	10^6	3.33×10^{-2}	3.33×10^{-8}
3.2	64,000	2.2×10^5	1.91×10^{-2}	8.68×10^{-8}
3.4	68,000	1.4×10^5	1.05×10^{-2}	7.52×10^{-8}
3.6	72,000	10^5	5.52×10^{-3}	5.52×10^{-8}
3.8	76,000	7.3×10^4	2.78×10^{-3}	3.82×10^{-8}
4.0	80,000	5.9×10^4	1.34×10^{-3}	2.27×10^{-8}
4.2	84,000	4.8×10^4	6.21×10^{-4}	1.29×10^{-8}
4.4	88,000	4.0×10^4	2.75×10^{-4}	$.688 \times 10^{-8}$
4.6	92,000	3.2×10^4	1.17×10^{-4}	$.366 \times 10^{-8}$

$$\sqrt{\overline{\sigma^2}} = 20,000 \text{ PSI}$$

$$N_R = \cfrac{1}{\displaystyle\int_0^\infty \frac{P(x)dx}{Nx}}$$

$$N_R = 1.41 \times 10^4 \text{ CYCLES}$$

$$\chi = \frac{\sigma}{\sqrt{\overline{\sigma^2}}}$$

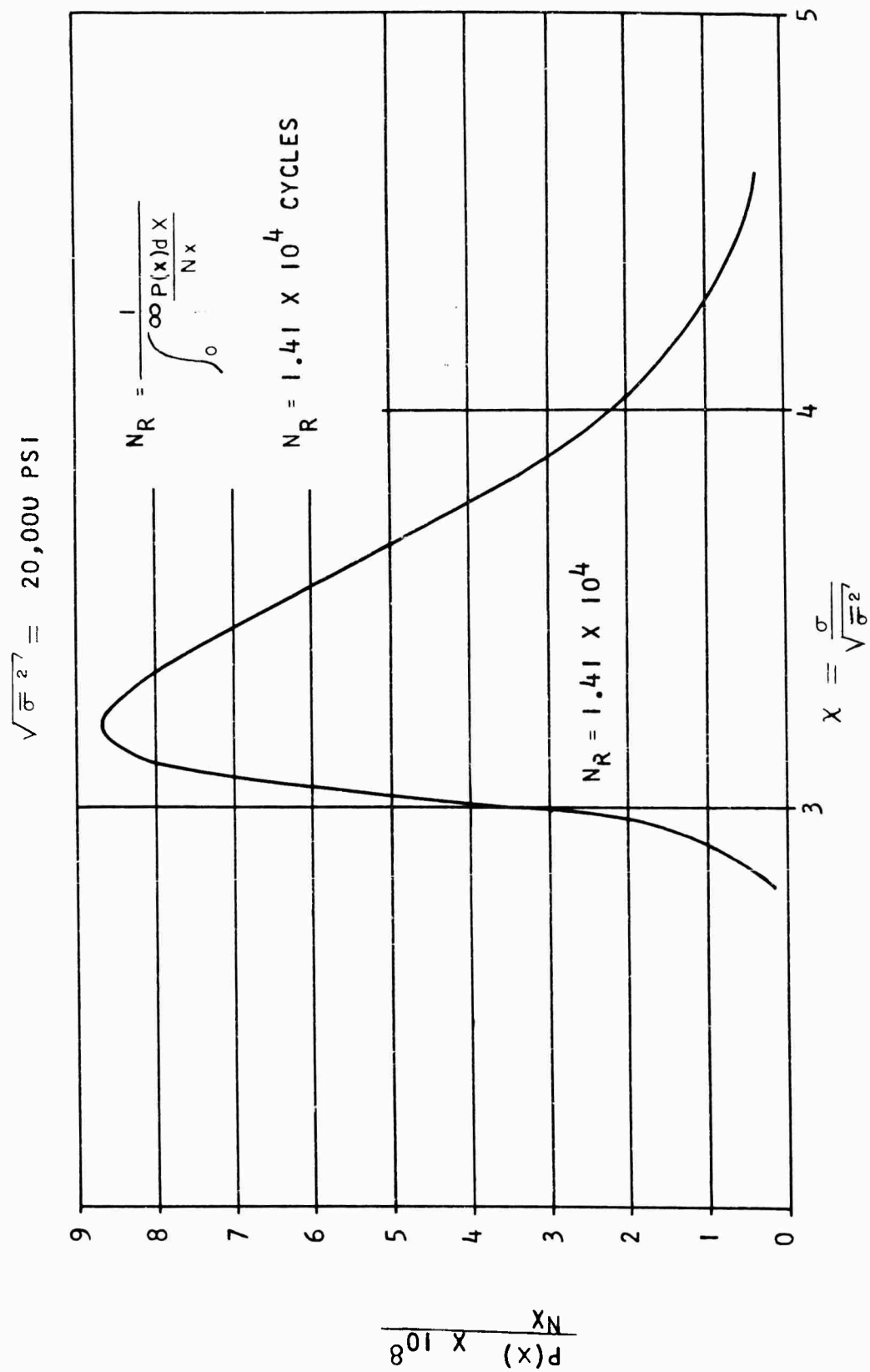$$N_R = 1.41 \times 10^4$$

$$\frac{P(X)}{N_X} \times 10^8$$

FIGURE 26 RELATIVE DAMAGE VS STRESS RATIO

The sample computation in Table 6 leads to evaluation of the integral of Equation 34 for one value of the RMS stress, 20,000 psi. Using arbitrarily chosen values of x, the ratio of $\sigma_m / \sqrt{\sigma^2}$, corresponding values of σ_m and P(x) are computed (second and fourth columns). The constant amplitude fatigue life, N_x, (third column) corresponding to the mean stress is obtained from reverse bending S-N data as in Figure 27. The relative damage $P(x)/N_x$ (fifth column) is computed and is plotted as shown in Figure 26.

The value of the integral in Equation 34 is represented by the area under the curve in Figure 26. This area is determined in an appropriate manner and the resultant value of the integral substituted into Equation 34 to obtain the value of N_R for the single RMS stress. Repetition of this procedure will develop the desired random S-N data from regular S-N data. The value of σ_m corresponding to the peak of the relative damage curve of Figure 26 is known as the peak damage stress.

A computer program exists to accomplish the preceding analysis and was used to randomize the Stress-Life data presented herein for the titanium 6Al-4V, Figure 27. A random Stress-Life curve for aluminum is presented in Figure 28. The computer print-out for this program is presented in Table 7.

Constant amplitude reverse bending S-N data is input to the computer as discrete points. The computer then simulates continuous data through these points with a series of parabolas. Sample input data and the smoothed data as printed out are presented in Table 7 (first through third columns). The RMS stress values of interest are shown (fourth column) with the corresponding random life and peak damage stresses (fifth and sixth columns). These result from a machine solution of the procedure presented in Table 6 and Figure 26. The remaining columns (seventh and eighth) are not essential data but are of interest. These data indicate, by a ratio of ordinates, the portion of the relative damage curve which is used in the solution.
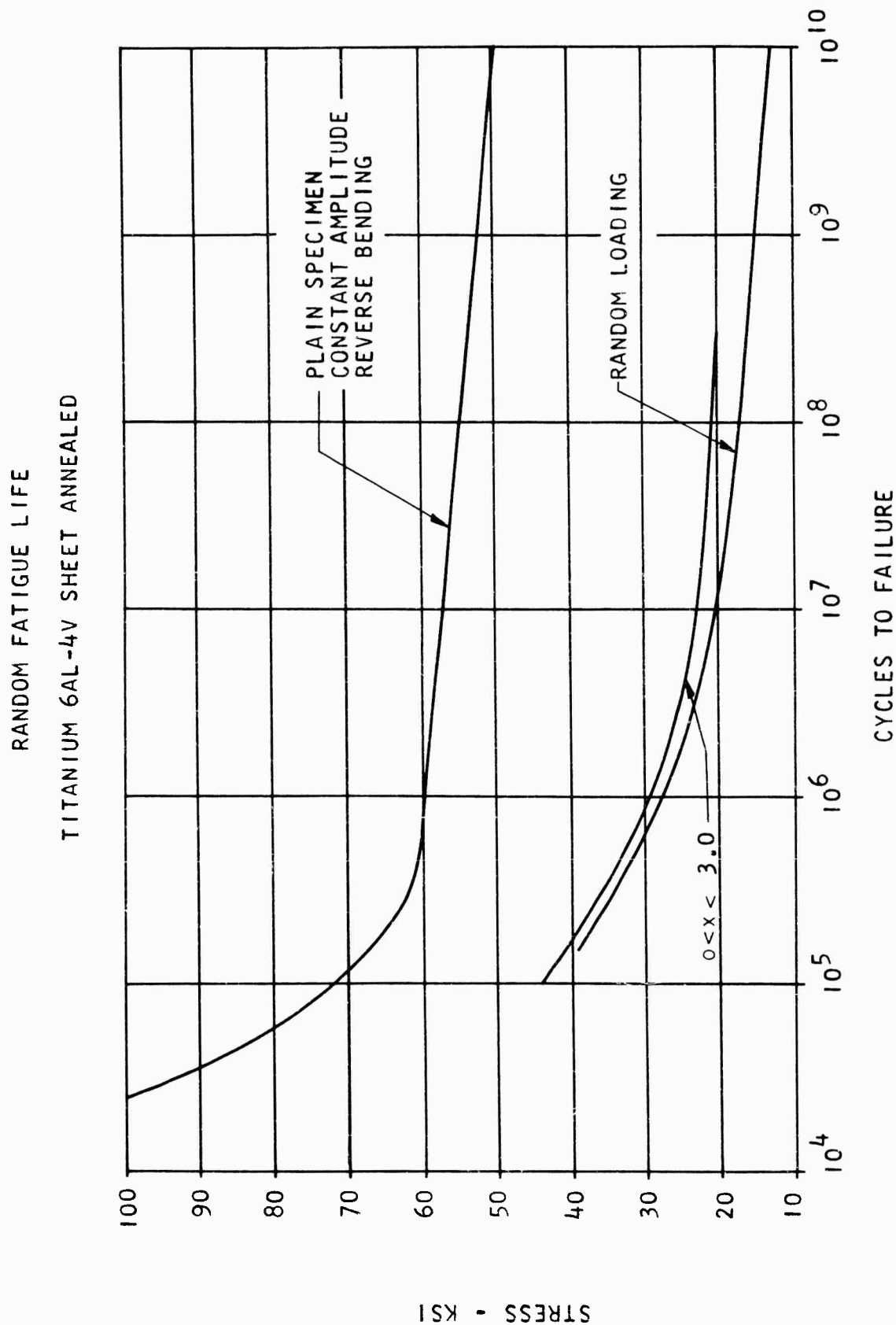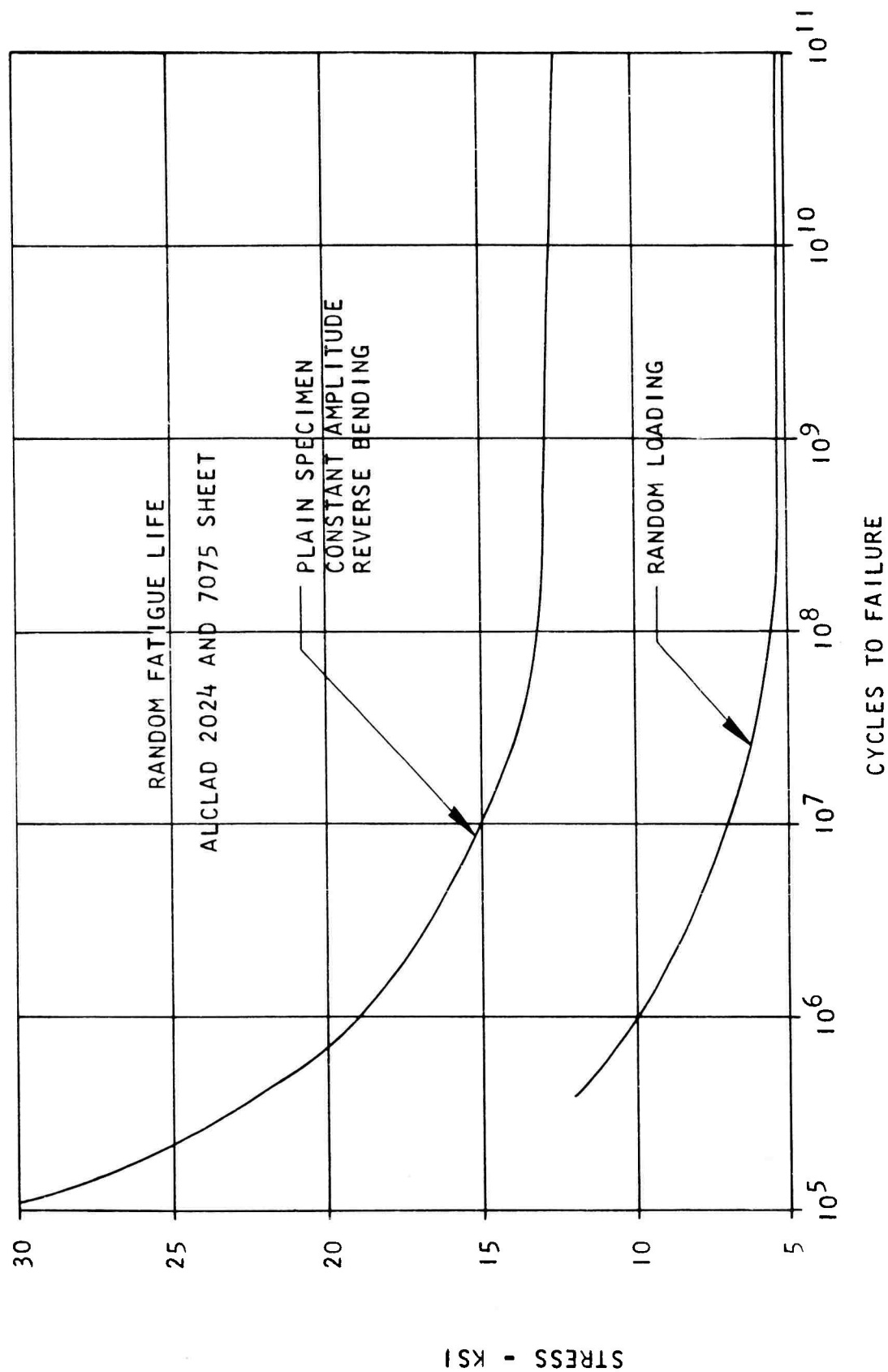
RANDOM FATIGUE LIFE

TITANIUM 6AL-4V SHEET ANNEALED

PLAIN SPECIMEN
CONSTANT AMPLITUDE
REVERSE BENDING

RANDOM LOADING

$o < x < 3.0$

STRESS - KSI

CYCLES TO FAILURE

FIGURE 27 RANDOM FATIGUE LIFE TITANIUM 6 AL - 4V SHEET ANNEALED

FIGURE 28 RANDOM FATIGUE LIFE ALCLAD 2024 AND 7075 SHEET

MINER CUMULATIVE FATIGUE DAMAGE THEORY
RAYLEIGH PROBABILITY DISTRIBUTION OF STRESS PEAKS

S-N INPUT

	INPUT STRESS	INPUT CYCLES/1000	SMOOTHED CYCLES/1000
1	55000.	100000.	99531.
2	60000.	1000.	810.
3	60500.	500.	622.
4	61000.	400.	521.
5	62000.	300.	373.
6	64000.	200.	231.
7	66300.	150.	155.
8	71500.	100.	94.
9	73200.	90.	86.
10	75000.	80.	79.
11	77300.	70.	70.
12	80100.	60.	60.
13	84000.	50.	50.
14	86000.	45.	45.
15	88200.	40.	40.
16	91300.	35.	35.
17	95100.	30.	30.
18	99200.	25.	25.

DELTA X = 0.015
DATA SMOOTHED 4 TIMES
UPPER 10 PRECENT OF CURVE USED TO FIND PEAK DAMAGE STRESS

TABLE 7 (CONT'D)

RANDOM S'N CURVE   COMPUTER PRINTOUT   ANALYSIS   2

MINER CUMULATIVE FATIGUE DAMAGE THEORY
RAYLEIGH PROBABILITY DISTRIBUTION OF STRESS PEAKS

MEAN FATIGUE LIFE

	RMS	NR/1000	SPD	Y1/YMAX	YN/YMAX
1	19000.	7300242.	65420.	0.00855	0.00491
2	20000.	351897.	66026.	0.00720	0.01037
3	21000.	60063.	66648.	0.00612	0.01944
4	22000.	21522.	67271.	0.00528	0.03332
5	23000.	10209.	67856.	0.00464	0.05329
6	24000.	5784.	68416.	0.00408	0.07943
7	25000.	3695.	68908.	0.00367	0.11342
8	26000.	2556.	69471.	0.00330	0.15409
9	27000.	1836.	70007.	0.00299	0.20144
10	28000.	1398.	70564.	0.00273	0.25540
11	29000.	1085.	71057.	0.00252	0.31646
12	30000.	857.	71763.	0.00234	0.38200
13	31000.	694.	72569.	0.00218	0.45271
14	32000.	568.	73459.	0.00203	0.52573
15	33000.	475.	74881.	0.00189	0.59783
16	34000.	400.	76380.	0.00177	0.66969
17	35000.	340.	79011.	0.00165	0.73724
18	36000.	293.	81133.	0.00153	0.79754
19	37000.	253.	83799.	0.00142	0.84751
20	38000.	222.	86129.	0.00131	0.89032
21	39000.	194.	88357.	0.00121	0.92551

ASD-TDR-63-820

CONVERSION OF DISCRETE TEST DATA TO EQUIVALENT RANDOM

The portion of the testing which was conducted in the discrete frequency siren facility produced data which required conversion to an equivalent random data for use in the design charts. This conversion relationship is developed below. Expressions are written for both the discretely and the randomly excited structural systems and combined to produce the required conversion equation.

Random Excitation

These systems are considered to be linear and excited in a single mode. Within these limitations Miles, Ref. 2, has presented the following equation for the RMS stress. In terms of this report

$$\sqrt{\sigma^2} = K\sigma_{o_i} \left[\int P_{R_f} A_{i_f} \, df \right]^{1/2} \qquad (35)$$

If the structure is considered to be essentially a single degree of freedom systems or to have principal modes well separated, this equation may be rewritten as

$$\sqrt{\sigma^2} = K\sigma_o \, P_R \left[\frac{\Pi A f}{2} \right]^{1/2} = K\sigma_o \, P_R \left[\frac{\Pi f}{4 \delta} \right]^{1/2} \qquad (36)$$

Discrete Excitation

The equation for the stress due to discrete frequency loading follows from the definition of the term "σ_o". This general stress per unit pressure is equal to the resultant dynamic stress divided by the applied pressure and the dynamic amplification factor or

$$\sigma_o = \frac{\sigma_H}{P_H A} \qquad (37)$$

This can be rewritten as

$$\sigma_H = K\sigma_o \, P_H A = K\sigma_o \, \frac{P_H}{2\delta} \qquad (38)$$

*Where the "K" is added to account for stress concentrations or other constants common to both expressions.

70

Combined Equations

If it is assumed that the similar factors in the random and discrete equations are truly similar (ie., the response to a single load of a random system is the same as the response to a single load of a discrete system within the limits of the load intensity) they can be combined as follows:

$$\frac{\sqrt{\sigma^2}}{\sigma_H} = \frac{P_R}{P_H} \, (\Pi\delta f)^{1/2} \tag{39}$$

By the use of this relationship and the appropriate fatigue data, siren test data was converted to equivalent random data.

Linearity Correction Factor

In using the discrete frequency test data an additional correction was made for linearity. This effect arises from the fact that the tests were conducted at high level to reduce the test time to a practical period. This factor was applied to the indicated test stress.

This factor consists of the quotient of two ratios. The numerator is a ratio of the test stress to the applied pressure at approximately the expected design level and the denominator is the ratio of the test stress to the applied pressure at the test failure condition. This factor applied to the test failure stress predicts a stress which would be indicated if the test structure response were linear throughout the test range. A clarifying sketch of this condition is presented in Figure 29.
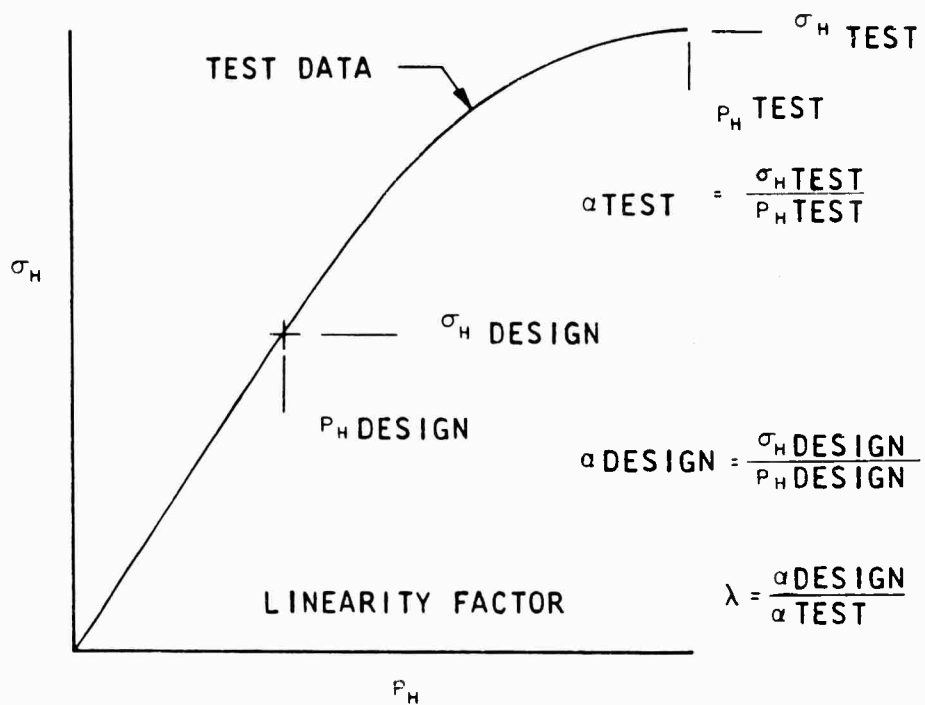
FIGURE 29 SKETCH OF LINEARITY DATA

SECTION 6   DESIGN NOMOGRAPHS

The relationship between the various factors is most usefully presented for design purposes in the form of a nomograph. Nomographs for the various structural configurations are presented on the following pages. In these nomographs, the sound pressure level is indicated in decibels/cps (Ref: .0002 dynes/cm^2), the panel dimensions in inches and the life in number of cycles. The stress-life curve is presented for only a single material.

Sketches of the structure and the design nomographs are presented in Figures 30 through 47.

For materials other than those shown in the design nomograph, the following procedure can be used to substitute the desired new material. Random S-N data are presented for several materials in Figure 48. This figure indicates a relative strength, expressed in decibels, for various materials and random life values. The difference in relative strength of the new material is determined for various lengths of life. These points are then plotted against the "relative strength" scale of the design nomograph to locate the new curve.

As an alternate method for quick single point comparison, the allowable db$_R$ can be determined for the material in the design nomograph and the relative strength difference at the appropriate life added to the answer.
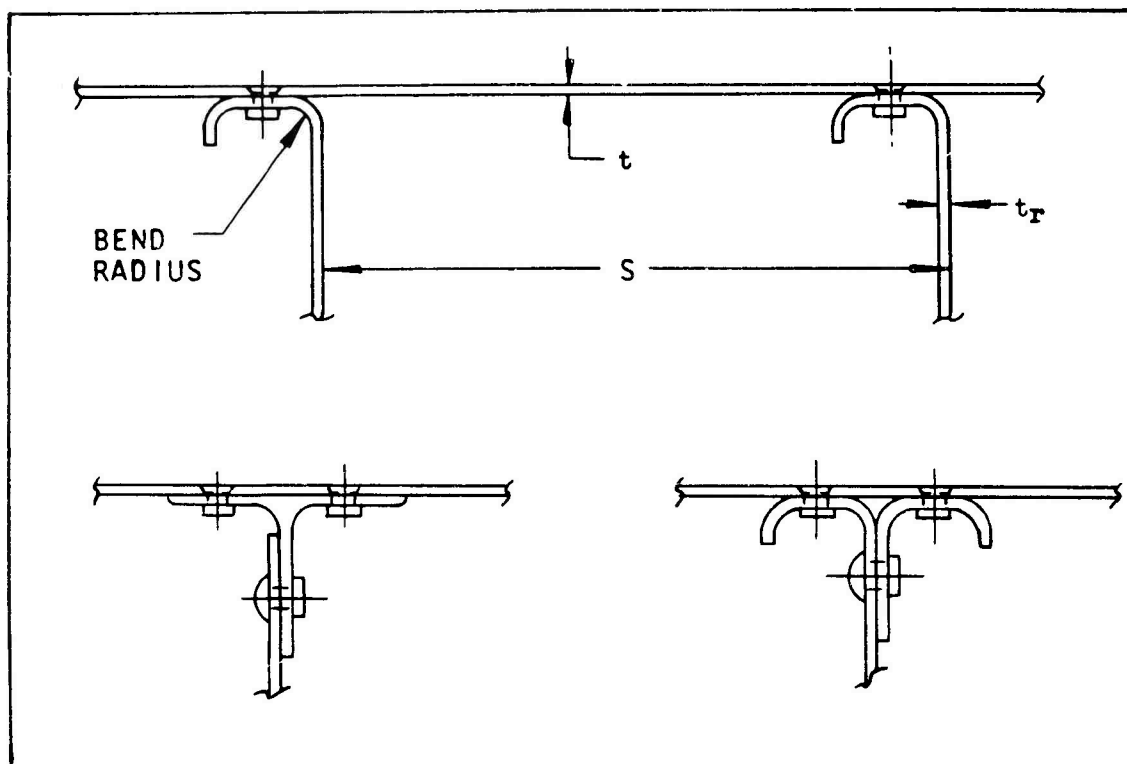
FIGURE 30 SKETCH SKIN AND RIB CONSTRUCTION

Skin and Rib Construction

This structural configuration is critical at either the bend radius of
the rib, in the skin at the rivet row on the side next to the heel of
the rib, or the skin to rib attachments may fail in tension. Improved
rib cap designs are shown and can be used when rib gage becomes excessive.

Example

A skin on rib structure of 2024-T3 material is required to withstand an
estimated spectrum level, db_R, of 118-1/2 db at the resonance frequency
of the structure. The design life is 1000 hours at this load or $N_R \simeq 10^9$
cycles. Following through the chart as indicated by the arrows to an
assumed rib spacing, S=4, a skin gage, t=.025 and a rib gage, t_r, of .038,
is found, (use t_r=.040). The approximate lowest resonance frequency is
found to be 250 c/s. At this frequency the spectrum level plot is checked
for agreement with the assumed spectrum level of db_R= 118-1/2 and a check
is made for agreement of N_R and the assumed value of 10^9 cycles. If
necessary an iteration is made to obtain agreement.
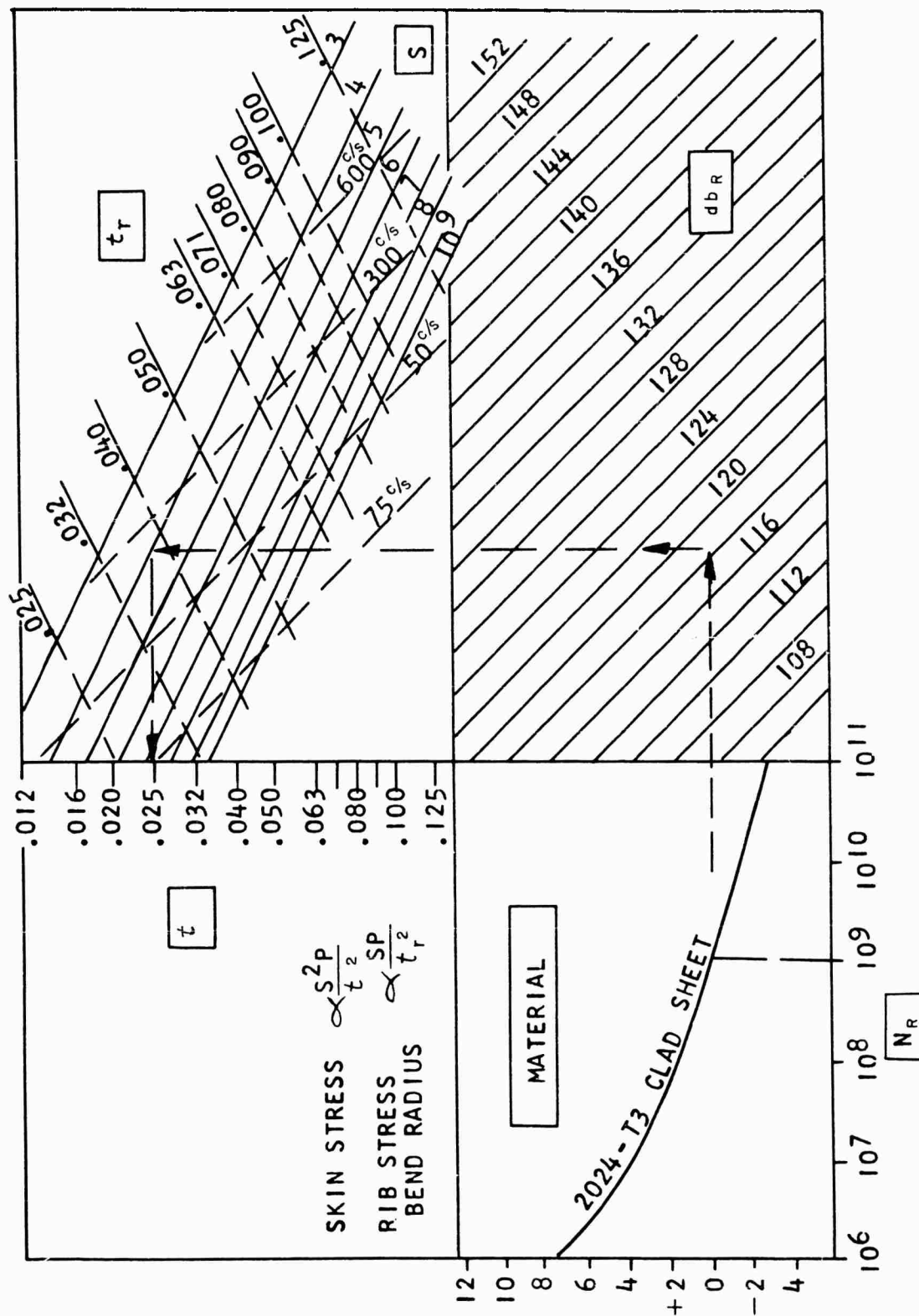
FIGURE 31 DESIGN CHART SKIN AND RIB CONSTRUCTION
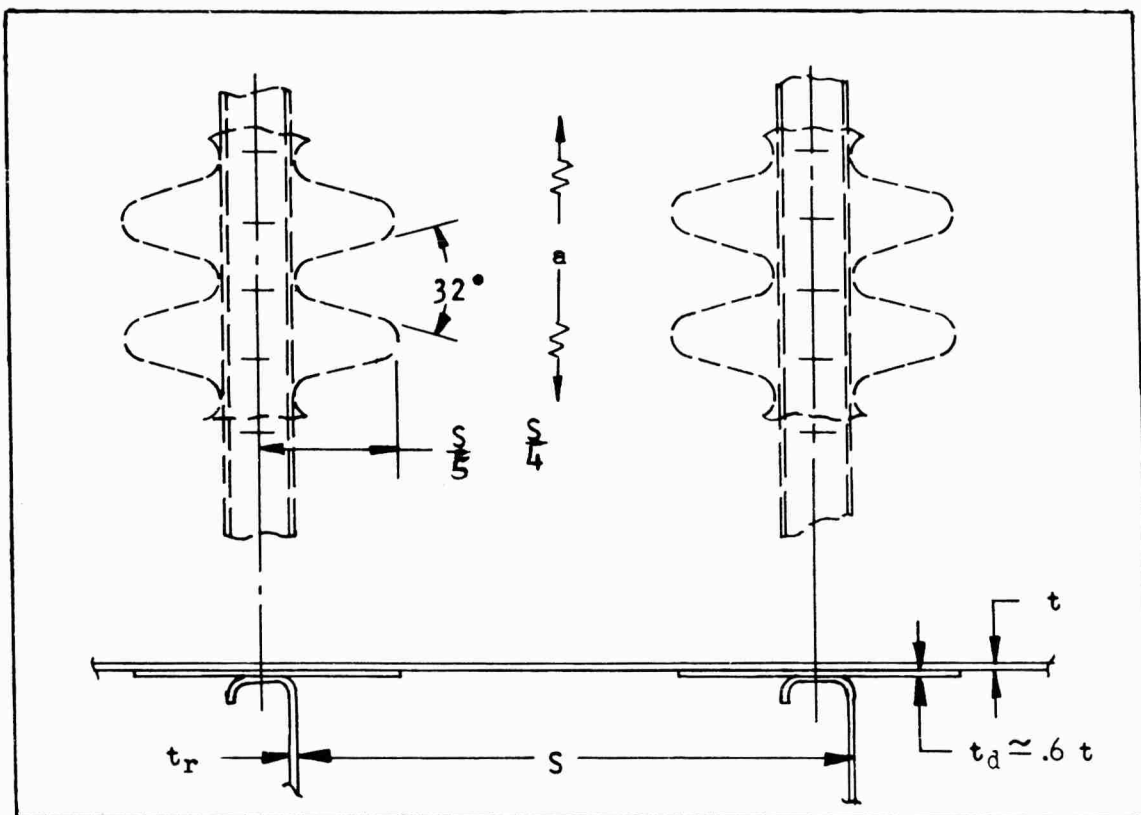
FIGURE 32   SKETCH SKIN AND RIB WITH BONDED DOUBLER

Skin and Rib with Bonded Doubler

The purpose of scalloped bonded doublers is to provide increased strength
at the skin to rib attachment with a minimum increase in weight.   Doublers
are scalloped to effect a stiffness taper and prevent premature cracking
at the edge of the doubler.

Example

A skin, doubler and rib structure of 2024-T3 material is required to withstand
an estimated spectrum level, db_R, of 124 db at the resonance frequency of the
structure.   The design life is 1000 hours at this load or $N_R \simeq 10^9$ cycles.
Following through the chart as indicated by the arrows to an assumed rib
spacing, S = 4-1/4, a skin gage, t = .023, and a rib gage, t_r of .043 is found.
The approximate resonance is 325 c/s.   The assumed values of db_R and N_R are
checked as in the example on page 74.   The value of N_R is found to be slightly
over 10^9 cycles but not enough to affect the results.   Thus, the structure
would be: S = 4-1/4, t = .025, t_d = .6 (.025) = .016, t_r = .050.
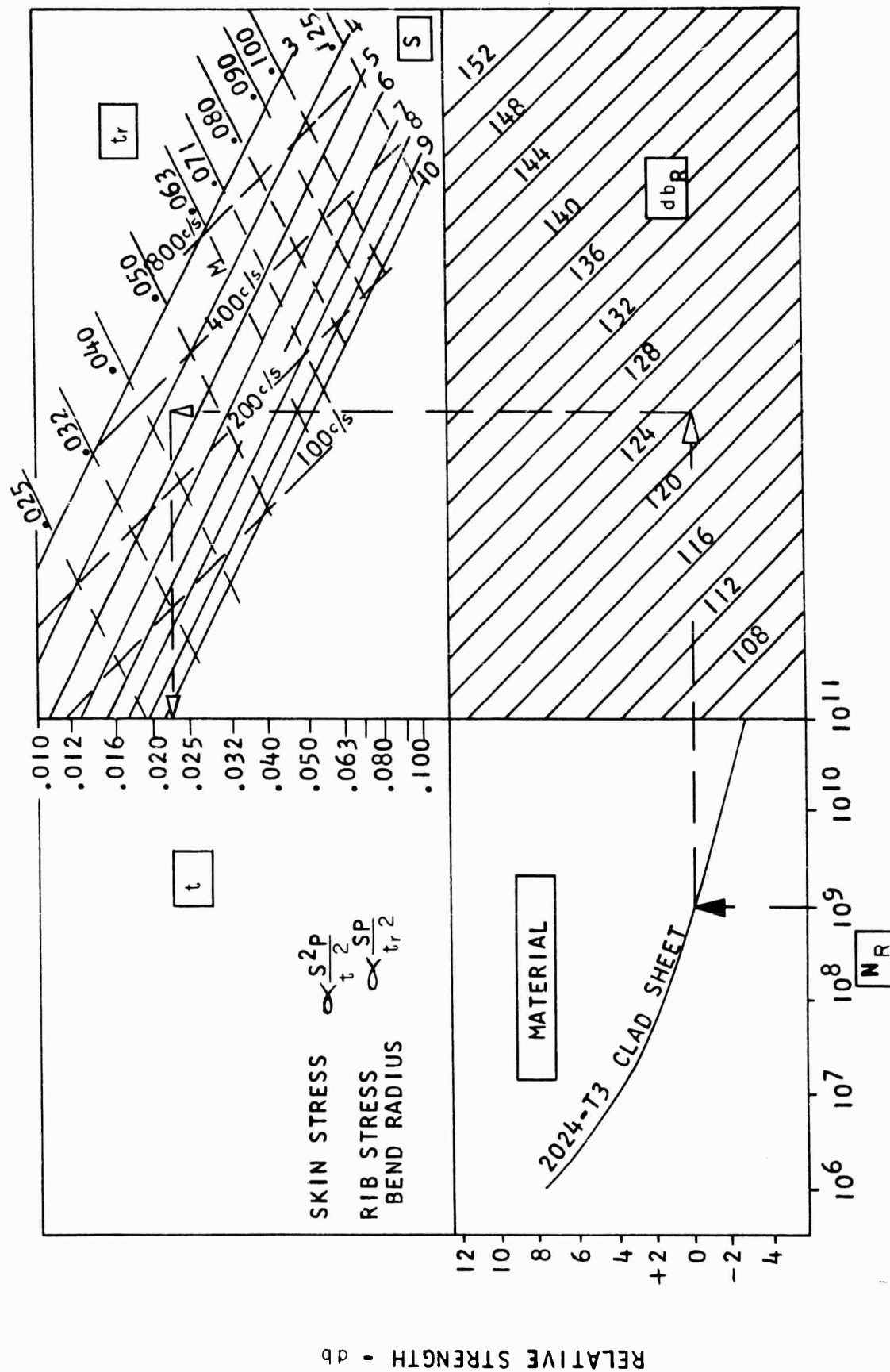
FIGURE 33 DESIGN CHART SKIN AND RIB WITH BONDED DOUBLER
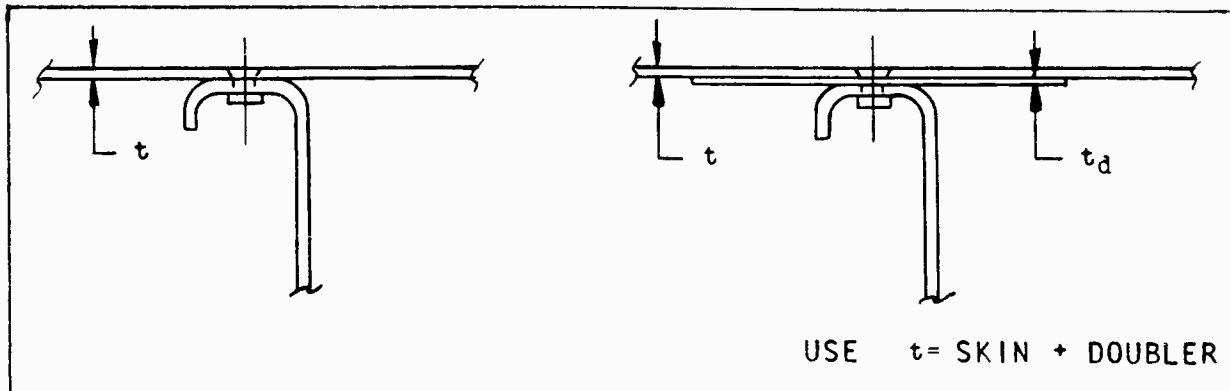
FIGURE 34   SKETCH ATTACHMENTS

USE   t= SKIN + DOUBLER

Attachment Requirements

Skin to rib attachments may be critical in tension if their spacing is large or if they are small in diameter. The chart on the facing page gives the upper limit for attachment spacing for a particular attachment and structural config-uration. Exceeding this limit will result in the attachment being of lower strength than the skin and ribs.

Example

A structure consisting of .063 skin supported by ribs at 5 inch spacing has been selected as satisfactory for acoustic loading. Skin to rib attachments are required to develop full strength of the skin and ribs.

Entering the chart at S=5 and following through to an assumed diameter of 5/32 and AD rivet, a maximum spacing of .75 is found.
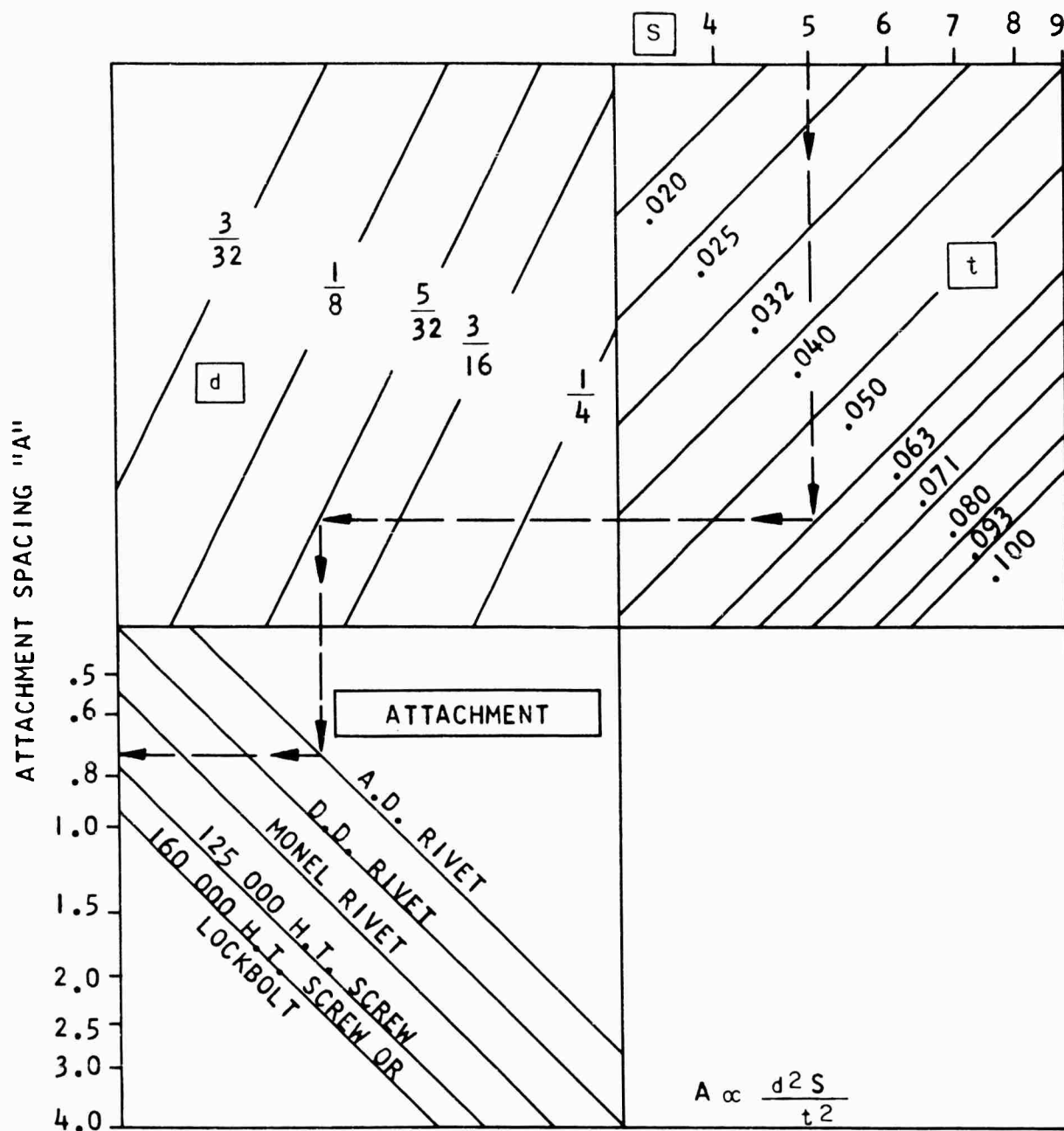
FIGURE 35 DESIGN CHART ATTACHMENTS
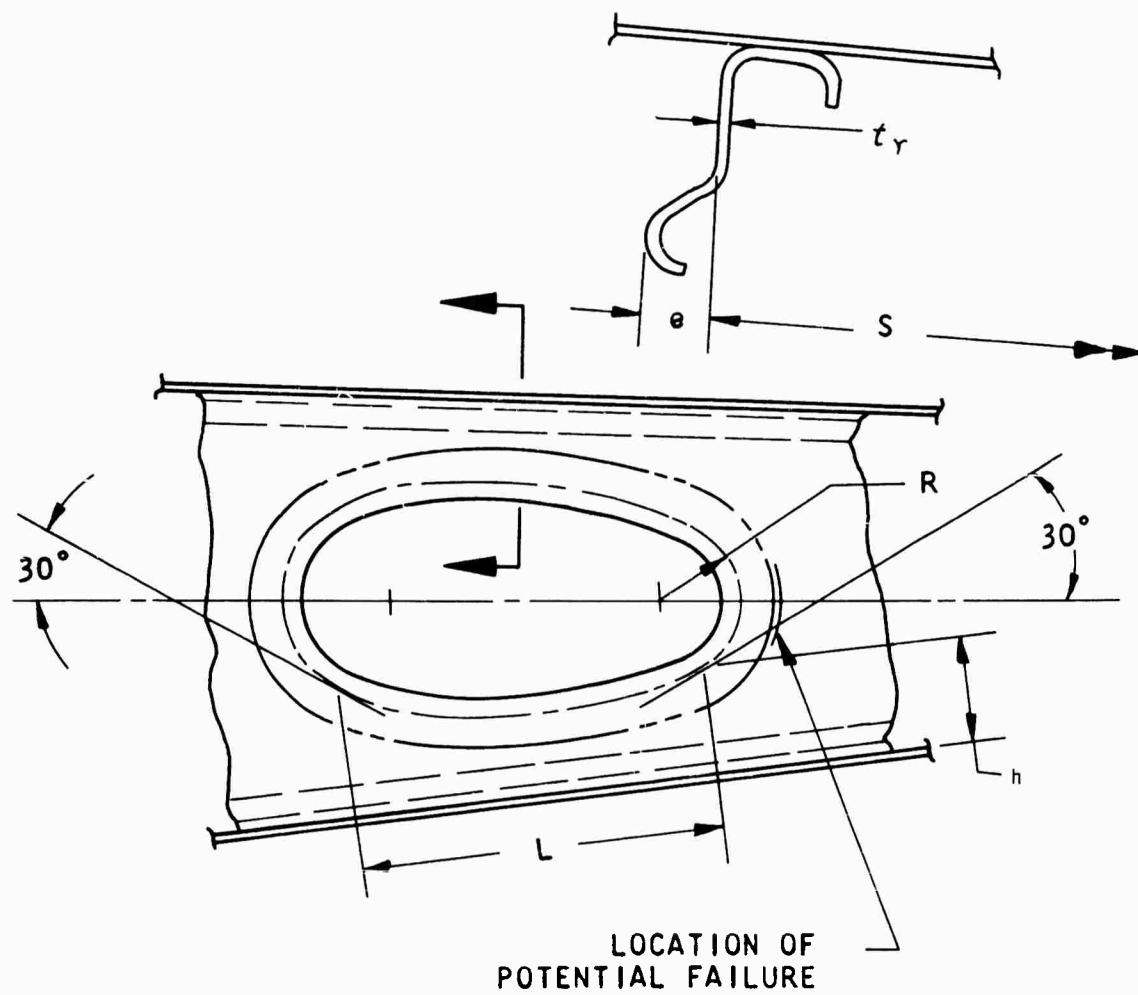
FIGURE 36 SKETCH RIB WITH LIGHTENING HOLE
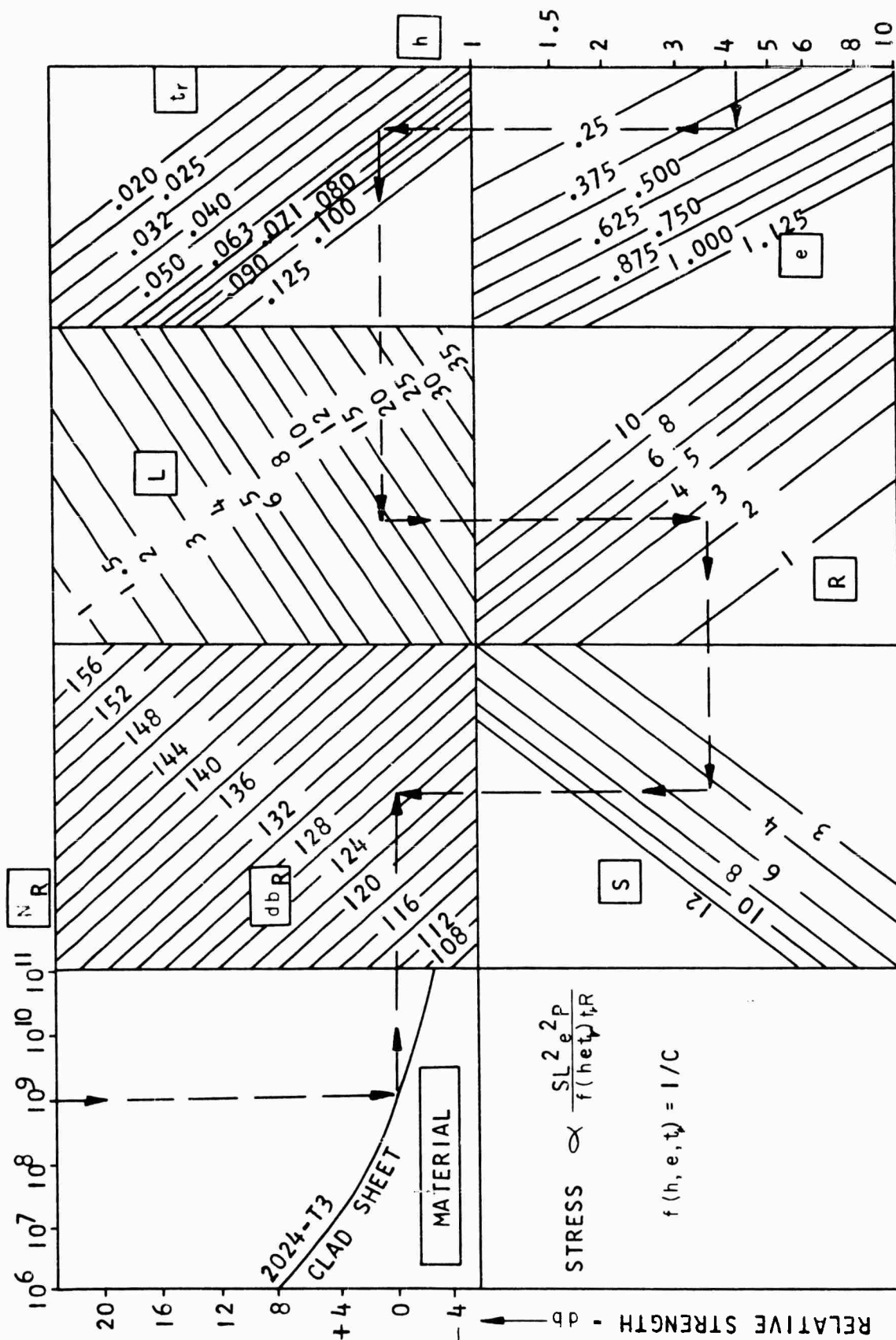
FIGURE 37 DESIGN CHART RIB WITH LIGHTENING HOLE

$$\text{STRESS} \propto \frac{SL^2 e^2 P}{f(h,e,t)\, tR}$$

$$f(h,e,t) = 1/C$$
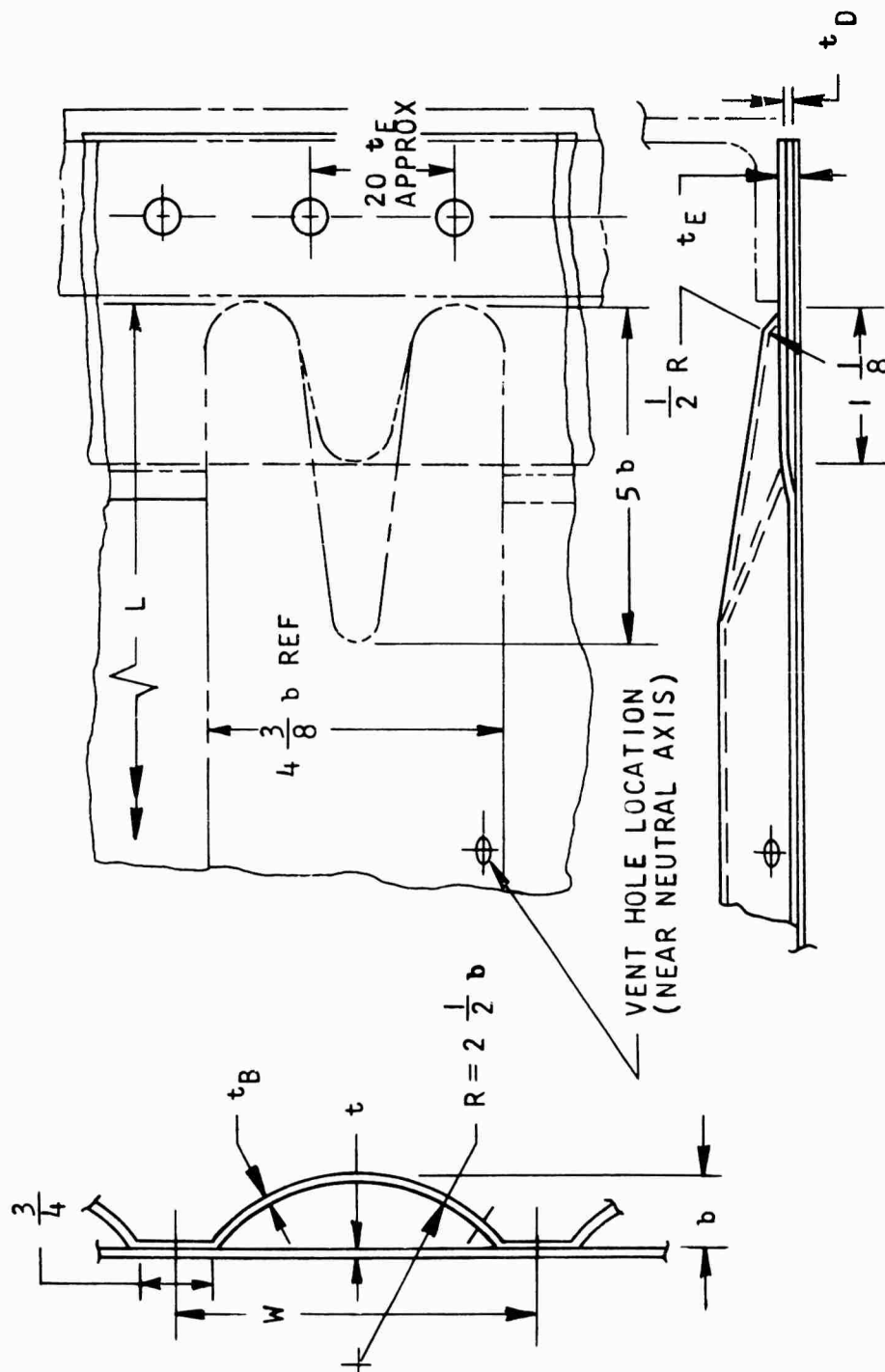
$t = t_B \pm \text{ONE GAGE}$

$t_E = t + t_D + t_B + \text{BOND THICKNESS}$

FIGURE 38 SKETCH BEADED PANEL
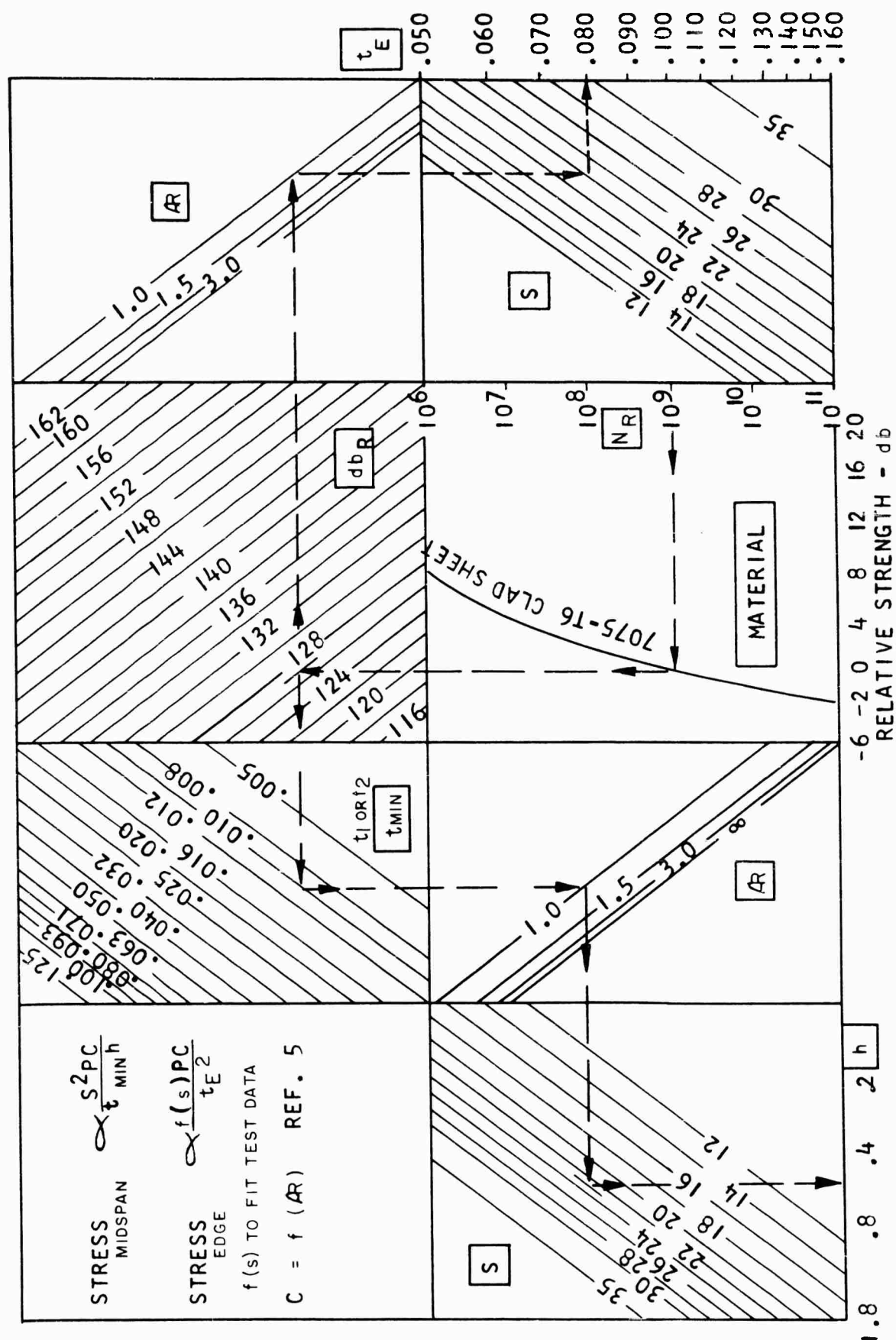
82
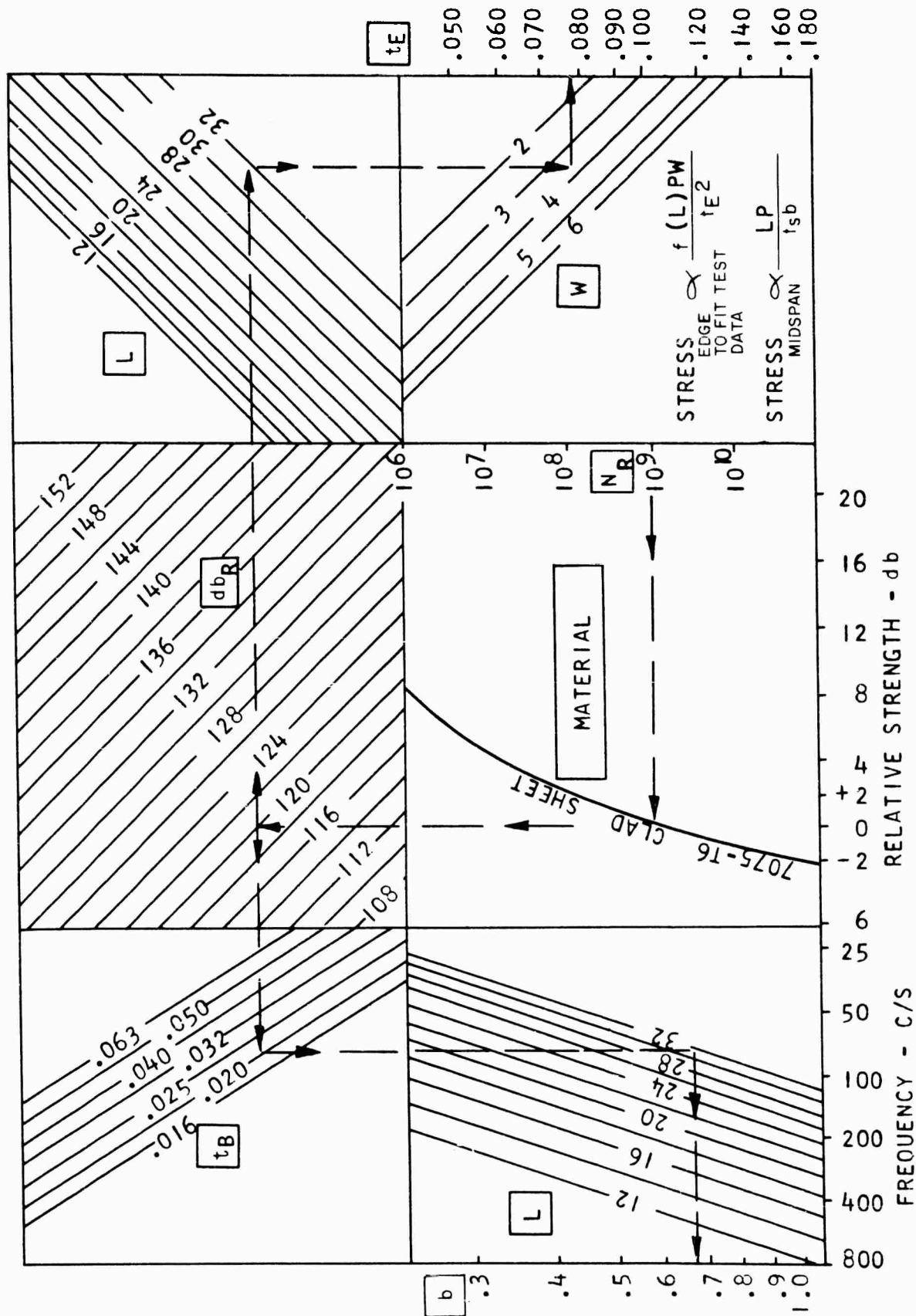
FIGURE 39 DESIGN CHART BEADED PANEL

$$20\ t_1\ \text{OR}\ \tfrac{1}{2}\ \text{MIN}$$

$$A = 20\ t_E$$

$$AR = \frac{a}{S}$$
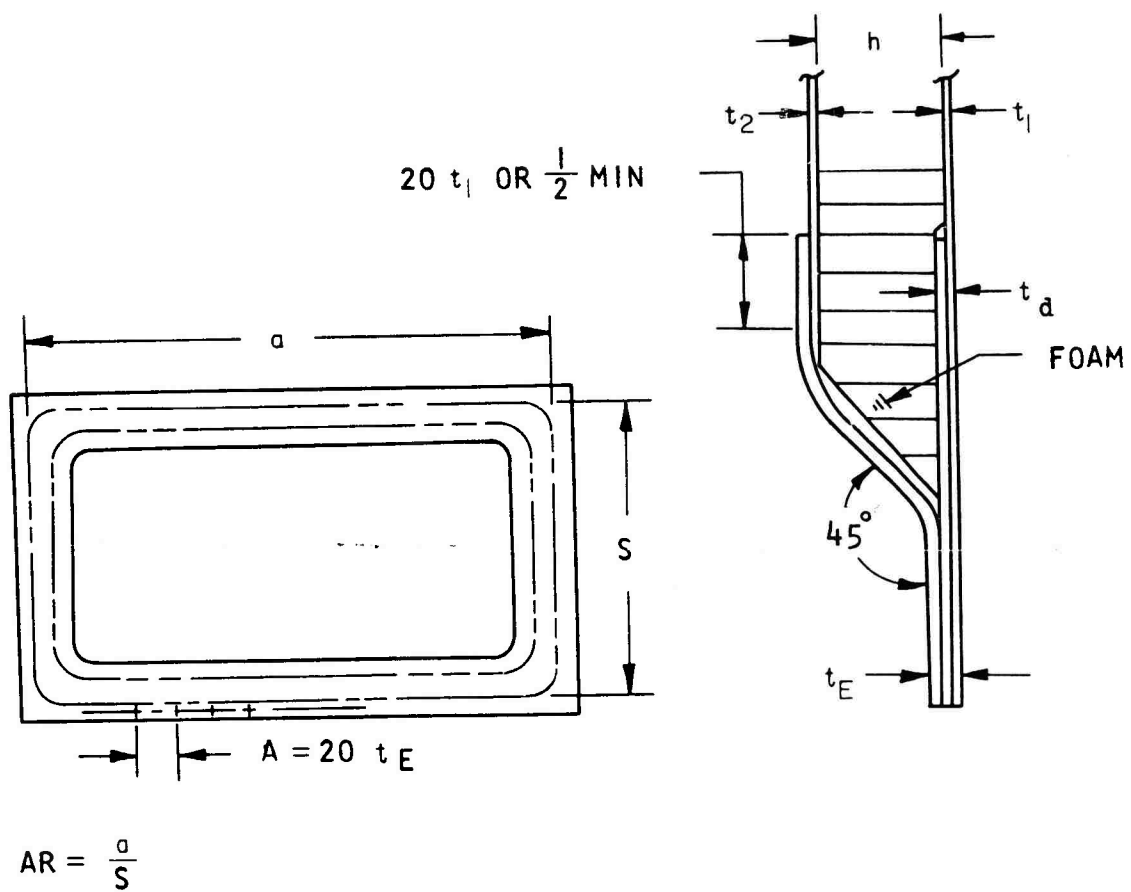
FIGURE 40 SKETCH HONEYCOMB PANEL

FIGURE 41 DESIGN CHART HONEYCOMB PANEL

$$\text{STRESS}_{\text{MIDSPAN}} \varpropto \frac{S^2 PC}{t_{\text{MIN}} h}$$

$$\text{STRESS}_{\text{EDGE}} \varpropto \frac{f(s) PC}{t_E^2}$$

f(s) TO FIT TEST DATA

C = f (ÆR) REF. 5
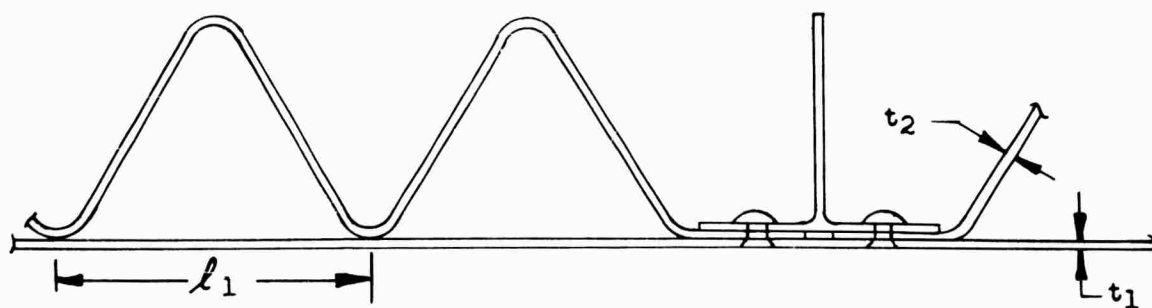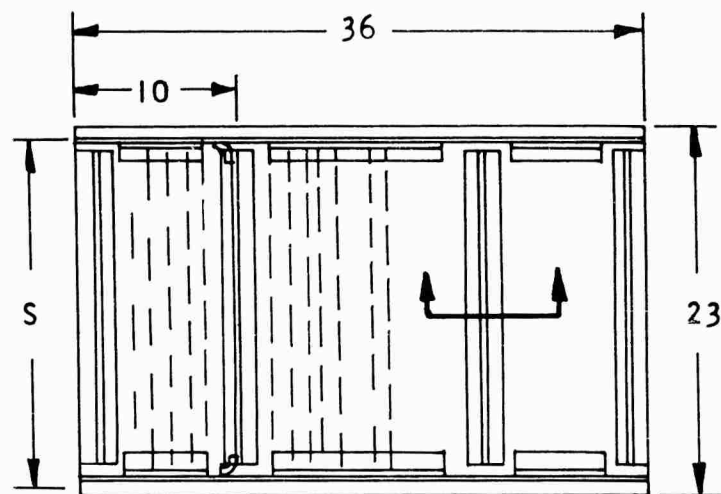
FIGURE 42 SKETCH CORRUGATED PANEL
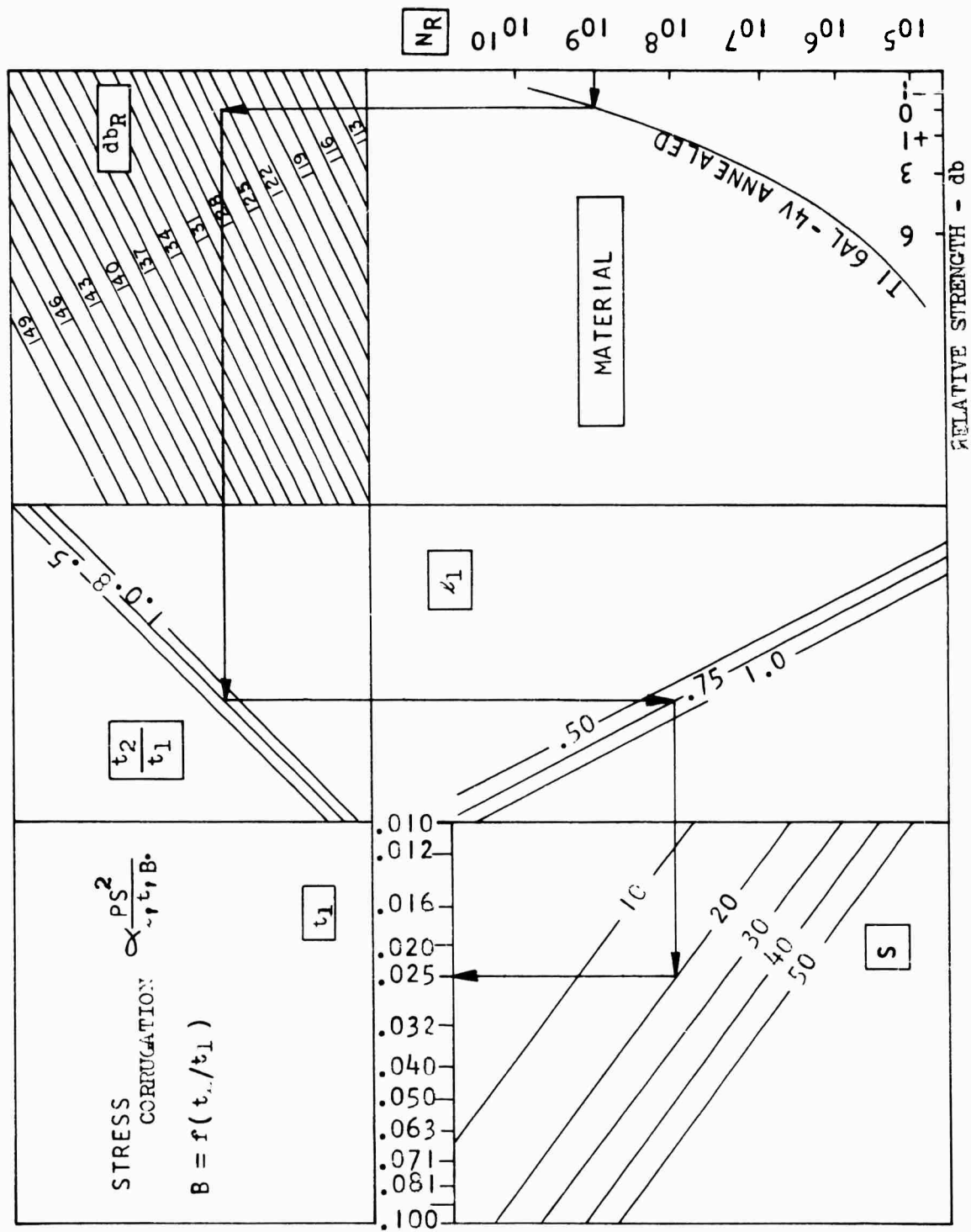
FIGURE 43 DESIGN CHART CORRUGATED PANEL - CORRUGATION
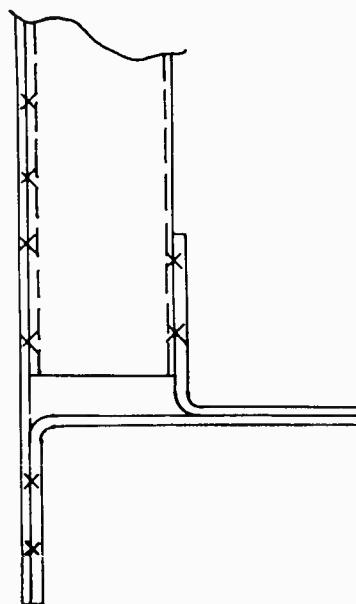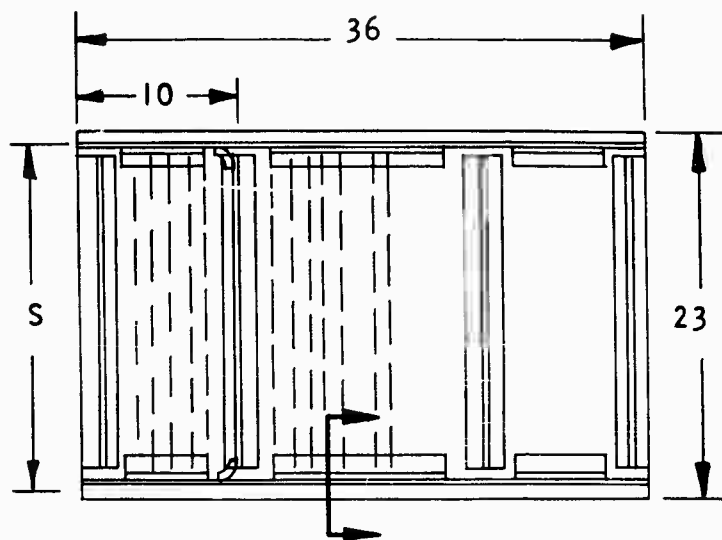
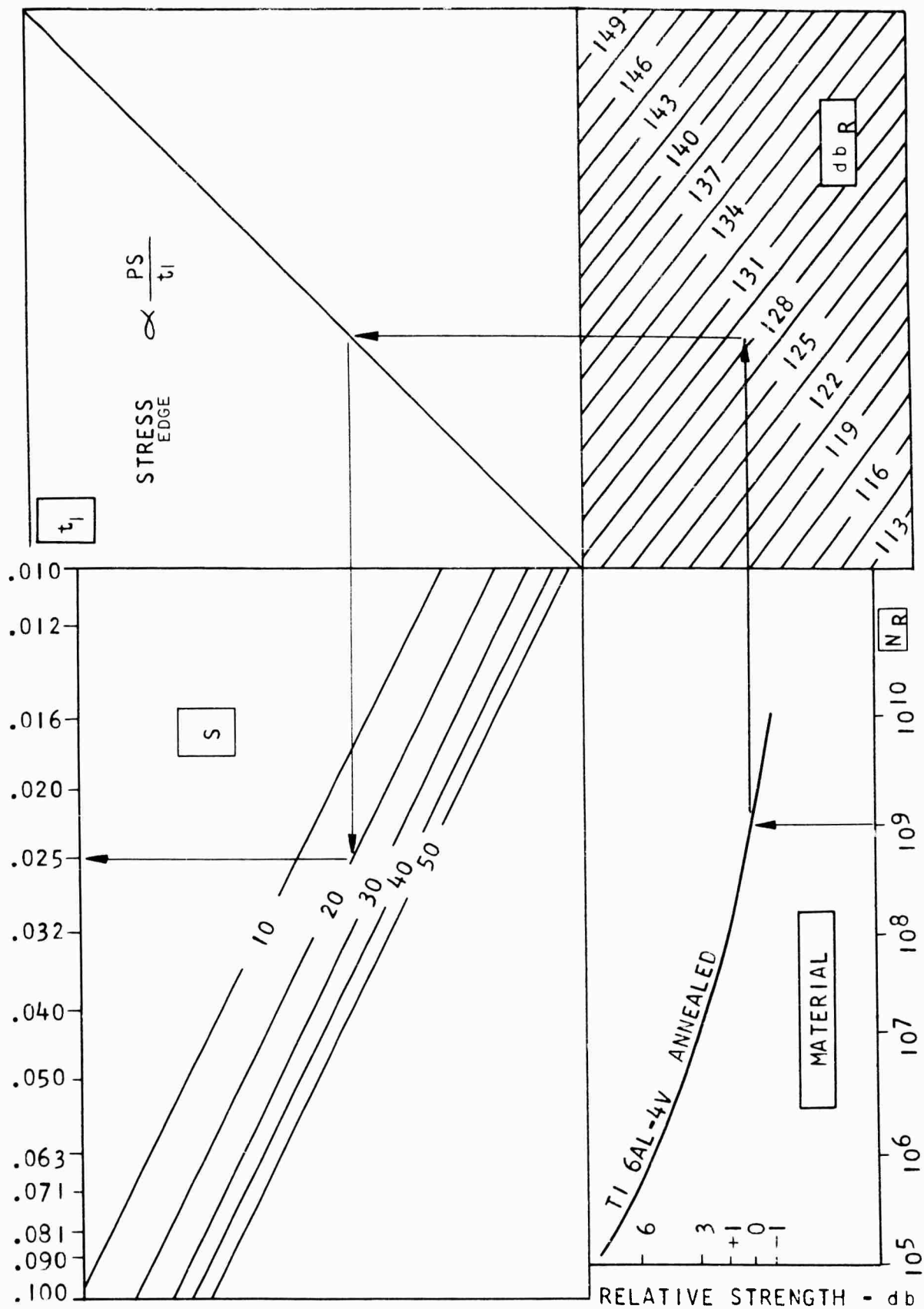FIGURE 44   SKETCH CORRUGATED PANEL - EDGE
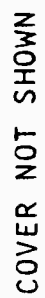
FIGURE 45 DESIGN CHART CORRUGATED PANEL - EDGE

COVER NOT SHOWN

ASPECT RATIO $= \dfrac{a}{b}$

A-A

B-B

FIGURE 46 SKETCH WELDED SKIN AND STRINGER
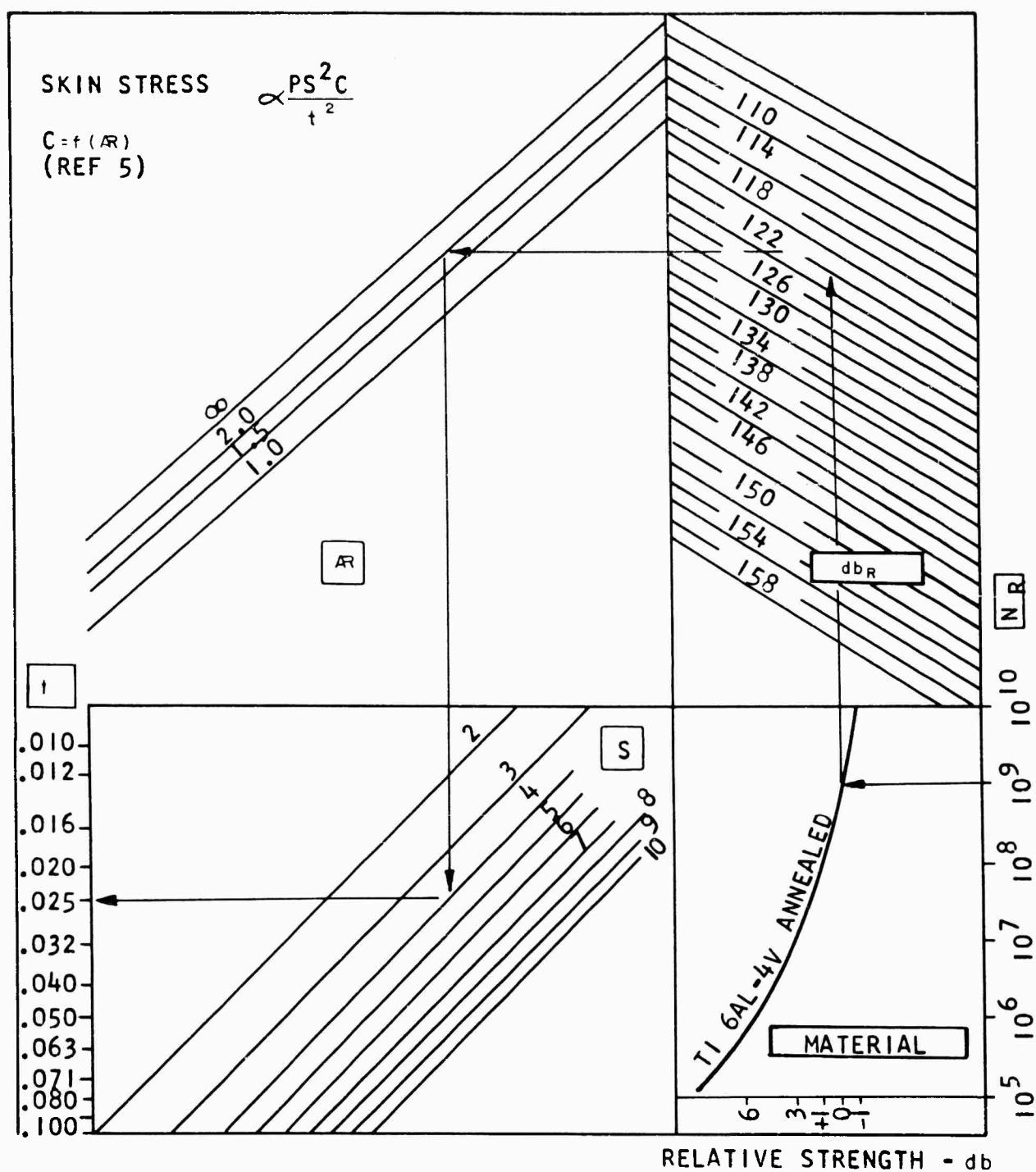
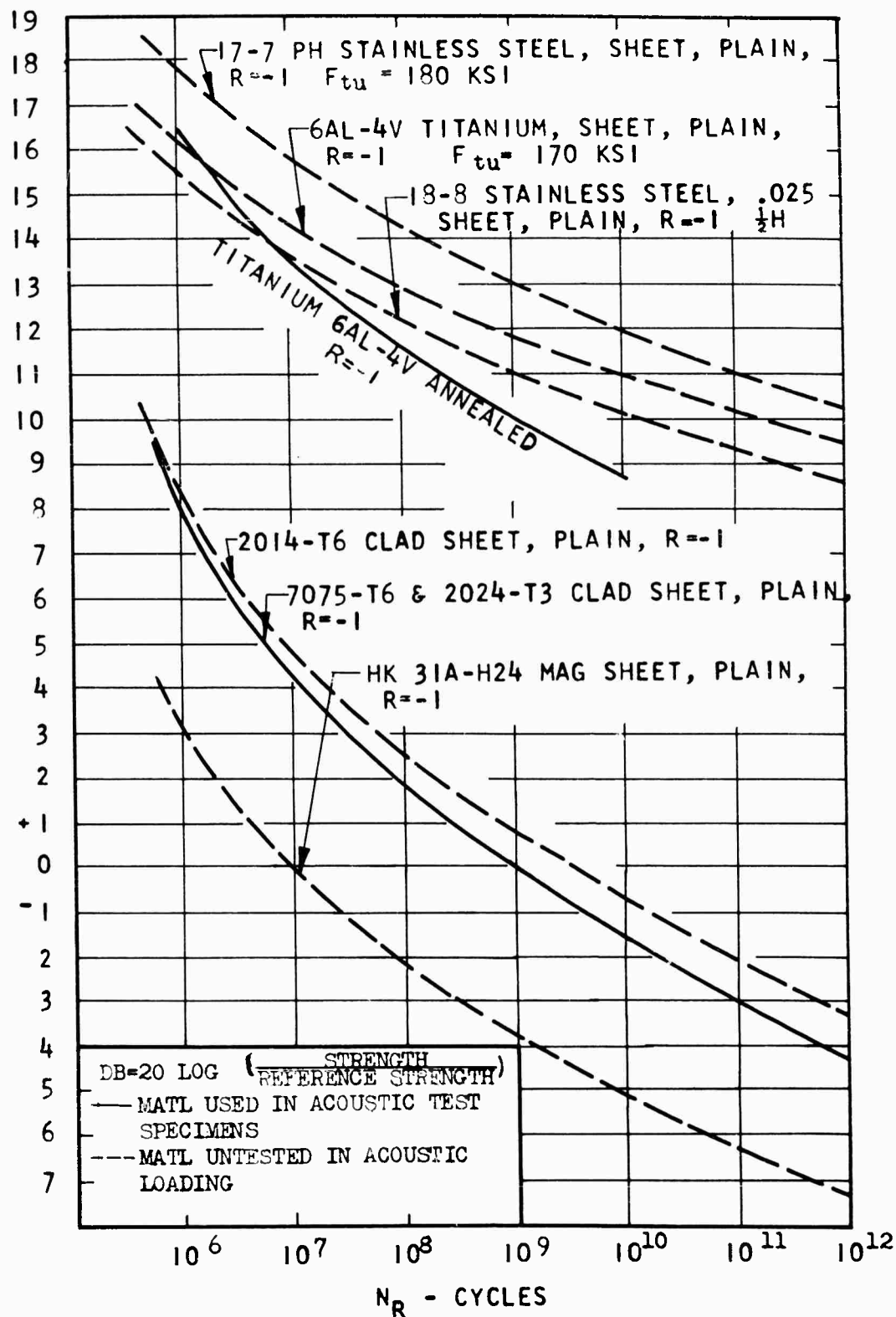FIGURE 47 DESIGN CHART WELDED SKIN AND STRINGER

FIGURE 48   RELATIVE FATIGUE STRENGTHS OF MATERIALS UNDER
RANDOM EXCITATION

SECTION 7   CONCLUSIONS

The design charts presented in this report will serve as a guide to the designer who is required to develop a structure that is resistant to acoustic fatigue. While the life under a specific distributed sound pressure level is not as predictable as a buckling or ultimate load under some static loading, it is still believed to be sufficiently accurate to aid in design.

These charts, for the specific structural configurations tested, are considered to be adequate to predict an allowable sound pressure level for a given life within a ± 6db range. If a design checks within less than this 6db or if acoustic fatigue is the primary design criteria, a simulated service test should be conducted.

Special attention must be given to the design of edges of panels which are of a sandwich type, such that the edges are inherently thinner than the central portion. This is equally true for both the aluminum and the titanium materials tested in this study.

SECTION 8 RECOMMENDATIONS

Acoustic fatigue, with the ever increasing engine power available, is becoming an ever more important design criteria. The general design data available to date of which these charts are a large portion is very incomplete. For present day efforts, the designer should have information on the direct effect of noise, of noise combined with direct stress and of noise combined with thermal stress.

The direct effect of noise is a fatigue phenomenom and is subject to all of the variability that exists in simple fatigue data as well as that due to random load distribution and various load spectra. For this reason, it is believed that the foremost requirement is for a continued investigation of the direct effect of noise on simple structure to improve the reliability, available data and to increase the number of structural configurations for which this data is available.

For the majority of current design combined flight or thermal and acoustic stresses are not critical. There are many projects for which this information would be most useful and the need is increasing continually. Thus, as an extension of the simple tests, information should be obtained on effect of combining other stresses with the acoustic stress.

REFERENCES

1. Van Dyke, J.D., Eshleman, A.L. and Belcher, P.M., "Method for Designing and Testing Structures Subjected to Random Acoustic Loading", Douglas Report, SM-22555.

2. Miles, J.W., "On Structural Fatigue Under Random Loading", Journal Aeronautical Sciences, Vol. 21, No. 11, pp 753-762, November 1954.

3. Kuhn, Paul, Peterson, J.P., Levin, L.R., "A Summary of Diagonal Tension", Part I, NACA TN 2661, May 1952.

4. Gerard, G., Becker, H., "Handbook of Structural Stability", Part I, NACA TN 3781, July 1957.

5. Roark, R.J., "Formulas for Stress and Strain", 2nd edition, McGraw-Hill Book Company, Inc., New York, N.Y., 1943.

BIBLIOGRAPHY

1. Schejelderup, H.C. and Galef, A.E., "Rationalization of an Aspect of Sonic Fatigue", Aerospace Engineering, June 1962, page 44.

2. Trapp, W.J. and Lazan, B.J., "Role of Structural Damping in Acoustical Fatigue", WADC TR 59-304, January 1960.

3. Clarkson, B.L., U. of Southhampton, "Note on the Use of Correlation Techniques to Determine the Forms of Vibration of a Continuous Structure Excited by Random Pressures"; WADC - University of Minnesota Conference on Acoustical Fatigue, WADC TR 59-676, March 1961, page 99.

4. Hess, Robert W., Herr, Robert W., Mayers, William H., "A Study of the Acoustical Fatigue Characteristics of Some Flat and Curved Aluminum Panels Exposed to Random and Discrete Noise", NASA TN D-1, August 1959.

5. Hubbard, H.H., NASA, "Design Considerations for Minimizing Acoustic Fatigue", WADC-University of Minnesota Conference on Acoustical Fatigue, WADC TR59-676, March 1961, page 321.

6. Jackson, C.E., Thorsen, K.R., Wherrey, J.E., Dempster, J.B., "The Influence of Dynamic Loads on Aircraft Fatigue", Proceedings of the Symposium of Fatigue of Aircraft Structures, WADC TR59-507, August 1959, page 449.

7. Lassiter, Leslie W., Hess, Robert W., and Hubbard, Harry H., "An Experimental Study of the Response of Simple Panels to Intense Acoustic Loading", presented at the Structures Session, Twenty-Fourth Annual Meeting, IAS, New York, January 23-26, 1956.

8. Lazan, B.J., "Review of Structural Damping Mechanisms", WADC -University of Minnesota Converence on Acoustical Fatigue, WADC TR 59-676, March 1961, page 168.

9. Mead, D.J., "Criteria for Comparing the Effectiveness of Damping Treatments", WADD TR 61-25, January 1961.

10. Oberst, Hermann, "Progress in the Development of Vibration Damping Materials", WADC - University of Minnesota Conference on Acoustical Fatigue, WADC TR 59-676, March 1961, page 185.

11. Edge, Phillip M., Jr., "Acoustic Fatigue Tests Relating to the Design of Structures for Elevated Temperatures". Symposium proceedings, Structural Dynamics of High Speed Flight, Los Angeles, California, April 1961. ACR-62, Vol. 1.

APPENDIX I

ADVANCED STRUCTURE DEVELOPMENT

For the advanced structural configuration to be tested in this work, an optimization study was carried out. The development of the relationships is presented along with curves of results. Two types of structure are considered, 1) the corrugated skin and 2) the melt-thru welded skin and stringers.

The corrugated skin panel is considered as an element in a control surface where torsional stiffness is important and therefore the panel is optimized on the basis of a shear loading. The optimum configuration is taken as that at which the three basic elements of the panel all buckle at the same time. These results of course present a variety of combinations each of which is optimum. These combinations are then considered in view of the effect of the noise loading acting on the elements as a beam.

The skin and stringer structure is conceived as a portion of a trailing edge and as such is required to carry axial loads in its cover plate. For this configuration the stringers with the adjacent effective skin are so selected that they will carry a chosen compressive load per inch for a minimum weight. The combination of elements is required to carry the load without failure as a column or in local crippling.

Skin and Corrugation Panel

The panel with the skin and corrugated inner skin is analyzed in the following paragraphs.

Critical Shear Buckling

The critical shear buckling stress of the skin and corrugation are given by the following equations:

$$* \ \tau_{cr_{ss}} = K_{ss}E(t/l)^2 \tag{40}$$

$$\tau_{1_{cr}} = K_{ss}E(t_1/l_1)^2 \tag{41}$$

$$\tau_{2_{cr}} = K_{ss}E(2t_2/l_2)^2 \tag{42}$$

$$(\tau_2/\tau_1)_{cr} = 4(l_1/l_2)^2 \ (t_2/t_1)^2 \tag{43}$$

Shear Distribution

The following analysis describes the shear stress distribution in the corrugation and skin based on equal shear deflections of these elements from node to node with the applied shear load acting in the direction of the corrugations, Figure 44.

$$\delta_1 = \frac{P_1 l_1}{A_1 G} = \delta_2 = \frac{P_2 l_2}{A_2 G} \tag{44}$$

Where the subscripts 1 and 2 refer to the skin and corrugation respectively. For one material, the G's are the same and the shear area A is equal to the thickness multiplied by the shear length which is the same for the two elements.
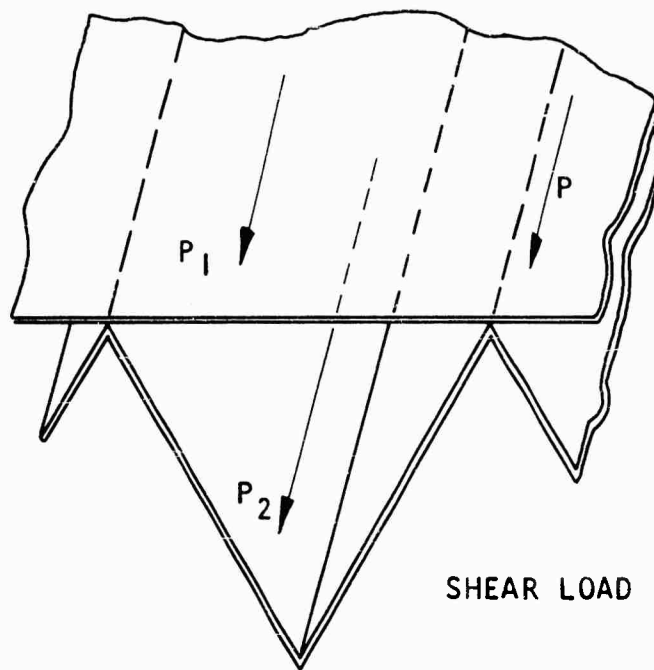
$$\frac{P_1 l_1}{t_1} = \frac{P_2 l_2}{t_2} \tag{45}$$

$$P_1 = P_2 \left(\frac{t_1 l_2}{t_2 l_1}\right) \tag{46}$$

The total load transferred from node to node, P, is equal to the sum of the loads in the elements.

$$P = P_1 + P_2 = P_2 \left(\frac{t_1 l_2}{t_2 l_1} + 1\right) \tag{47}$$

$$P_2 = P \left(\frac{t_2 l_1}{t_1 l_2 + t_2 l_1}\right) \tag{48}$$

* NACA TN 2661, A Summary of Diagonal Tension, Part I, page 26
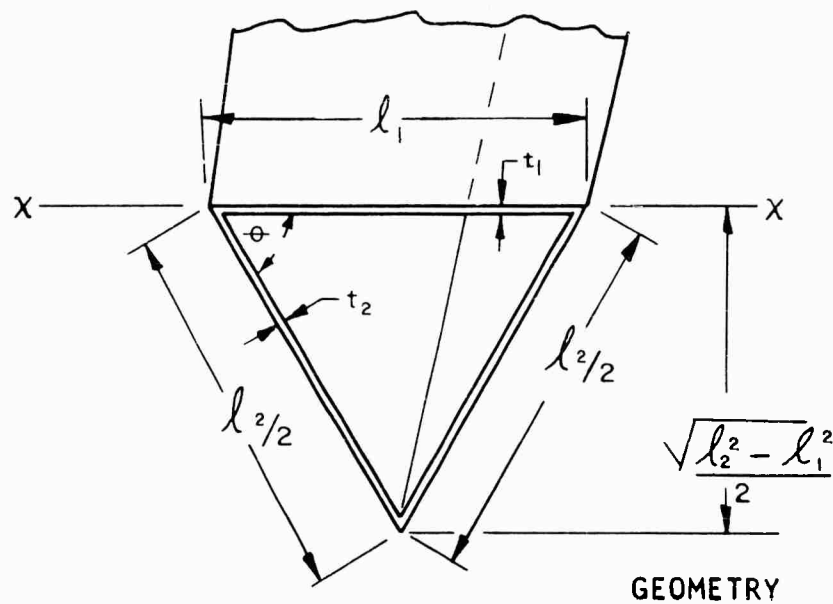
SHEAR LOAD DISTRIBUTION

GEOMETRY

FIGURE 49   ELEMENTAL BEAM - CORRUGATED PANEL

In a manner similar to the derivation of the expression for P_1

$$P_2 = P_1 \left(\frac{t_2 l_1}{t_1 l_2} \right) \tag{49}$$

$$P = P_1 + P_2 = P_1 \left(\frac{t_2 l_1}{t_1 l_2} + 1 \right) \tag{50}$$

$$P_1 = P \left(\frac{t_1 l_2}{t_2 l_1 + t_1 l_2} \right) \tag{51}$$

Shear stress is the shear load divided by the shear area

$$\tau_2 = \frac{P_2}{A_2} = P \left(\frac{t_2 l_1}{t_1 l_2 + t_2 l_1} \right) \tag{52}$$

$$\tau_1 = \frac{P}{A_1} \left(\frac{t_1 l_2}{t_1 l_2 + t_2 l_1} \right) \tag{53}$$

As previously, A is the product of thickness and the shear length

$$\tau_2 / \tau_1 = l_1 / l_2 \tag{54}$$

Optimum Shear

Optimum configurations are assumed to exist for the following condition

Actual distribution of $\left(\tau_2 / \tau_1 \right)$ shear stress equals critical distribution

of $\left(\tau_2 / \tau_1 \right)_{cr}$ shear buckling stress, and from the two previous sections

$$\tau_2 / \tau_1 = l_1 / l_2 = 4 \, (l_1 / l_2)^2 \, (t_2 / t_1)^2$$

$$4 \, l_1 / l_2 = (t_1 / t_2)^2 \quad \text{(for equal shear buckling)} \tag{55}$$

Allowable Buckling Stress in Corrugation in Bending

The following equation relates the allowable buckling stress in the corrugation
to the various parameters involved with the element of skin and corrugation
acting like a beam

$$* \; \sigma_{Al} = \frac{K_b \Pi^2 E}{12(1 - \gamma^2)} \left(\frac{t}{l} \right)^2 \qquad \text{(REF: 4)} \tag{56}$$

* NACA TN 3781, Handbook of Structural Stability, Part I, page 19

For a given material and aspect ratio and based on the corrugation parameters this reduces to

$$\sigma_{A1} = K \left(\frac{t_2}{l_2}\right)^2 \tag{57}$$

If both sides of the equation are multiplied by $(l_1/t_1)^2$ and the terms are rearranged, the following expression results:

$$\left(\frac{l_1}{t_1}\right)^2 \frac{\sigma_{al}}{K} = \left(\frac{l_1}{l_2}\right)^2 \left(\frac{t_2}{t_1}\right)^2 \tag{58}$$

This bending stress factor is thus expressed in the same terms as occur in the optimum shear expression. As the pertinent corrugation length is $l_2/2$

$$(t/l)_2^2 = \left(\frac{2t_2}{l_2}\right)^2 = 4 \left(\frac{t_2}{l_2}\right)^2 \tag{59}$$

For an infinite aspect ratio $K_b = 24$ **

Thus K may be evaluated as follows:

$$K = \frac{4K_b \Pi^2 E}{12(1-\nu^2)} = \frac{(4)(24)(\Pi^2)(16 \times 10^6)}{12(1-.3^2)} = 1.28 \times 10^9 \tag{60}$$

Bending of Corrugations

The following analysis results in a general equation relating the bending stress of the corrugations to the various parameters involved:

$$\sigma_{ap} = \frac{M}{Z} \qquad M = \frac{PL^2}{8} \tag{61}$$

Where Z is the section modulus, L is the beam length and B is the running load

$$\sigma_{ap} = \frac{PL^2}{8Z} \tag{62}$$

A stress parameter equivalent to that developed for the allowable buckling is derived based on the assumption that the final stress will be approximately 50 times the stress indicated by the above equations and using the panel dimensions indicated below. This permits direct comparison of the applied and allowable buckling stress in terms of the critical shear factors.

** NACA TN 3781, Handbook of Structural Stability, Part I, page 92

For: $L = 23"$, $l_1 = .75"$, $t_1 = .025"$, $p = .104$ psi, a sample case follows,

$$\left(l_1/t_1\right)^2 \left(\frac{\sigma_{ap}}{K}\right) = \frac{\left(l_1/t_1\right)^2}{K} \left(\frac{AF_x PL^2}{8Z}\right) = \left(\frac{(.75/.025)^2}{1.28 \times 10^9}\right)\left(\frac{(50)(.104)(23)^2}{8Z}\right) \quad (63)$$

$$\left(l_1/t_1\right)^2 \left(\frac{\sigma_{ap}}{K}\right) = \frac{2.406 \times 10^{-4}}{Z} \quad (64)$$

Developing an expression for "Z" where the geometry is shown in Figure 44

$$I_x = 2(1/3) \left(t_2/\sin\Theta\right)\left(l_2/2 \sin\Theta\right)^3 = 1/12 \left(t_2\right)\left(l_2\right)^3 \sin^2\Theta \quad (65)$$

where $\sin^2\Theta = \dfrac{l_2^2 - l_1^2}{l_2^2}$ and $l_2 t_2 = A_2$

$$I_x = \frac{l_2 t_2 \left(l_2^2 - l_1^2\right)}{12} = \frac{A_2\left(l_2^2 - l_1^2\right)}{12} \quad (66)$$

$$d = \frac{\int y\, dA}{\int dA} = \frac{(1/2)\left(l_2/2 \sin\Theta\right)\left(A_2\right)}{A_1 + A_2} = \frac{A_2\sqrt{l_2^2 - l_1^2}}{4\left(A_2 + A_1\right)} \quad (67)$$

$$I_{cg} = I_x - \sum Ad^2 \quad (68)$$

$$I_{cg} = \frac{A_2}{12}\left(l_2^2 - l_1^2\right) - \left(A_1 + A_2\right)\left[\frac{A_2^2\left(l_2^2 - l_1^2\right)}{16\left(A_2 + A_1\right)^2}\right] \quad (69)$$

$$I_{cg} = \left[\frac{A_2}{12} - \frac{A_2^2}{16\left(A_2 + A_1\right)}\right]\left(l_2^2 - l_1^2\right) = \left[\frac{A_2^2 + 4A_1 A_2}{48\left(A_1 + A_2\right)}\right]\left(l_2^2 - l_1^2\right) \quad (70)$$

The peak distance from the neutral axis, C, is

$$C = \frac{\sqrt{l_2^2 - l_1^2}}{2} - d \quad (71)$$

$$C = \left(\frac{2A_1 + A_2}{A_1 + A_2}\right)\frac{\sqrt{l_2^2 - l_1^2}}{4} \quad (72)$$

$$Z = \frac{I_{cg}}{C} = \frac{A_2^2 + 4A_1 A_2}{12\left(A_2 + 2A_1\right)}\sqrt{l_2^2 - l_1^2} \quad (73)$$

$$Z = \frac{A_2(A_2 + 4A_1)}{12(A_2 + 2A_1)} \; (1_2) \; \sqrt{1 - (1_1/1_2)^2} \tag{74}$$

Rewriting the areas as products of length and thickness

$$Z = \frac{1_2{}^2 t_2 \left[1_2 t_2 + 4 1_1 t_1 \right] \sqrt{1 - (1_1/1_2)^2}}{12 \left[1_2 t_2 + 2 1_1 t_1 \right]} \tag{75}$$

$$Z = \frac{1_2{}^2 t_2}{12} \left[\frac{t_2/t_1 + 4 1_1/1_2}{t_2/t_1 + 2 1_1/1_2} \right] \sqrt{1 - (1_1/1_2)^2} \tag{76}$$

Eq 76 Results from dividing Eq 75 numerator and denominator by $1_2 t_1$

Multiplying and dividing the first factor by $\dfrac{(t_2/t_1)}{(1_1/1_2)^2}$

$$Z = \frac{(1_1{}^2 t_1)}{12} \left[\frac{t_2/t_1}{(1_1/1_2)^2} \right] \left[\frac{t_2/t_1 + 4 1_1/1_2}{t_2/t_1 + 2 1_1/1_2} \right] \sqrt{1 - (1_1/1_2)^2} \tag{77}$$

Rearranging

$$Z = \frac{(1_1{}^2 t_1)}{12} \left[\frac{(t_2/t_1)^2}{(1_1/1_2)^2} \right] \frac{\left[1 + 4 \frac{(1_1/1_2)}{(t_2/t_1)} \right]}{\left[1 + 2 \frac{(1_1/1_2)}{(t_2/t_1)} \right]} \sqrt{\frac{1}{(t_2/t_1)^2} - \frac{(1_1/1_2)^2}{(t_2/t_1)^2}} \tag{78}$$

Optimum Section Modulus

The value of Z is defined earlier as

$$Z = \frac{1_2{}^2 t_2 \left[1_2 t_2 + 4 1_1 t_1 \right] \sqrt{1 - \frac{1_1{}^2}{1_2}}}{12 \left[1_2 t_2 + 2 1_1 t_1 \right]} \tag{79}$$

which for the optimum condition of 1_2 equals $2(1_1)$ reduces to

$$1_1{}^2 t_1 \, B$$

Where

$$B = \frac{2 + \dfrac{t_2}{t_1}}{1 + \dfrac{1}{t_2/t_1}} \qquad (80)$$

A sample computation of the applied stress factor due to pressure is presented
in Table 8. These results are plotted with the allowable stress factor data
in Figures 45 through 48. The permissible conditions are those for which the
allowable stress factor is greater than the applied stress factor. The
condition at which these are equal is the minimum weight condition for the
configuration. These points of equal stress factor are replotted with the
conditions for optimum shear. These are shown in Figure 49 and 50 for the
.025 and .020 outer skins respectively.

Table 8
SAMPLE COMPUTATION FOR FIGURE 45
For $l_1 = .75"$, $t_1 = .025"$ and $p = .104$ psi

1	2	3	4	5	6	7	8	9	10
l_1/l_2	t_2/t_1	$\dfrac{l_1/l_2}{t_2/t_1}$	$\left[\dfrac{l_1/l_2}{t_2/t_1}\right]^2$	$\left[\dfrac{1}{t_2/t_1}\right]^2$	$\left[\dfrac{l_1/l_2}{t_2/t_1}\right]^2 - \left[\dfrac{1}{t_2/t_1}\right]^2$	$\dfrac{1}{(l_1/l_2)^2(t_2/t_1)}$	$\dfrac{1+4(l_1/l_2)/(t_2/t_1)}{1+2(l_1/l_2)/(t_2/t_1)}$	$\left[\dfrac{l_1/l_2}{t_2/t_1}\right]^2 - \left[\dfrac{1}{t_2/t_1}\right]^2$	$(l_1/l_2)^2\dfrac{p}{\sigma_K}$
.4	.5	0.800	.640		3.36	1.562	1.615	1.835	0.040
.6		1.200	1.440	4.0	2.56	0.694	1.705	1.600	0.103
.7		1.400	1.960		2.04	0.510	1.737	1.428	0.151
.8		1.600	2.560		1.44	0.391	1.760	1.200	0.237
.9		1.800	3.240		0.76	0.309	1.782	0.872	0.406
.4	.6	0.667	0.445		2.335	2.247	1.571	1.528	0.036
.6		1.000	1.000	2.78	1.780	1.000	1.667	1.333	0.088
.7		1.166	1.360		1.420	0.735	1.699	1.191	0.131
.8		1.333	1.777		1.003	0.566	1.726	1.002	0.199
.95		1.583	2.505		0.275	0.360	1.760	0.524	0.620

Column (10) is plotted versus columns (1) and (2) in Figure

OPTIMUM WEIGHT
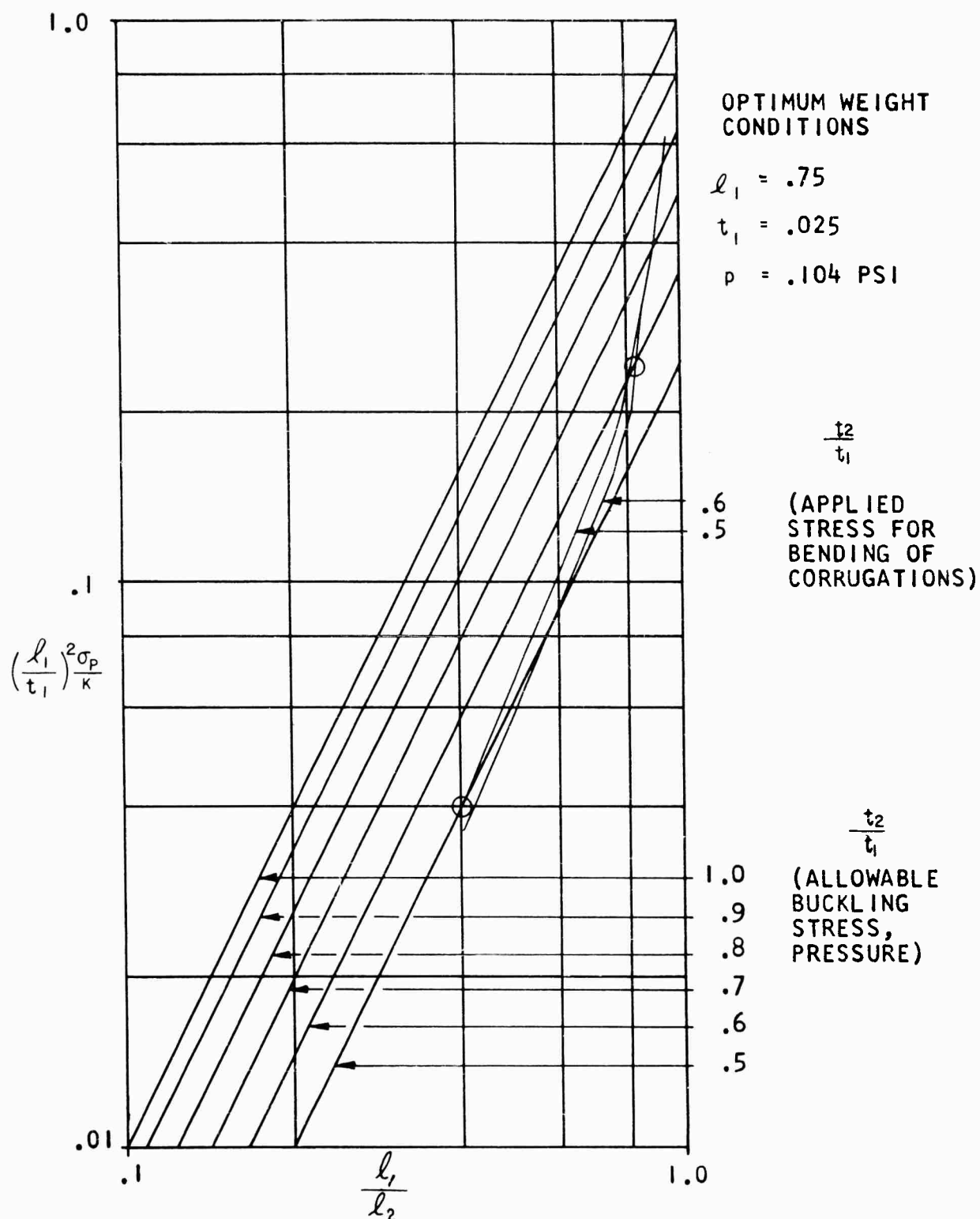CONDITIONS

$\ell_1 = .75$

$t_1 = .025$

$p = .104$ PSI

FIGURE 50   LENGTH AND THICKNESS RATIOS FOR EQUAL APPLIED
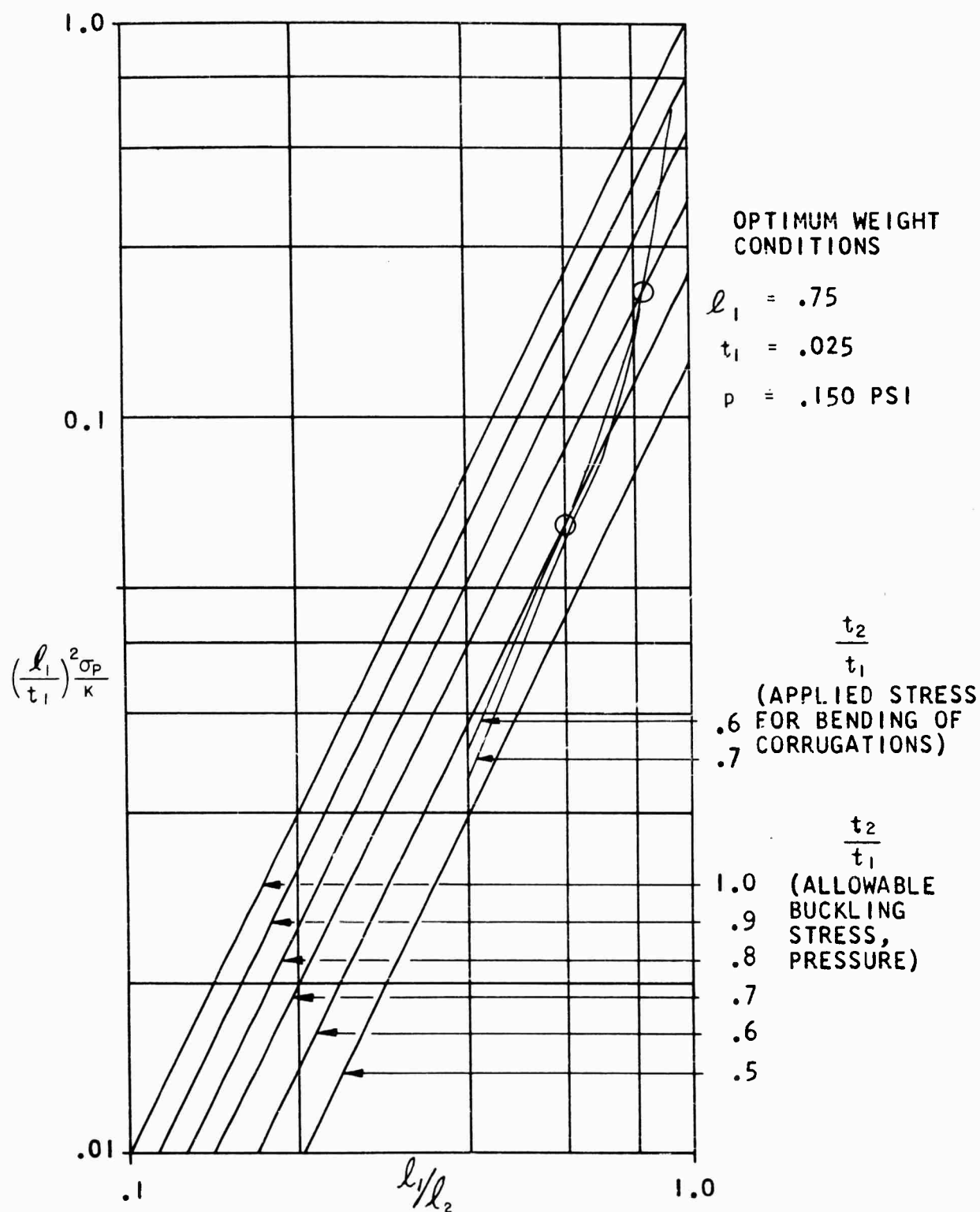AND ALLOWABLE BENDING AND BUCKLING STRESS
$p = .104$ PSI

FIGURE 51   LENGTH AND THICKNESS RATIOS FOR EQUAL
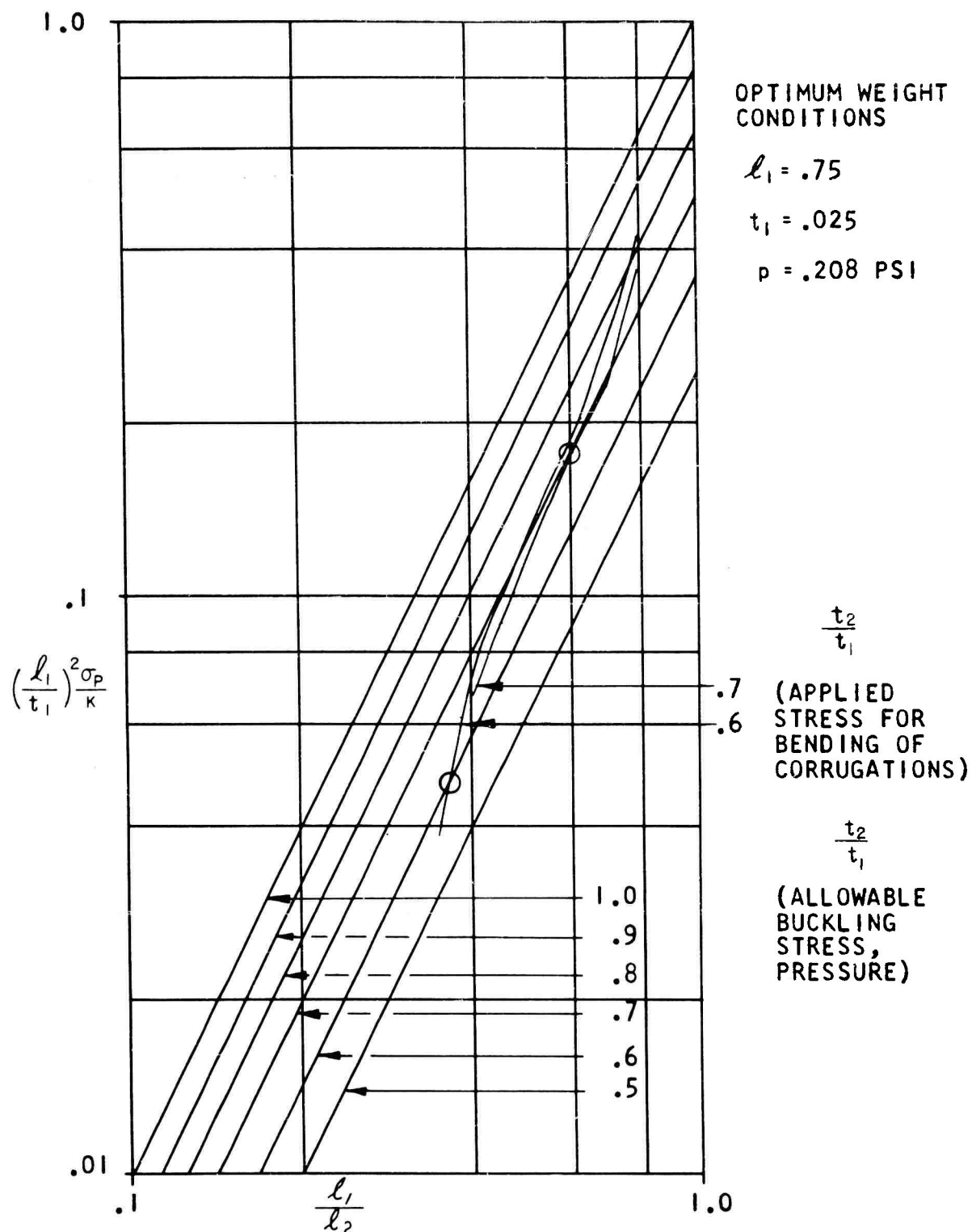APPLIED AND ALLOWABLE BENDING AND
BUCKLING STRESS p = .150 PSI

FIGURE 52   LENGTH AND THICKNESS RATIOS FOR EQUAL APPLIED
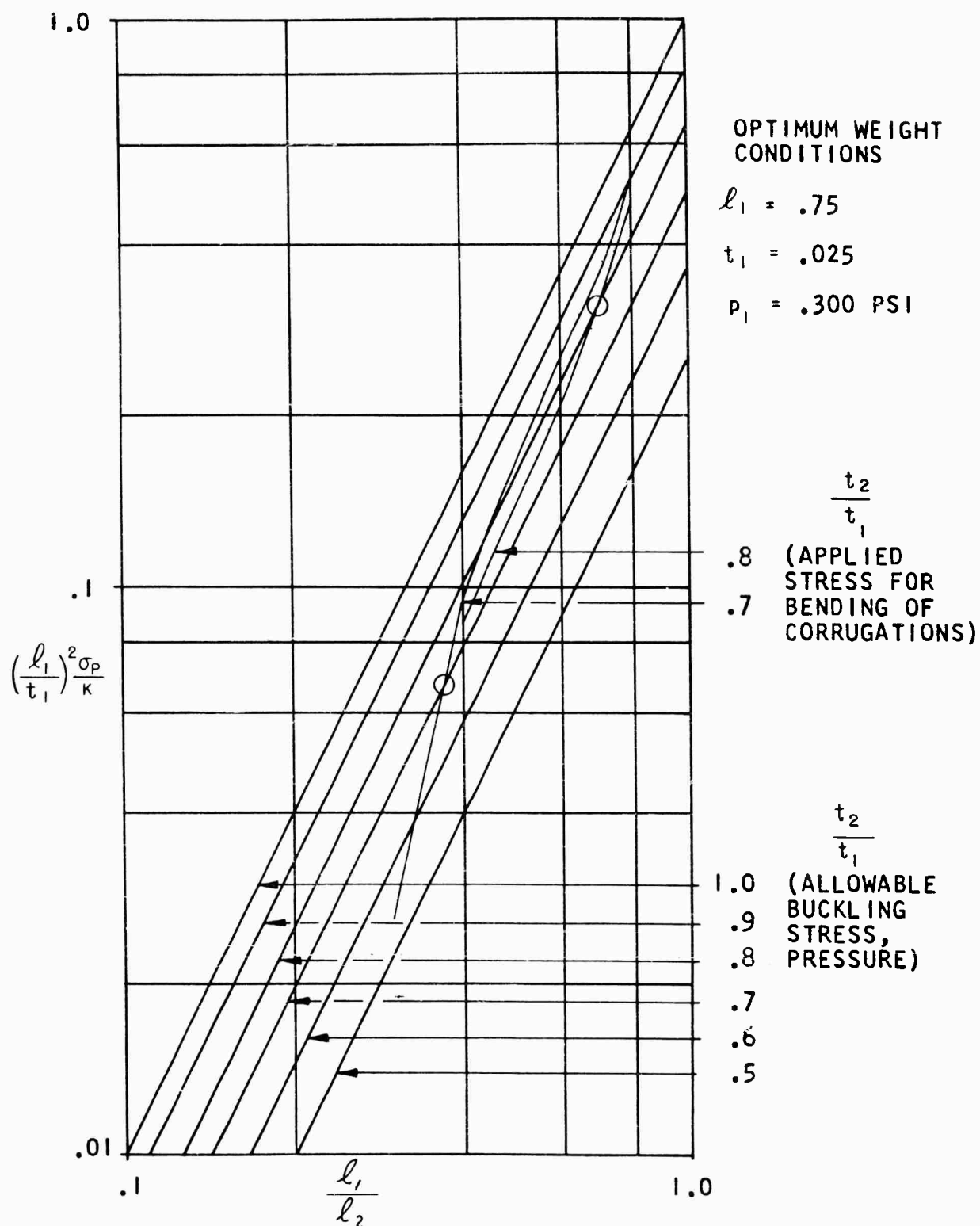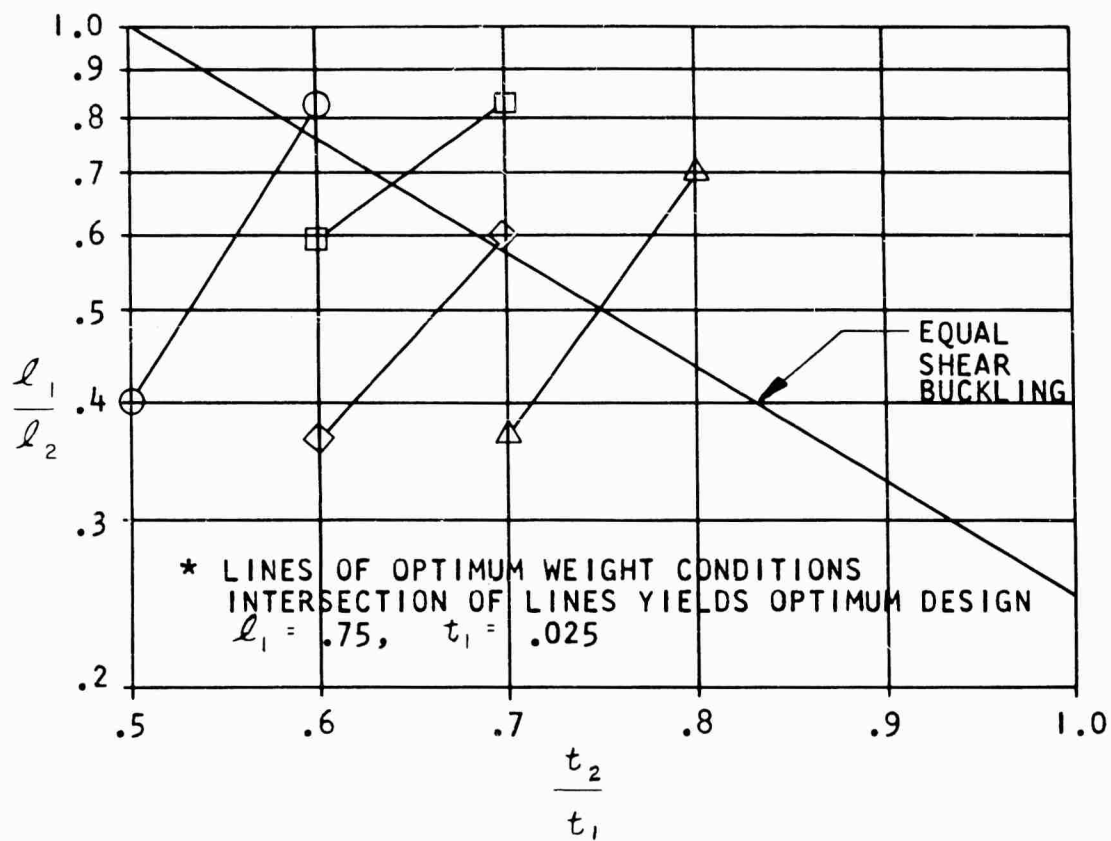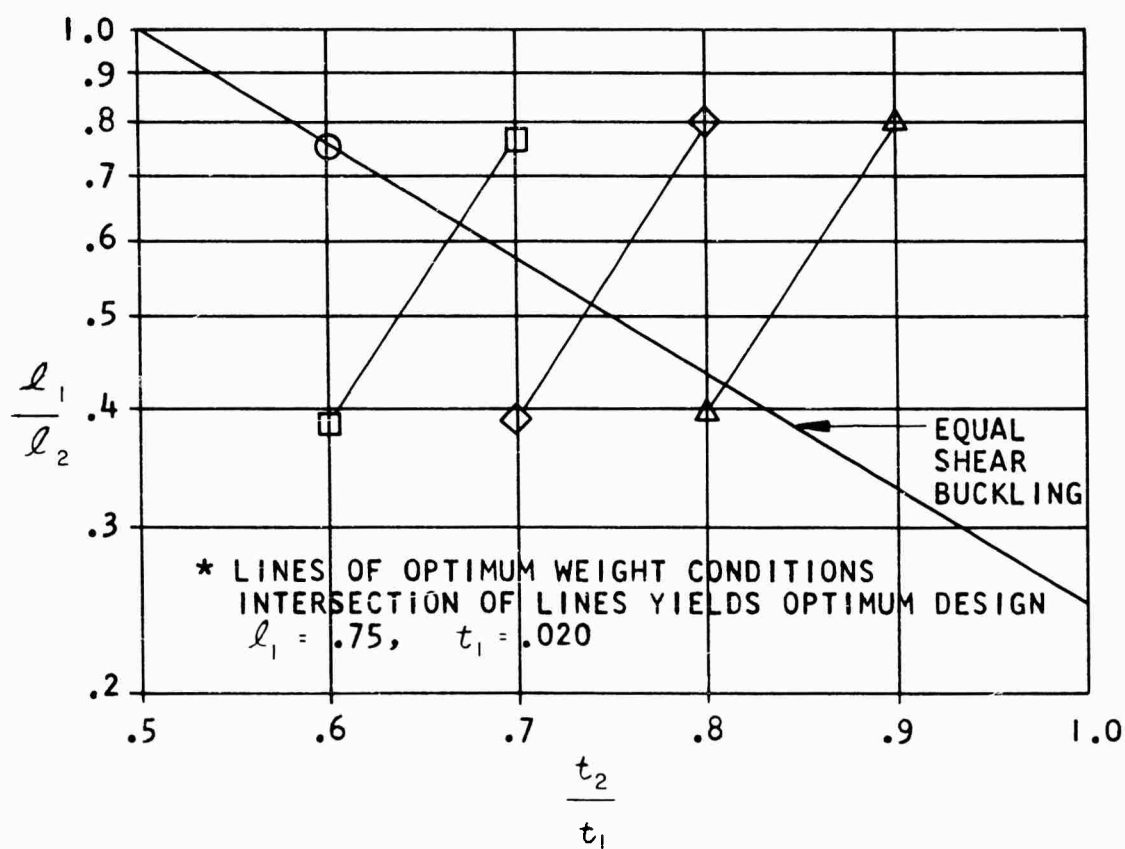AND ALLOWABLE BENDING AND BUCKLING STRESS
p = .208 PSI

FIGURE 53   LENGTH AND THICKNESS RATIOS FOR EQUAL APPLIED
AND ALLOWABLE BENDING AND BUCKLING STRESS
p = .300 PSI

FIGURE 54 OPTIMUM DESIGN FOR VARIOUS SOUND PRESSURE
LEVELS RANDOM LOADING $t_1 = .025$

FIGURE   55   OPTIMUM DESIGN FOR VARIOUS SOUND PRESSURE
LEVELS RANDOM LOADING t_1 = .020

SKIN AND STRINGER

The following procedure determines the cap width (b_c) and web width (b_w) for which the applied, crippling allowable, column allowable, and skin stresses are equal. A typical cross section is shown in Figure 51, the section properties are presented in Table 9, and the optimum stringer configurations are shown in Table 10. Tangent modulus and column data are presented in Figures 52 and 53.

The procedure is as follows: Assume an applied stress (f). Using equation 82 determine the value of $(b_c + b_w)$. From Figure 53, find the ratio (b_w/t_w) at which the crippling stress is equal to the applied stress. Under these conditions, determine the corresponding value for (b_c), (b_c/t_c), and the crippling stress in the cap. If it is less than (f), revise (f) as indicated and repeat the above procedure. If the allowable crippling stress in the cap is equal to or greater than (f), determine the allowable column buckling stress (F_c) for that configuration. If it is not equal to f, repeat the above procedure.

The crippling stress in the web, instead of the crippling stress in the cap, is set equal to the applied stress because the resultant material distribution yields the greatest allowable column stress. A sample computation is shown below:

Sample Computation

$$(t = .020", 1000 \text{ lb/in}, S = 4", t_w = t_c = .030")$$

$$f = P/A = \frac{(1000 \text{ lb/in})(4 \text{ in})}{(A)_{skin} + (A)_{web} + (A)_{cap}}$$

(the resulting b_c and b_w will be the same for any combination of spacing and load per inch which yields 4000 pounds).

The effective width (W_e) is used in computing the skin area

$$(A)_{skin} = (W_e)(t) = \frac{1.7 \, t^2 \, E}{f_s} = \frac{2.67}{f_s} \quad \text{(For Ti-6Al-4V)} \quad (81)$$

$$f = \frac{4000}{\frac{2.67}{f_s} + t_w(b_c + b_w)} \quad (82)$$

The applied stress in the skin (f_s) is set equal to the applied average stress (f).

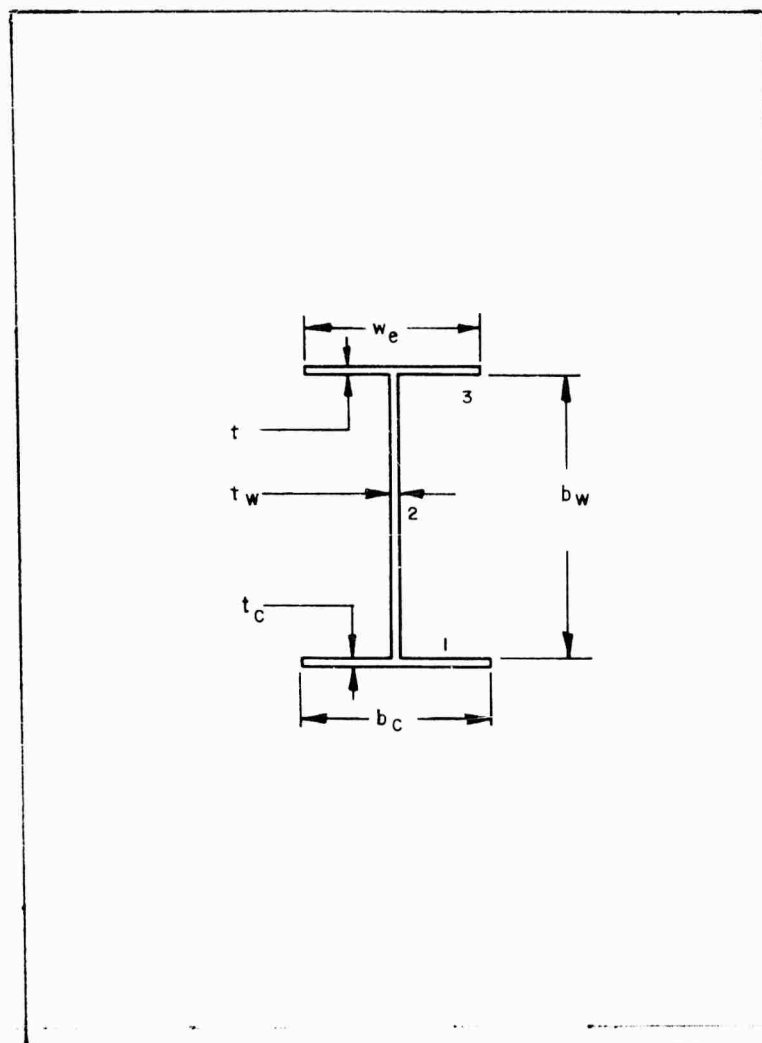$$(b_c + b_w) = \frac{4000 - 267 \ f}{.03 \ f}$$

FIGURE 56 STRINGER CROSS SECTION

Table 9

STRINGER SECTION PROPERTIES

Case	t	w_e	t_w	$(b_c + b_w)$	b_c	b_w	f	$*(F_c)$
1	.020	.454	.030	1.23	.48	.75	87,000	87,200

Case	Section	A X10^{-3}	y	y^2	Ay X10^{-3}	Ay^2 X10^{-3}	I_{cg} X 10^{-3}
	1	14.40	.015		.216		
	2	22.50	.405	.164	9.120	3.69	
1	3	9.08	.790	.624	7.170	5.72	1.05
	$\sum(1-3)$	45.98			16.51	9.41	

$$I = \sum(Ay^2) - \frac{\sum(Ay)^2}{\sum A} + \sum(I_{cg})$$

$$(I)_1 = .00941 - .00595 + .00105 = .00451 \text{ in}^4$$

$\rho = .313$

(83)

$*L^1 = 13.05$ inches

Table 10

OPTIMUM STRINGER CONFIGURATIONS

		S = 4"			S = 5"		S = 6"
t = .020" at 1000 #/in.	t_w	= .030"	= .035"	= .040"	= .035"	= .040"	= .040"
	b_c	.48"	.15"	.11"	.38"	.15"	.34"
	b_w	.75"	.87"	.88"	.83"	.97"	.92"
	W	.01870 #/in.	.01851 #/in.	.01755 #/in.	.02277 #/in.	.02316 #/in.	.02726 #/in.
t = .025" at 1135 #/in.	t_w	= .030"	= .035"	= .040"	= .035"	= .040"	= .040"
	b_c	= .48"	= .15"	= .00	= .42"	= .14"	= .43"
	b_w	= .75"	= .86"	= .94"	= .82"	= .92"	= .94"
	W	.02190 #/in.	.02165 #/in.	.02244 #/in.	.02694 #/in.	.02674 #/in.	.03277 #/in.

TANGENT MODULUS CURVE
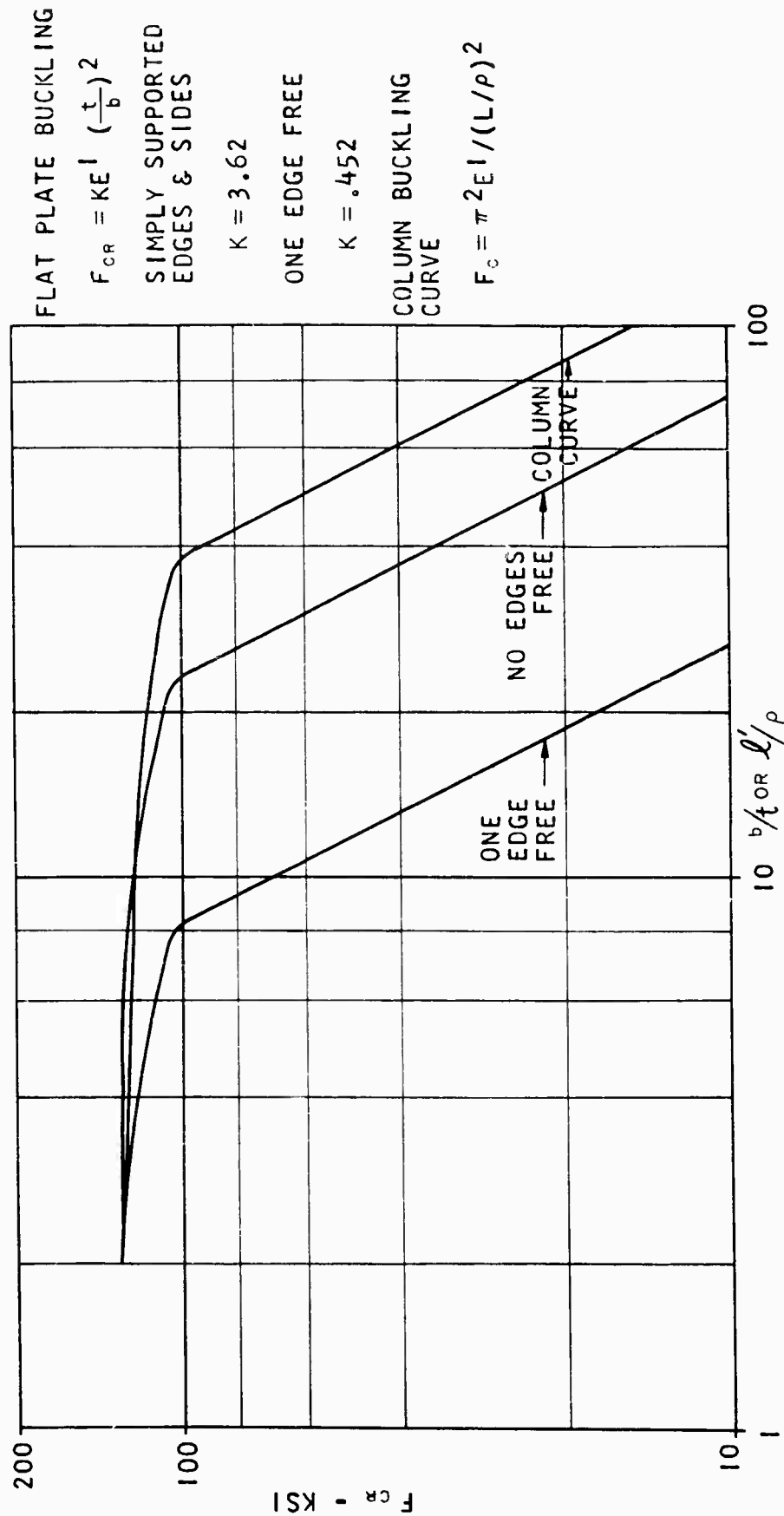
FOR TI 6AL-4V ANNEALED, TYPICAL
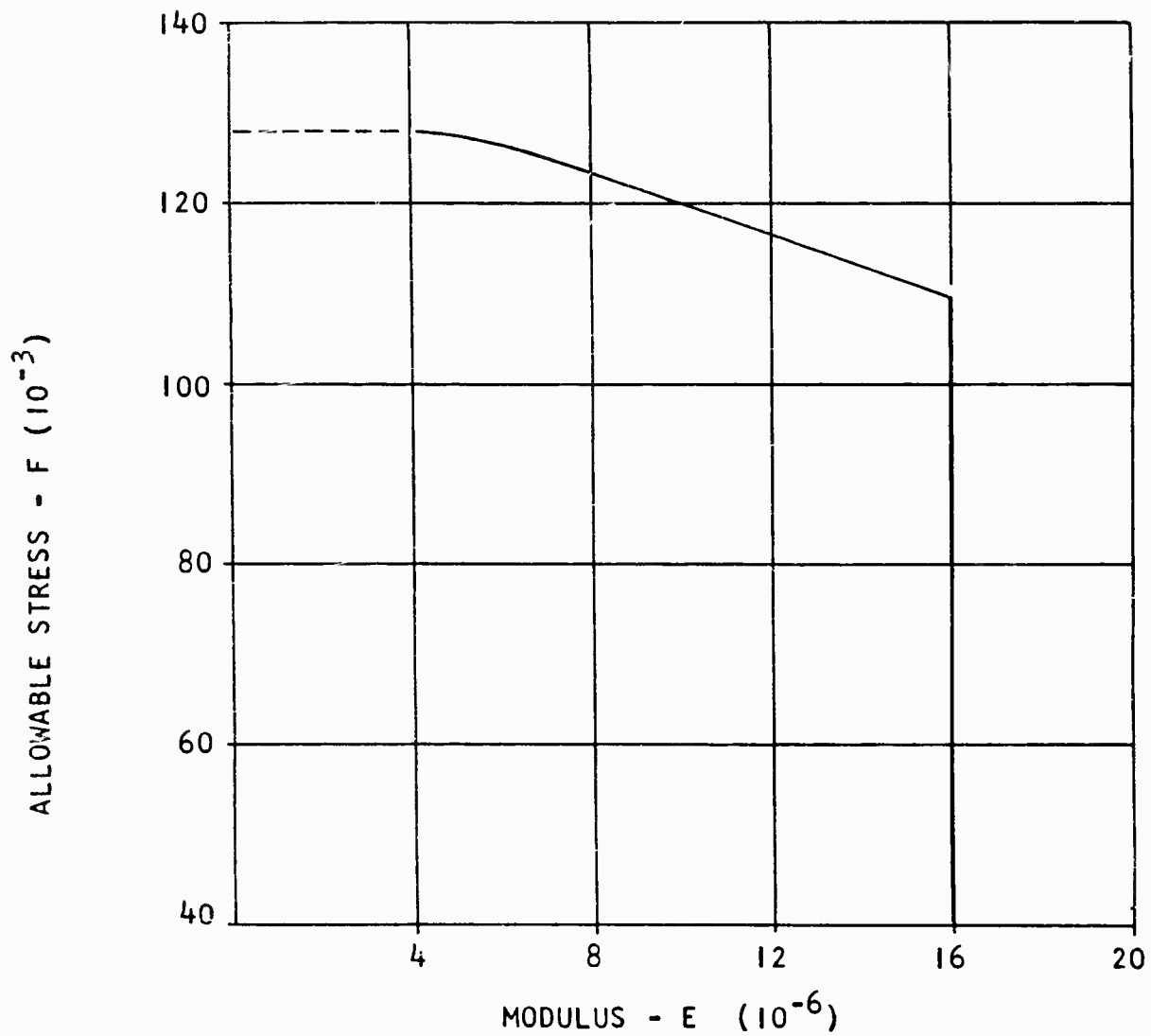
FIGURE 57   TANGENT MODULUS CURVE
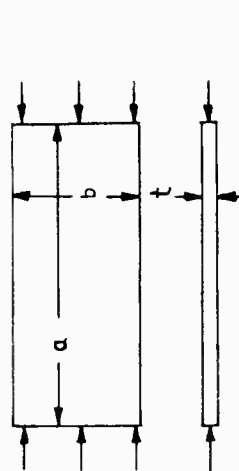
FIGURE 58 FLAT PLATE AND COLUMN PANEL BUCKLING